Al-Farabi Kazakh National University

UDC 662.141 On manuscript rights

YELEMESSOVA ZHANERKE KOMEKOVNA

New nano metal-organic framework energetic materials for pyrotechnics

6D073400 – Chemical technology of explosives and pyrotechnics

Dissertation submitted in fulfillment of the requirements for the degree of

Doctor of Philosophy (PhD)

Scientific supervisors:
Candidate of Chemical Sciences,
Lesbayev B.T.

Professor, PhD
Nanjing University of Science and Technology,
Nanjing, China
Ruiqi Shen

Republic of Kazakhstan

Almaty, 2020

Acknowledgement

I would like to appreciate *Prof. Z.A Mansurov* for all his direction, promotion and invaluable mentorship during my PhD research.

I would like to acknowledge *Prof. Ruiqi Shen* and the staff of Chemical Engineering School of Nanjing University of Science and Technology (Nanjing, China) *Dr. Wu Lizhi, Tang Yue, and Haonan Zhang* for all their help and support.

CONTENTS

NORMATIVE REFERENCES

In the present thesis, the following references have been used:

GOST 3885-73. Reagents and highly pure substances. Sampling, packing, packaging and labeling.

GOST 24104-88. Laboratory scales.

GOST 50431-92. Thermocouples. Nominal static conversion characteristics.

GOST 8.417-81. Government system for ensuring the measurements uniformity. Physical quantities units.

GOST 7.32-2001. Report on scientific - research work. Structure and rules for formulation.

GOST 7.1-2003. Bibliographic record. Bibliographic description. General requirements and compilation rules.

SYMBOLS AND ABBRIVIATIONS

AC	activated carbon
AN	ammonium nitrate
AP	ammonium perchlorate
BET	specific surface analysis
β	heating rate
CNT	carbon nanotubes
CRH	carbonized rice husk
DSC	differential scanning calorimetry
DTA	differential thermal analysis
EM	energy materials
EIL	energetic ionic liquid
EDS	energy-dispersive X-ray spectroscopy
E_a	activation energy
GO	graphene oxide
HEM	high energy materials
HMX	octahydro-1,3,5,7-tetranitro- 1,3,5,7-tetrazocine
LAG	liquid-assisted grinding
MB	methylene blue
MOF	metal-organic framework
NASA/CEA	computer software for thermodynam. calculations
NC	nitrate cellulose
RDX	hexahydro-1,3,5-trinitro-1,3,5-triazine
SEM	scanning electron microscopy
TATNB	1,3,5-triazido-2,4,6-trinitrobenzene
TG	thermogravimetric analysis
TNT	2,4,6-trinitrotoluene
T_p	peak temperature of the DSC curve

INTRODUCTION

General characteristics of the work. This dissertation is devoted to the developed of highly effective catalytically active energy additives designed to enhance the basic characteristics of the combustion process of pyrotechnic compositions. The goal was solved by the development and design of metal-organic framework structures (MOF) based on rice husk and transitional metal oxides and the study of the effect of MOF on the kinetics of the process of thermal decomposition and combustion of a pyrotechnic composition based on ammonium nitrate.

Relevance of the research topic. Energy materials (EM) are materials with a high content, accumulated internal energy, which is released during a chemical reaction. The list of energy materials includes hydrocarbon fuel, rocket fuel, explosives, pyrotechnic compositions, etc. Energy materials consist of chemical compounds, which are combustible and oxidizing substances that, when entering into a chemical reaction, intensively release energy. Energy materials differ in energy intensity - the amount of energy released during complete combustion relative to their specific volume. An intensive search for new compositions to increase the energy intensity of energy materials is carried out without compromising their important characteristics, such as decomposition initiation temperature, burning rate and temperature, as well as environmental cleanliness. One of the classic ways to increase the efficiency and optimize the properties of energy materials is to use metal nanoparticles and their oxides as well as various carbon and carbon-containing materials as catalytic additives.

Currently, pyrotechnic compositions belonging to the class of energy materials are used in many industries. Pyrotechnic compositions are used in pyro automatics, in pyrotechnic heaters, in airbags, as igniters in rocket engines, in fireworks, in compositions causing rainfall to extinguish fires, etc. In this regard, the creation of environmentally friendly pyrotechnic compositions with predetermined performance characteristics is an urgent task. To solve this problem, one of the promising areas is the development and creation of special additives for pyrotechnic compositions that would allow you to adjust the main parameters, such as the initial decomposition temperature, ignition delay time, burning rate, the formation of toxic gases and pressure increase (in order to prevent transition combustion process in explosive mode). To optimize the listed performance characteristics of pyrotechnic compositions, the most promising materials as catalytic additives are metal nanoparticles or their oxides. In turn, the processes of aggregation and agglomeration of introduced nanoparticles, which leads to uneven distribution in the bulk of the powder material, always complicate the process of adding nanodispersed additives to a powdery material. To prevent the agglomeration process, methods of fixing nanoparticles in the pores of a porous material can be used. Carbon nanoporous materials are characterized by a fairly ordered structure, and the content of many surface defects allows various metal centers to be embedded in their structure and thus create metal-organic framework structures (MOFs) based on

them, which have a number of unique properties, such as ordered crystalline structure, strong metal-ligand interaction, high porosity and high specific surface. It should be noted that the use of highly porous systems with an ordered structure also helps to achieve a uniform local distribution of active centers on their surface, which can significantly increase the efficiency of the catalysts. Thus, the possibility of changing the catalytic activity of MOF by introducing specified metal centers into their structure defines these materials as the most promising as catalytic additives for improving the performance of pyrotechnic compositions.

A promising and economical method for the production of nanoporous carbon material with a high specific surface is to obtain it from renewable plant waste. In connection with the foregoing, in the dissertation, research was conducted on the creation of new MOFs based on waste from vegetable raw materials of rice husks and nanoparticles of metal oxides and their influence on the main characteristics of the combustion process of pyrotechnic compositions was studied.

The purpose of research. To develop metal-organic framework structures (MOF) based on waste plant materials and metal oxide nanoparticles and explore the possibilities of their use to increase the burning rate, lower the decomposition temperature, and also reduce the concentration of toxic gases during the burning of pyrotechnic compositions.

Tasks of research. To achieve this goal the following tasks were set:

1. To develop and create a metal-organic framework structure (MOF) based on waste plant materials and metal oxide nanoparticles;
2. To study the kinetics of thermal decomposition of a pyrotechnic composition based on ammonium nitrate in the presence of a metal-organic framework structure (MOF) with various metal oxides;
3. To determine the effect of a metal-organic framework structure (MOF) with various nanoparticles of metal oxides on the combustion conditions of pyrotechnic compositions at initial pressures from 1 to 3.5 MPa;
4. To study the possibilities of initiating the combustion process of a pyrotechnic composition by laser radiation with the addition of a metal-organic framework structure (MOF);
5. Determine the effect of the metal-organic framework structure (MOF) on the activation energy of the pyrotechnic composition AN/Mg/NC.

The main provisions for the thesis defense.

1. Prevention of the process of agglomeration of metal oxide nanoparticles by the isolated distribution of nanoparticles in a porous carbon matrix increases the catalytic activity of the created metal-organic framework structures (CRH/Me_xO_y).
2. Achieving a high burning rate of the pyrotechnic composition to 20.5 mm/s, with a low-pressure value n=0.42 by adding an additive of a metal-organic framework structure (CRH/CuO) at an initial pressure in the system of 3.5 MPa.
3. Ensuring the reduction of the activation energy of the pyrotechnic composition to 8 kJ/mol by the introduction of an additive of a metal-organic framework structure (CRH/CuO).

4. Ensuring the ignition of the pyrotechnic composition by laser initiation using a metal-organic framework structure without adding optical sensitizers with an ignition delay time of 506 ms at a laser energy of 4.35 J.

Object of the study: metal-organic structural composites (MOF) based on carbonized rice husk with the addition of nanosized transition metal oxides (CuO, NiO, FeO, TiO, Zr_2O) and pyrotechnic compositions based on them containing ammonium nitrate, magnesium, cellulose nitrate.

Subject of study: study of the specific effect of MOF (CRH/Me_xO_y) on the kinetics of thermal decomposition of the pyrotechnic composite (AN/Mg/NC) and the promoting effect of MOF (CRH/Me_xO_y) on the AN/Mg/NC combustion process.

Research methods: The following research methods were used to achieve and solve the necessary goals and tasks: BET analysis (low-temperature nitrogen adsorption) to determine the specific surface area of activated carbons; scanning electron microscopy (SEM) to study the characteristics and surface morphology of activated carbons; energy dispersive analysis to study the elemental composition; adsorption capacity of methylene blue to study the adsorption capacity; differential scanning calorimetry (DSC); differential thermal and thermogravimetric analysis to study the kinetics of decomposition of compositions (DT-TGA); high-speed camera (MotionXtra HG-100K); NASA-CEA software (chemical equilibrium and application) for thermodynamic calculations of adiabatic combustion temperatures.

Scientific novelty of the work. The scientific results presented in this work contain new experimental and theoretical data on the influence of metal-organic framework structures MOF (CRH/Me_xO_y) on the combustion and thermal decomposition of pyrotechnic compositions based on ammonium nitrate.

The following results for the first time were obtained:

1. Activated carbon-based MOF (CRH/Me_xO_y) metal-organic frameworks have been developed based on carbonized rice husk and transition metal oxide nanoparticles, which were first used as a combustion catalyst in pyrotechnic compositions.

2. It was found that the MOF (CRH/CuO) additives provide the pyrotechnic composition AN/Mg/NC with a high burning rate of 11.6 to 20.5 mm/s at an initial pressure in the system of 1 to 3.5 MPa, while the calculated value of the indicator pressure *n* is in the range of 0.53-0.42. From the obtained results follows an important conclusion that the addition of MOF provides the opportunity to significantly increase the burning rate of the pyrotechnic composition without the transition of the combustion process to explosive mode.

3. It was revealed that the additives of MOF (CRH/Me_xO_y) have a direct effect on the decomposition mechanism of the pyrotechnic composition AN/Mg/NC and reduced its activation energy to 8 kJ/mol.

4. It was established that the developed AN/Mg/NC/CRH/Me_xO_y pyrotechnic composition is highly energy-efficient material, which is suitable for direct ignition by laser initiation. The developed combustible composition does not require the addition of optical sensitizers to ensure stable ignition by laser radiation, which means to safe for its chemical properties. The pyrotechnic composition

AN/Mg/NC/CRH/CuO stably ignites at a laser energy of ≥4.35 J (without MOF, the laser energy was 25.97 J), the ignition delay time was 506 ms (without MOF, the ignition delay time was 902 ms).

The theoretical significance. The theoretical significance of this work is to establish the basic laws of the influence of metal-organic framework structures (MOF) on the characteristics of thermal decomposition and combustion of energy-intensive materials. The obtained scientific results could be useful in fundamental and applied research related to the composition and properties of energy materials.

The practical significance. The developed metal-organic framework structures (MOF) are promising materials for use as effective additives for improving the useful characteristics of energy-intensive materials. The results could be used in applied research related to the development and creation of high-energy energy-intensive materials.

Approbation of the work results. The results of the dissertation were reported and discussed in the following international scientific conferences:

• Proceedings of IV Conference of Students and Young Scientists «Chemical Physics and Nanomaterials» (Almaty, March 19, 2019);

• Proceedings of the Conference of the Students and Young Scientists dedicated to the 30th anniversary of the Institute of Combustion Problems creation (Almaty, November 30, 2017);

• X International Symposium «The Physics and Chemistry of Carbon and Nano energetic Materials» (Almaty, September 12-14, 2018);

• International Scientific Conference Modern Problems of Condensed Physics States, Nanotechnologies and Nanomaterials (Almaty, May 17-18, 2018);

• The First International Conference on Defense Technology Proceedings (Beijing, China, October 21-25, 2018);

• The 4th International Nano-Structured Energetic Materials Workshop (Nanjing, China, November 2-4, 2018);

The personal contribution of the author consists in the formulation and conduct of experiments, the synthesis and interpretation of the results obtained, the writing of articles and reports. Goals and objectives, experiment planning, discussion of the results and the main points of defense were discussed with both scientific consultants.

Publications. The main results of the thesis were published in 12 publications, of which 2 articles is included in the Scopus database and 1 article included in the Thomson Reuters database, 4 - publications were published in publications recommended by the Committee on Control in Education and Science of the Republic of Kazakhstan, 4 - in the proceedings of International and regional scientific conferences, application for utility model No. 2019/0488.2.

The scope and structure of the work. This thesis work is presented on 94 pages of printed text and contains 64 figures and 16 tables. The work consists of introduction, review of literature, description of research objects and methods, results and discussion, conclusion, list of references contain 116 names.

1 LITERATURE REVIEW

1.1 High energy materials

High-energy materials (HEM) - class of compositions with a high content of accumulated internal chemical energy which might be emitted while a specific chemical reaction or physical process occurs. The HEM concept covers a large list of various substances: hydrocarbon combustible, rocket fuels, gunpowder, explosives, pyrotechnic means, incendiary means, etc. These materials mainly consist of one or several classes of chemical compounds, such as: combustible, oxidizing agents, promoters, binders (organic polymers, providing mechanical strength and density), etc., which quickly react with each other when initiated and release a large amount of energy [1]. The onset of the HEM reaction most often occurs under conditions of fairly extreme temperatures and pressures. In terms of heat generation Q_v, when fully burned, energetic materials differ in their energy intensity. Energy intensity is the amount of heat released during the complete combustion of the HEM, relative to their unit volume. In liquid or suspension fuels, due to the low density of HEM, additional additives are introduced into their composition, such as metals (aluminum), carbon-containing materials (technically carbon), borides, binders, catalysts and other technological additives that increase the energy intensity of materials [2].

Energy materials with their chemical formula and the oxygen atoms ratio to hydrogen, carbon and nitrogen, can have oxidizing and reducing (combustible) properties. There are also substances with a balanced oxygen content, which simultaneously combine both properties (oxidant-reducing agent). Such formulations are called monopropellant [3].

Some advantages of using HEM: (1) non-oxygen technology (internal oxygen resources consume while chemical transformation reactions occur; (2) possible to control the rate of a chemical reaction in a rather wide range from burning to explosion (10-5 seconds); (3) allow in the shortest possible time to obtain large amounts of the required energy for the target application. The above listed advantages continue to attract the attention of researchers for more than a hundred years, the results of previous work in this area have opened up access to the development of technical progress that we have today.

New directions for energetic materials are to find the high-energetic, high-dense, and non-sensitive materials. Early scientists [4-7] showed that MOFs have high potential and preferences in this field. Due to the high mechanical strength, thermostability and high detonation heats, MOFs were prognosticated to be applicable as HEMs. However, the process for preparing these bulk polymers is expensive and multistage. In this connection, it is of interest to search for alternative methods for obtaining bulk materials, one of which are structures based on graphene oxide frameworks and activated carbon materials. The growing popularity of multilayer graphene’s is due to the uniqueness of their physical and chemical properties. A promising, simple and cost-effective method is the production of activated carbon materials from plant wastes like rice husk or walnut shell [8-10].

Mixtures of certain fuel (e.g. magnesium bits) and oxidizer (e.g. CuO, Fe_2O_3 etc.) are energy-saving composites [11,12]. The energy produced by the gas products is determined by the enthalpy reaction that occurs from the oxidation-reduction process between the fuel and the oxidizer. Even though these materials usually have a much higher energy density [13] than organic explosives (such as 2,4,6-trinitrotoluene, nitrocellulose, hexahydro-1,3,5-trinitro-1,3,5-triazine), their generated energies are lower than the theoretical values because a large portion of the fuel powders is usually unreacted owing to the low reaction rates between the fuel and oxidizer and the slow mass transfer rate between the reactants. What is more, such powders without reactions are significant pollutants [14] and, due to their size distribution and the complexity of their decomposition, are important sources of particulate material 2.5. Most recently, many other important molecules with their high-energy content and intense action have been included in formulations. Others compose consist of salts (NaN_3, NH_4ClO_4, and $KClO_4$), in fact. Such molecules have very positive gas generation behavior, but in the process of production, transport and operation, they can cause severe environmental pollution [15].

High explosives, pyrotechnic powder and chemicals releasing their chemical energies at a rate much higher through decomposition than in the mixture of common materials, usually known as HEMs. Such products have a very different reaction than other materials with thermal and mechanical energies inputs. The analysis of HEMs has been recently conducted using state-of - the-art methoodology and theory and evolved from conventional synthetic approaches from a field with limited functional concerns to an established area of fundamental research [16].

To sum up, there are some advantages of using HEM: (1) non-oxygen technology (internal oxygen resources consume while chemical transformation reactions occur; (2) control the rate of a chemical reaction within a rather wide range from burning to explosion (10-5 seconds); (3) allow large amounts of the energy required for the target application to be obtained in the shortest time possible. For more than a hundred years, the above-mentioned advantages continue to attract researchers' attention, the results of previous work in this area have opened access to the development of the technical progress we have today.

1.2 Energy propellants (fuels) designed for explosives and pyrotechnics

People began to use the fire as fuel for home heating and cooking from the beginning of human creation. Carbon was used to melt metal golds the most popular technical use of the past years [64]. Earlier on, the first carbon powder was developed in China, which was the start of a new military and mining age and the first powder was made. Carbon has a wide variety of different kinds and allotropic shapes, from graphite to fullerenes and nanotubes. It has been introduced into the formulation of carbon products for energy density, among the most well-known industrial additives. Carbonaceous products are widely used in the aerospace industry in solid fuels to enhance combustion properties and to minimize thermal radiation within the grain [18].

A missile or rocket is a launch system that is sent to a desired destination, whether as a warhead or as a satellite. The response to the energy of the hurled stuff, called the 'propellant', which is filled within the rockets chamber [16], passes the forward force to the rocket. A propellant could therefore be defined as a controlled energy source that contains the materials needed for the combustion or conversion of this energy into usable cinematics. One of the main rocket or missile subsystems is the propulsion system. Propellants can be either rigid or liquid in a chemical propulsion system. Solid propellants, though, are commonly used for both satellite defense and launch vehicles [18].

The strength, density and capacity to customize the properties needed for the task at hand should be the perfect propellant for rockets [2,3]. Propellants should treat various loads over a large temperature spectrum -55 to +65°C. Whilst solid propellant output typically is smaller than liquid, in view of its versatility, consistency in construction, stability, protection, long life range and lower cost, solid propellants are favoured for military purposes [27,28]. Recent specifications have driven the production of massive engines, burning process control and efficiency, energy and mechanical properties changes. Thus, solid propellants should have the following desirable properties:

• High release of chemical energy and low molecular weight combustion products (high I_{sp}).

• High density (reduction in motor volume and thereby weight).

• Low pressure index, low temperature sensitivity coefficient, smokeless exhaust.

• High mechanical properties (ultimate tensile strength, ultimate compressive strength, and elongation %.

• Unable to deteriorate through transport either chemically or physically.

• High autoignition temperature and insensitivity to impact to prevent accidental initiation.

• The processing process is easy and cost-effective.

Intrinsic/constitutional and environmental factors are the key determinants of solid rocket propellants ' mechanical properties. Constitutions involve chemistry, bonding properties and microstructuring, while atmospheric variables include temperature, distance, duration, air temperatures, etc.

An explosive substance is an explosive substance (or a substance mixture) that is itself capable of causing damage to the environment through a chemical reaction that produces gas at such a temperature and pressure. Even if gas does not grow, pyrotechnic compounds are included [19].

The classification of explosives is shown in Fig. 1. Primary and secondary explosives may be grouped together. Primary explosives are considered sensitive explosives because if they are exposed to an ignition temperature, flame, friction or a heated wire, a crystal will detonate. Lead azide, plum trinitroresorcinate (lead styphnate) and tetrazolyl guanyletracene (tetrazene) are the most frequently used key explosives. Mercury fulminate was used in earlier times as well [29,30].

The existence of plum due to its significant environmental impact as primary explosives come into service is a frequent problem for most main explosives. Biometric explosive plum-free main explosives are therefore favored, for example 1.3.5-triazido-2,4,6-trinitrobenzene (TATNB). In a few milliseconds or less, however, the key explosive reaction starts with deflation. Main load explosives can greatly differentiate and depend heavily on their use. Such systems usually have also different binders, in which the binder amount can be as small as 5%. Blasting bombs, including ammonium nitrate (AN), which may be used to oxidize a liquid fuel, may be very heterogeous. Nearly all variations can be found between these instances [20].

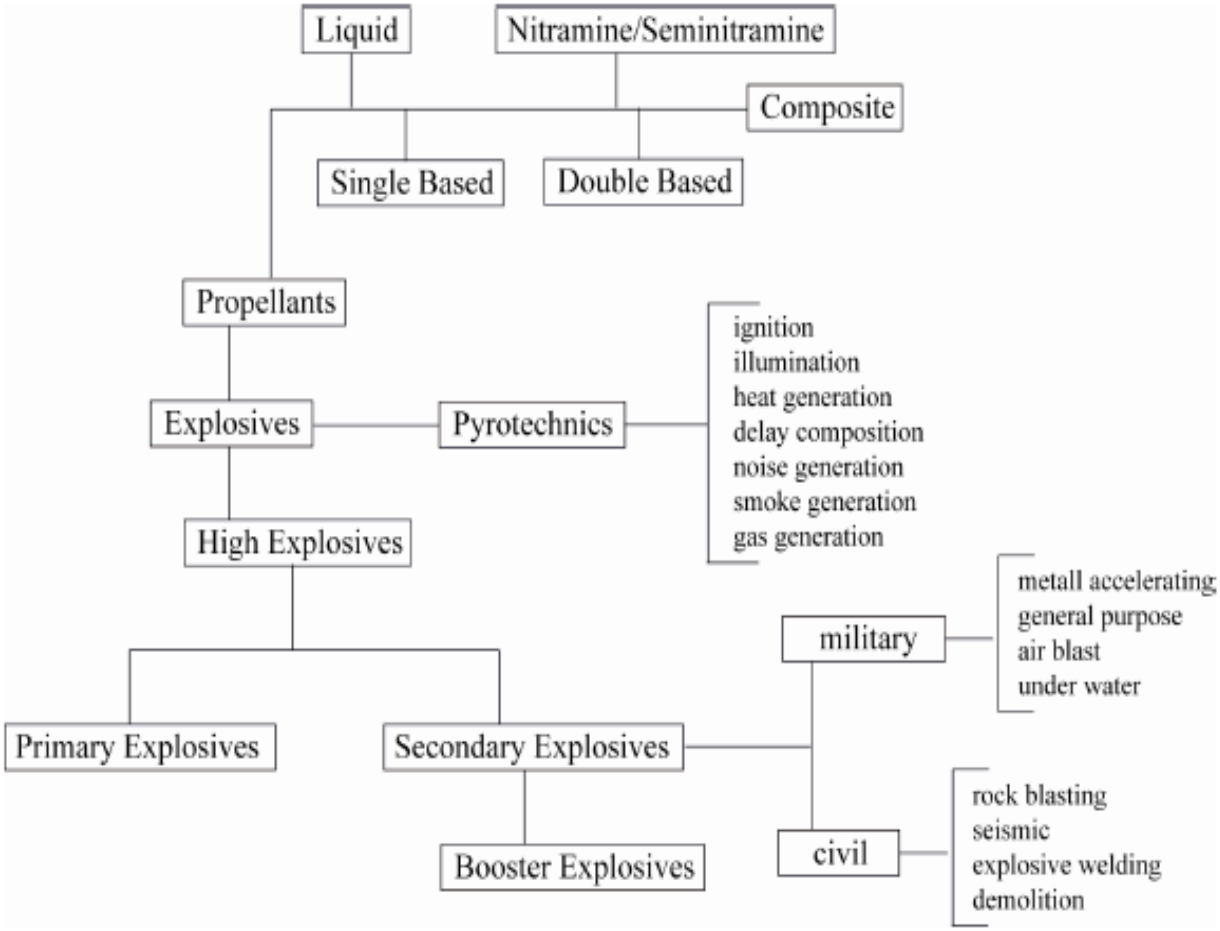

Figure 1 - Classification of explosives [23]

Many new energy molecules have been synthesized in the field of main load explosives, especially in military applications [33]. Based on computer simulations, and expertise in organic chemistry, high-density explosive target molecules have been defined and can be achieved by fused ring and/or stretched ring systems in the molecular structure.

The term pyrotechnics derives from the Greek terms 'pyros-fire, flame' and 'techne-art' and is one of the closely related subjects: high explosives, propellants and pyrotechnics themselves. Since these three subjects have a more or less similar physicochemical history, they also overlap in structure and intent. The most noticeable traditional manifestation for pyrotechnics however is that pyrotechnic

composition creates beautiful optical and acoustic effects. Optical effects: Motion (rockets, fire wheels, bombs); color (stars, various colored smoke); sparks (candles, volcanoes, fountains). Bang ('swissbanger', thunderbangers, crackers); Whistle (wailing sirens, banshees); Rustle (cracklestars). A pyrotechnic process is different from ordinary combustion, because it does not require ambient air [20]. In pyrotechnics, the exothermic reactions are based on simple chemical redox reactions. Experience has long been the fundamental basis of pyrotechnics. In order to obtain the desired, well-defined effects, the redox reaction can be influenced by clever choice of reduction agents and oxidizers as well as variation of the composition. The term 'effect' in pyrotechnics includes: reaction rate, reaction heat, reaction temperature, gas production, reaction products/flashing particles and colored light.

The burning of large quantities of traditional pyrotechnics, for example used to launch hundreds of fireworks projectiles, produces large quantities of smoke, and depending on the specific weather conditions, such as wind direction, wind speed and relative humidity, the smoke may block the view of additional fireworks or surround the audience. Most compositions of pyrotechnics show a very high sensitivity to electrostatic discharge and friction, and since particle size distribution and morphology affect the sensitivity and reactivity of pyrotechnic composition systems, special manufacturing requirements make production difficult and dangerous. For instance, a human being's electrostatic charge is strong enough to cause a tripping of certain pyrotechnic redox reactions. In addition, pyrotechnic coloring is still a difficult subject, as the absence of any metal ions (transition metals) is best for controlling the color of the fireworks and removes any ash residue [26]. Ammonium perchlorate and ammonium nitrate are therefore preferred oxidizing agents. Though chlorates may be used as an oxidizer, due to their extreme sensitivity they are not preferred. With regard to color, it is difficult to realize blue (in most cases arising from copper salts). Some alkali or earth-alkali metals (e.g., red (strontium salts), green (barium alts), yellow (sodium salts)) that do not produce ash residue easily produce the other colors [20].

1.3 Pyrotechnic gas-generating compositions

There are several gas-generators for sudden pressure or inflation, such as seat-belt tensioners, fire-fighting equipment and inflating passive restraint systems for occupants of vehicles (colloquially known as "air bags"). Another form of known inflators makes use of a quantity of stored compressed gas that is released selectively to inflate the air bag. A related inflator type generates a gas source from a gas-generated fuel, which, when ignited, provides a sufficient quantity of gas to inflate the air bag. The airbag inflates the gas by means of a mixture of a supplied compressed gas and the combustion products of a gas-generating device, another inflator (called a composite inflator). There are several drawbacks for inflators which are entirely or partly dependent on the production of gases due to combustible materials. For example, in such inflators, the burning of the propellant and the inducing materials lead to the production of undesirable particulate matter [37-39].

The use of particle producing or combustion-generating inflators as part of a passive retaining device in the vehicle could therefore contribute to the introduction of harmful particulates into the vehicle occupant zone and thus to the inhalation by the occupants [20].

The inhalation of particulate matter will, in fact, cause asthmatic reactions, posing a health risk to the inhabitants. Therefore, the volume and form of particulates emitted by the inflator device are restricted by automotive companies. Insoluble particulates rather than soluble, as the latter are thought to cause a greater reaction. Particulates that occur through the secondary combustion of the inert components of rocket and acceleration systems as well as from some components of solid rockets or gas turbines. The decrease in particulates in one or more of these components would result in the positive reduction for the whole assembly of measurable ("smokelike") pollutants [20].

The toxicity of the gasses emitted after the gas turbine is fired is also a concern (for example, NH_3, HCN, NO_x, CO). Sodium azide is widely used in small gas generators. Such products, sadly, have drawbacks in terms of toxicity and gas production. Dual base propellants are other conventional gas-generating weapons. They thus produce toxic and reactive gases and are highly combustible [40]. Alternative gas-generating compounds were suggested that are associated with Double Basis (DB), azodicarbonamide (ADCA) nitrate and potassium-nitrate (KNO_3) or potassium perchlorate ($KClO_4$) and ammonium nitrate oxidized [20].

The development of gas generating compositions that satisfy all the requirements is an extremely difficult task, since there are no suitable organic compounds, solid and thermostable, for this purpose, and the creation of a stoichiometric mixture is possible only on the basis of ammonium nitrate.

1.4 Ammonium nitrate: a promising propellant oxidizer

Ammonium nitrate (AN) is one of the ammonium compounds that is most commercially important in terms of use. It is commonly used for nitrogen and explosive fertilizers [41]. For explosives and propellants, the nitrate ion is an oxygen supply and it requires its added oxidant when serving as a source of ammonia and nitrate ion essential to the product, for form of a nitrogen fertilizer. Most commercial explosives have AN as their principal feature. ANs are well-known to contain several components such as ammonium nitrate-fuel (ANFO), amatol, etc. However, its use in the field of propellant pyrotechnics, unlike the potassium nitrate used in earliest solid cockets or ammonium perchlorate (AP), which is the principal element of the black powder or piston powder and is known to have been used. That is rather minimal which is the key oxidant for conventional solid propellants. Its use in key propellant applications is limited to small burn speeds, low performance applications including gas generators for liquid propellant engine turbopumps and jet aircraft emergency starters [43].

The solid propellants have been used widely in both space missions and military missions due to their technical versatility. Main ingredients in solid propellents are a gas generating strong oxidizer and an aromatic carbon solvent that

is also a bonding agent. AP is currently employed as the primary oxidizer for most solid rocket engines. Late, with the growing concern for chlorine-free environmentally friendly propellants, AN is growing as a rocket-propellant oxidizer for safe combustion products even if inorganic nitrates are known to be a low-power oxidation compared to perchlorate. AN is hygroscopical, undergoes a room temperature change that involves a significant change in volume and burns very slowly, in addition to its low energy content. Such detrimental features make it as an alternate oxidizer even less desirable. However, many of these AN problem, which limit its use as an efficient oxidizer, have proven to be overcome by extensive literature. Nevertheless, much of the information concerning the different properties of salt, in particular the information concerning its use as an oxidizer, remains, owing to its use in strategic areas, restricted or scattered.

In nature as such, AN does not occur. The salt was first invented in 1659 by Glauber, who produced nitric acid on toxic alkals, ammonium carbonate, and named it nitrum flammans because of its yellow flames from sodium residues. Was distinct from potassium nitrate. Mellor reviews many of the early procedures mentioned in the literature for planning AN [44-45].

The ammonium nitrate compound is a whole in which a strong ammonium ion (NH^{4+}), as a cationic ion, is present and a negative nitric acid salt ion (NO^{3-}) functions as an anion. Fig. 2 demonstrates the molecular structure and stable phase.

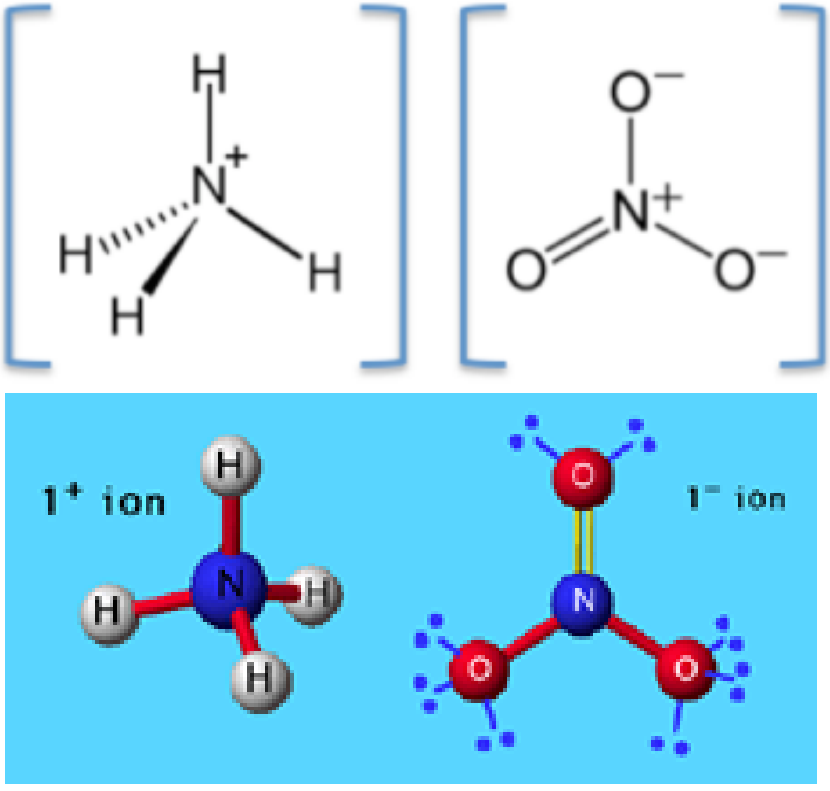

Figure 2 - The structural and molecular form of ammonium nitrate [41]

AN is the cheapest oxygen source for industrial explosives usable in condensed form. In the second half of the nineteenth century the original experiments with it as part of explosive mixes started. Grindel and Robin were the

first to use AN as an incendiary alternative for potassium nitrate in black powder at the beginning of the 19th century [46]. In 1867 the Swedish chemists Ohlosson and Norrbin developed the Ammoniakust explosive. In the beginning of the present century, explosive properties of AN, such as detonation intensity, impact and fire, exposure rate etc., were first reported [21].

AN is used by itself for more prone explosives in tandem with chemicals, or for admixture with stronger fuels and sensitizers such as nitroglycerin or TNT [48]. Amatol, ammonal and minols are some of the known military explosives that use AN. AN properties, such as density and porosity, must also be modified according to specification. AN should be dense and non-absorbent in order to achieve maximum strength per unit volume, and this should be achieved by achieving highest densityfor use in explosives sensitized by explosive ingredients [21].

AN are mainly used in the explosives and fertilizers field. Most ANs were consumed in high explosives before World War II. Instead, it grew significantly, consuming nearly 90% of output in 1975 [48] as a nitrogen fertilizer. It accounts for 24 percent of the world's nitrogen consumption as a straight fertilizer and also is found with many compositions and complex fertilizers such as calcium AN, ammonium sulphate nitrate, potassium AN, nitro magnesia, etc. Also, in fluid fertilizers is used with urea. As stated, the nitrogen in both plant types, ammonia and nitrate ion, are integrated into the AN fertilizer [21].

Areas include coal mining, metal extraction, non-metal mining and quarries are commonly use AN as an explosion. AN being an oxidizer has seen widespread use in formulations and propellants containing steam. Ellern provided some descriptions of these compositions [47]. It was used in the manufacture of nitrous oxide however in small quantities. Controlled heating of AN [21] produces nitrous oxide, which is primarily used as an anesthetic and an aerosol propellant for food products.

1.5 Metal-organic frameworks (MOFs)

Based on their intriguing and detailed molecular structures (Fig. 3), metal-organic frames are a new class of porous material and were attracted by great attention in catalyst, gas sturgeon and chemical sensors [22, 49–52]. Energetic OMFs an important category of materials, primarily using azole heterocycles and their compounds as ligands. They are an important form of materials. Significantly, combustion prducts are harmless, produce less smoke and are environment friendly with these nitrogen-rich ligands. Energy MOFs are a special type, owing to their unusual architectures, their high energy density ligands and the subsequent intriguing compositions that reveal their fuel capacity at high heat exposure. Therefore, MOFs may generate two-phase flow, because they have their porous structure [53-55], improving the reacting of gas flows to unburnt porous solides which help convective transportation and thus affect the efficiency of the composites. In addition, the energetic MOF components contain large amounts of gaseous element(s) (i.e. CHON elements), which make them conducive to gaseous prducting generation in combustion. Energetic MOFs are therefore suitable fuels

because they are eco-friendly fuels for burning, high thermal explosives and different molecular structures. While many energetic MOFs were synthesized [56,57] over the last several years, there has been no evidence of exploration of MOFs in compound energy materials [22].

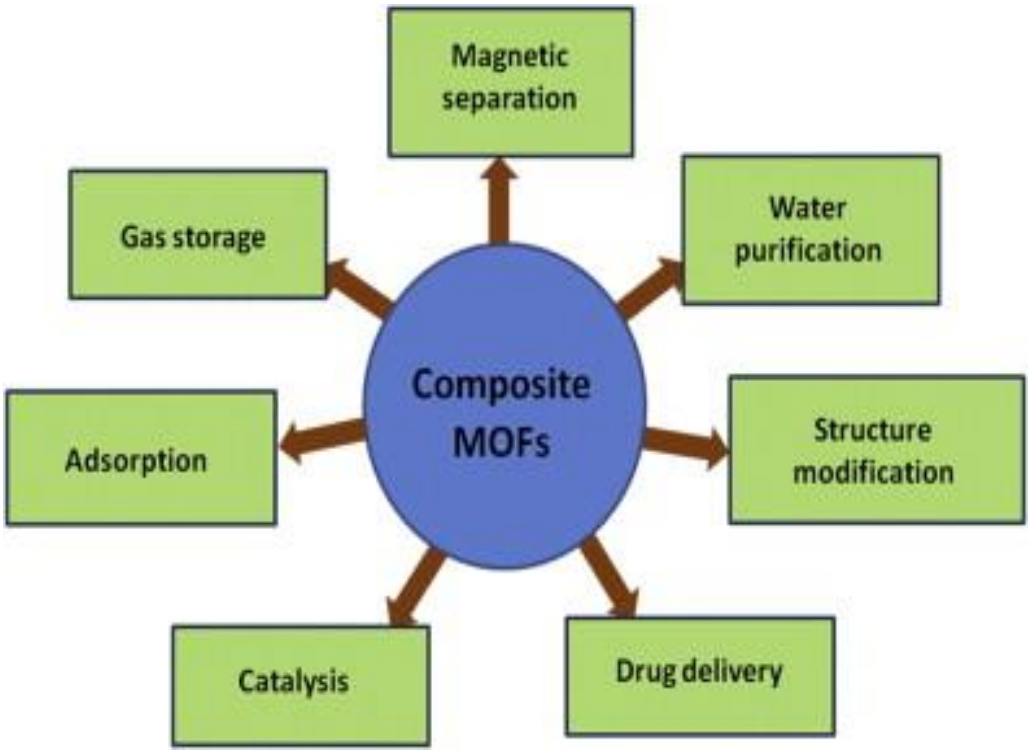

Figure 3 – The field application of metal organic frameworks [39]

In the work Hui Su etal.al [58], documented a novel form of composite energetic materials based on strong three-dimensional, energetic MOF ($[Cu(atrz)_3(NO_3)_2]_n$ (MOF(Cu), atrz=4,4-azo-1,2,4-triazole]). They chose the fuel of fuel MFO(Cu): (1) it is highly exposed to heat and has a high level of nitrogen (53.35%), which could improve the performance of gas production; (2) it is porous in nature, thus encouraging convective transport, and can promote the full combustion; (3) because the MOF(Cu) meets the needs for green material production, the high nitrogen content of its combustion goods is safe, smoke less and environmentally friendly. Period salts have also been used as an oxidizing agent despite their low toxicity and a high level of oxygen [22].

Due to its intriguing molecular topicology and potential applications in chemical separation and gas stockpiling, drug delivery, catalytic and chemical sensor technology, metal-organic frameworks have attracted considerable attention. In fact, due to its high densities and high exposure heat MOFs could also be potential energy resources. Thanks to its high surface characteristics and the possibility of changing its physical-chemical properties through the introduction of metal centers, the porous crystalline structure is attractive. But it is expensive and time consuming to manufacture such bulk polymers. In this context, it is interesting to find alternative methods for obtaining bulk materials, including structures based on graphene oxide

frameworks and carbon active substances. Multilayer graphens grow in popularity due to their special physical and chemical characteristics. The processing of activated carbon content from plant waste such as rice husk or walnut shell is a promising, easy and cost-effective method [59-61].

1.5.1 Method for preparation and synthesis of MOF

Fig. 4 provides a description of the different approaches for MOF planning. Many MOF syntheses are liquid-phase synthetic solutions, where a combination of solid salt and ligand in a reaction vial comprises different metal salt and ligand solutions, or solvent. A solver can be selected based on several factors, including reactivity, solubility, redox propensity, consistency constant etc. For these liquid-phase reactions. The thermodynamics, and activation energy for a specific reaction, are also characterised by solvents. In addition to liquid phase syntheses, researchers have also been trying to produce solid phase MOF syntheses, because it is quicker and easer, but the synthesis of solid states is continuously met with difficulties getting individual crystals and thus deciding the chemical structure. A common crystallizing process that has been used to produce MOF crystals during the last few decades has been the slow evaporation procedure. The method of slow evaporation is a constant crystallisation cycle used for the preparation of MOF crystals over the last decades [24].

While solvothermal methods are used in the routine synthesis of MOFs, alternatives to MOF synthesis have been implemented for additional methods, including micro-wave, electrochemical synthesis, mechanochemical syntheses, and sonochemical synthesesis.

The slow evaporation method. A conventional way of handling MOF's is by slow evaporation, which usually requires no external power source. Although this method is occasionally preferred because it is a room temperature process, it still takes more time than other well-known conventional methods. In the slow evaporation process, solvent slow evaporation at a fixed temperature, often room temperature, concentrates the solution of the original materials. Sometimes the process involves a solvent combination that can improve reactant solubility and making the cycle quicker by evaporating low boiling solvents faster [24].

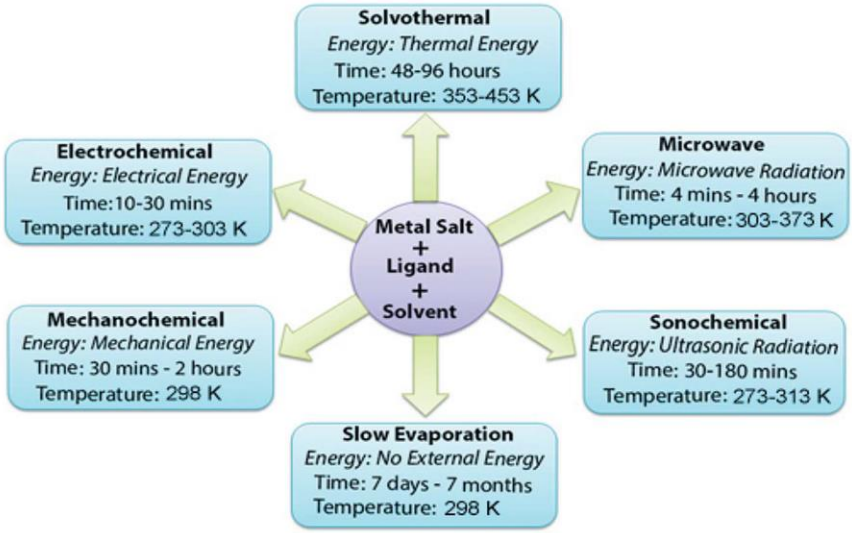

(*a*)

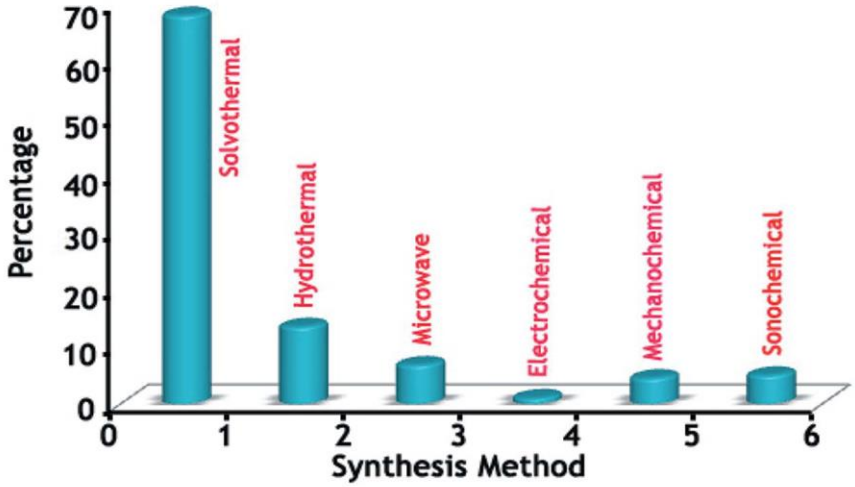

(*b*)

Figure 4 - (a) Synthesis conditions commonly used for MOF preparation; (b) indicative summary of the percentage of MOFs synthesized using the various preparation routes [24]

Solvothermal synthesis. In closed vessels under autogenous pressure over the boiling point of the solvent, solvothermal reactions are performed. In solvothermal conditions, many starting materials can undergo quite unexpected chemical changes, often accompanied by nanoscale morphologies which can not be achieved by conventional methods. In most cases solvothermal reactions have been conducted using high-boiling organic solvents. Dimethyl formamide, diethyl formamide, acetonitrile, acetone, ammonia, methanol etc are the most widely used industrial solvents. Solvent mixtures were also used to avoid differential solutions to the various starting materials. Based on the requirement for the reaction, solvothermal reactions may occur in different temperature ranges. Glass vials are typically used for low temperature reactions, whereas autoclaves filled with teflon allow reactions at temperatures greater than ~400 K. A huge number of inorganic compounds and

inorganic organic composite products have been successfully employed for synthesis [24].

Microwave-assisted synthesis. Synthesis aided by microwave gives a very fast synthesization process of MOFs. To order to produce nanosize metal oxides, widely utilizing microwave-assisted techniques have been used. Such methods include the heating of nanosize crystals with microwaves for about an hour. The process was alluded to as solvothermal microwave-assisted synthesis for the preparation of MOFs. In general, the consistency of the crystals produced from microwave processes is the same as that created from standard solvothermal processes, but synthesis is much faster [24].

Electrochemical synthesis. While it is possible to prepare broad MOF crystals under mild conditions by modifying the pH / solvent at room temperature for certain application and in order to produce large amounts of MOF samples rapidly, modern mild and rapid synthetic methods are continuing to be established and understood. As one such process, Electrochemical synthesis does not require metal salts and offers a continuous production in an industrial process of MOF crystals. The basic principle is that the metal ion can be released into mixtures of organic connector and electrolyte through anodic dissolution [24].

Mechanochemical synthesis. The method for MOFs is a mechanochemical synthesis, which is solvent-free. Mechanochemistry is the process by applying mechanical strength to perform a chemical reaction. Bonds are of considerable interest in modern synthetic chemistry through simple, economic and environmentally-friendly mechanochemical pathways. Mechanochemical syntheses for fast synthesis of liquid assisted grinding (LAG), which incorporates small amounts of solvent into a solid reaction mixture, have recently been employed effectively. Frissic and colleagues demonstrated that they could generate single-dimensional, bi-dimensional and 3-dimensional coordinating polymers of the same reaction mix by adjusting the added solvent in a LAG cycle. This strategy is further applied to synthesize certain zeolitic frameworks of imidazolates [24].

Sonochemical synthesis. Sonochemistry is a process through the use of intense ultrasonic radiation (20kHz–10MHz) that affects the molecules chemicalally. Extremely high temperatures and pressure causes chemical or physical changes attributable to the phase of cavitation, which required formation, through and an abrupt collapse of bubble in a liquid. Extreme conditions can promote chemical reactions by forming a crystallisation nuclei surplus immediately. In contrast to conventional hydrothermal procedures sonochemical techniques can generate homogeneous nuclear centers and a significant reduction in crystallization time. Synthesis MOF-5 with 1-methyl-2-pyrrolidinone (NMP) sonochemical irradiation will generate 5-25 mm crystals within 30 minutes close to those with solvothermal or microwave process synthesization MOF-5 [24].

1.5.2 New directions for metal–organic frameworks: fuels for «green» composites

Energetic materials are commonly used as a source of large amounts of hyperthermal gas components in micropropulses, mines, air bag systems, ammunitions and propellants. With increasing awareness of environmental and environmental concerns, a considerable effort has been made to find green composite compounds of the next generation which have excellent characteristics to fulfill the needs of their broad range of applications, but also to prevent deleterious components and components that comply with environmental protection requirements [22].

Based on its interesting molecular structures and broad uses in the fields of catalysis, gas storage and chemical sensors, MOFs (Metal-Organic Frameworks) are a new class of porous materials. Energy MOFs, a large category of these porous materials, primarily use azole heterocycles as ligands. Importantly, these nitrogen-rich ligands combustion product is innovative, produces less smoke and is ecologically friendly. Energy MOFs are unique due to the high-energy ligands and the subsequent intriguing structural motifs that arise from elevated detonation temperatures and demonstrate their ability as fuels. Furthermore MOFs can produce two-phase fluid due to their porous structure, enhancing the reaction between the gas flux and unburned pore solids that support convective transport, and therefore affect the performance of these composites. In addition, energy MOF compounds produce large quantities of gas elements (for example, CHON elements) that enable gaseous products to be produced during combustion. A environmentally-friendly combustion products, heat and different molecular frameworks make efficient MOFs suitable fuels, thus. Although several energetic MOFs have been synthesized over the last couple of years there have been no reports of exploratory MOFs in composite energy materials [22, 62].

In fact, due to their high density and high heat rates, MOFs could also be possible energetic products. For reference, in Hope-Week'sand co-workers' papers, the two hydrazine-perchlorate 1D MOFs[$(Ni(NH_2NH_2)_5(ClO_4)2)_n$(NHP) and the linear polymeric (CHP)] structure with thrombosis of detonation comparable to that of hexanitrohhexaazaisowutzitane (CL-20; approximately 1,5 $kcalg^{-1}$ is considered as perhaps the most effective metal-oriented energizing agent known to date). These coordination polymers were unfortunately highly sensitive to their impact, due to the low rigidity of such linear polymer structures. To decrease sensitivity the same writers also used a hydrazine-carboxylate derivative $(ClO_4)_2 \cdot H_2O$)n(CHHP), as well as $(Zn_2(N_2H_4)_3(N_2H_3CO_2)_2)(ClO_4)_2 \cdot H_2O$)n(CHHP) and $((ClO_4)_2 \cdot H_2O)n(ClO_4)_2 \cdot H_2O)n(ClO_4)_2 \cdot H_2O$), which showed a considerable decrease in sensitivity, but at the same time decreased their detonation heats [23].

Given these advancement, the current framework for teamwork remains restricted to a 1D or 2D layout. The 3D (Fig. 5) architectures have more dynamic communication modes compared with 1D linear and 2D structured systems, maximizing network stabilization and therefore increasing stability. Several 3D MOFs, some with a number of energetic motives like nitrate anions (NO_3(-)), and

perchlorate anions ($ClO_4(-)$) have been synthesized with significant magnetic, catalytical, and luminescents properties [23, 63].

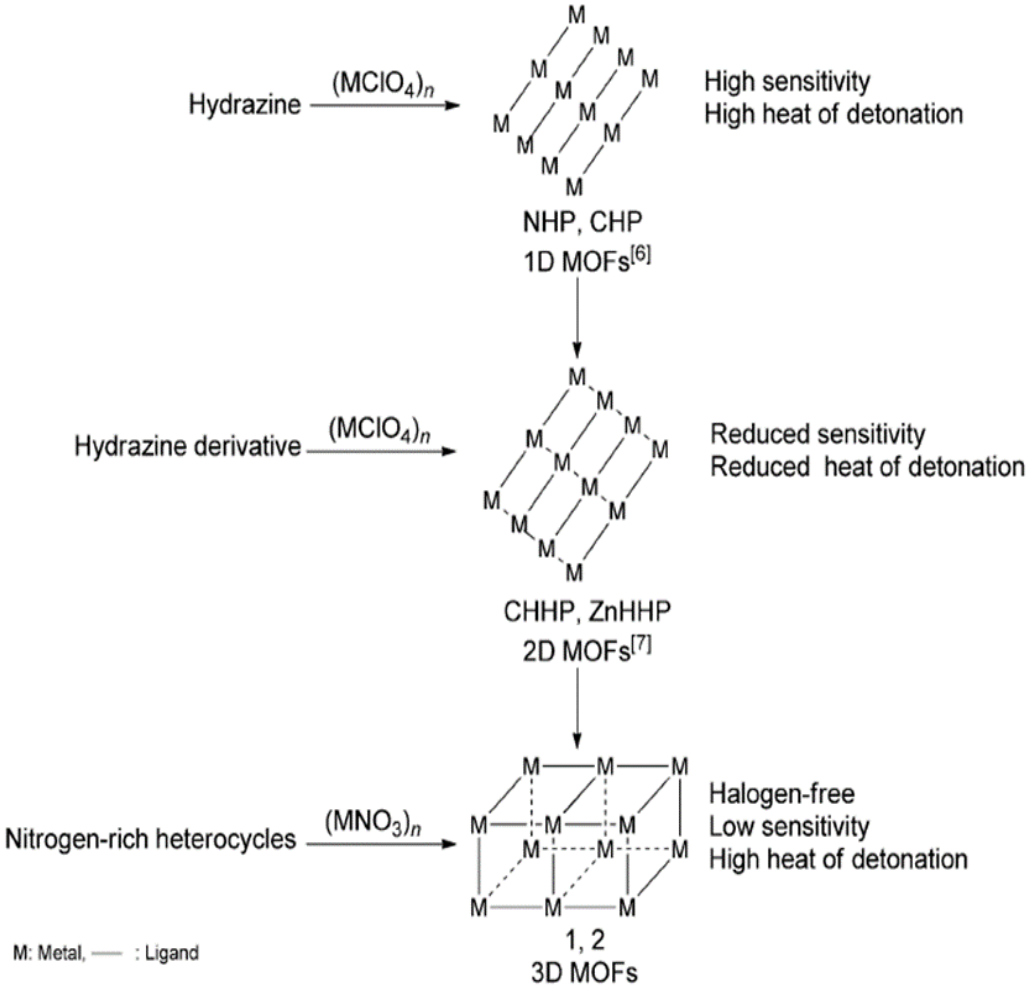

Figure 5 - Energetic MOFs with different topologies [63]

Nevertheless, the use of energetic materials when practicable was not revealed or discussed; the literature still lacks specific energy properties details. In fact, all 1D and 2D active perchlorate-based MOFs have been tested for thyroid dysfunction and teratogenic in the U.S. Environmental Protection Agency (EPA) [23].

1.6 Carbon containing materials

The beneficial properties of carbon-containing materials have been known since ancient times. Since the beginning of human development of fire, people began to use them as fuel for heating homes and cooking. The most previously known technological application of carbon dates back to many years, where charcoal was used to melt metal ores [64]. Later in China, the first powder, consisting of coal, appeared, which gave a start to the beginning of a new era in the military and mining. Carbon has many types and allotropic forms, from graphite, graphene oxide to fullerenes and nanotubes, each of which is distinguished by its uniqueness and structure. Carbon is one of the well-known technological additives that are

incorporated into the composition of energy materials to ensure their energy intensity. In the aerospace industry, carbonaceous materials are often used in the composition of solid fuels to improve the characteristics of combustion and reduce thermal radiation inside the grain. For example, charcoal, which is an integral component of the earliest known chemical explosive, gunpowder, has been extensively studied for use as a modifier of the burning rate of chemical rocket fuels [64-66].

1.6.1 Graphene oxide frameworks

Due to its unmatched properties and various applications, the study of carbon nanostructures is very extensive. Graphene is one of the most widely talked about among the various species of carbon because of the remarkably excellent properties of it in the present era [67,68]. The use of powerful oxidizing substances to produce graphene oxide (GO), a nonconductive hydrographic carbon content, is an important factor for graphite syntheses, and one of the most common solutions to graphite exfoliation. For bulk graphene synthesis, chemical medications are a practical approach. While GO is hard to determine its exact composition, it is obvious that GO interferes with epoxide, alcohol, ketone and carboxylic groups as previously contagious aromatic lattice. The low cost, easy access and widely available graphic conversion capable of GO is of great interest. Flake graphite is the most common source of graphite. Smooth graphite is a stone that is naturally produced and extracted through heteroatomic degradation.

In 1859 Brodie first revealed GO synthesis by applying potassium chlorate in the nitric acid bowl to slurry graphite. By using a combination of sulfuric acid and fuming sulfuric acid, Staudenmaier strengthened this technique in 1898 with a progressive introduction of chlorates in the reaction blend. A minor change in the method allowed for the development of heavily oxidized GOs with a single and updated procedure. Hummers documented the use of $KMnO_4$ and $NaNO_3$ in condensed H_2SO_4 in 1958 as an alternative method for the synthesis of graphemium oxide. This approach could be used to create massive graphic films with GO [69-71].

GO is mainly synthetic in two stages: graphite oxidation and graphite oxide exfoliation, as shown in Fig. 6.

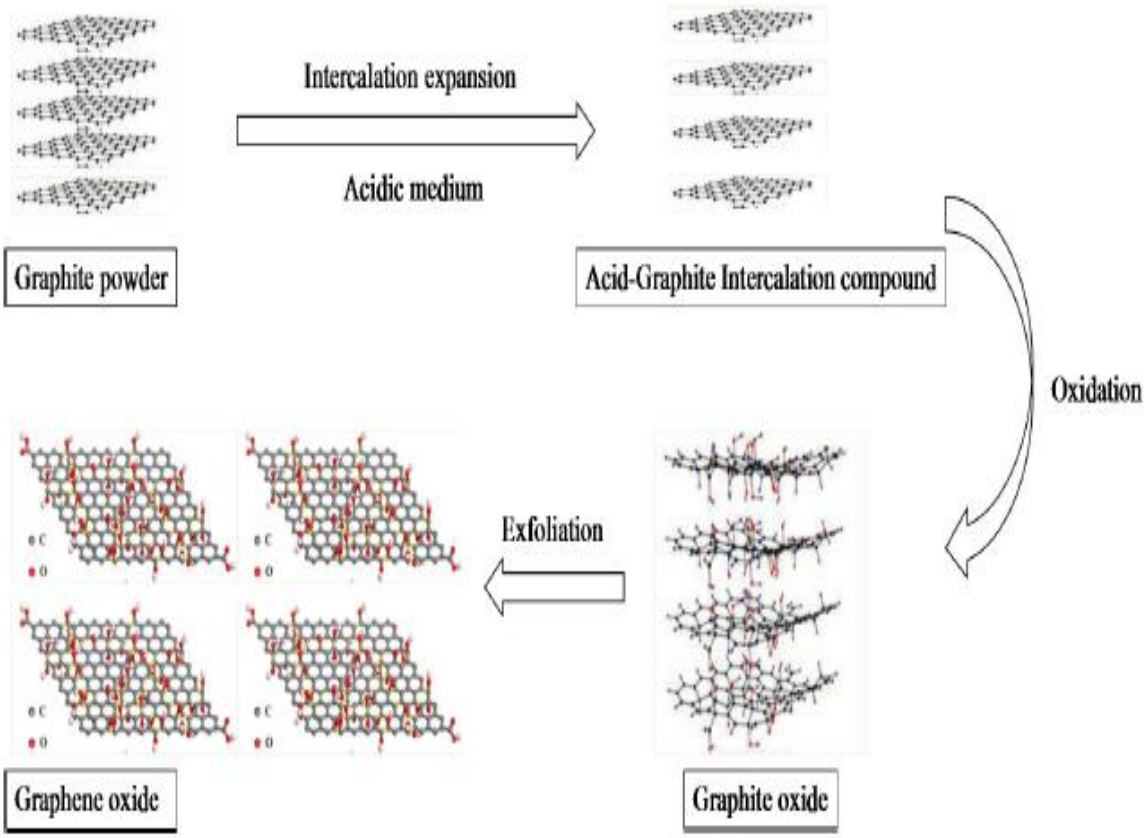

Figure 6 - Schematic description of the process of GO preparing [69]

2D-layered nanomaterials of graphene oxide (GO)-and reduced GO (rGO) were reported to be energentic and exothermic for heating [72]. These nanomaterials could be used to bind various crystalline EMs, including 1,2-dinitroethene-1,1-diamine and 1,3,5,7-tetrazocane (HMX) nitro-cellulose (NC). Either these EMs can be deposited on the GO surface or they can be covered with thin layers of GO [73]. A decrease of the intensity of these EMs would be attempted by depositing various energy compounds on the surfaces of nanosheet GO orrGO (or intercalation of nanosheets). As energy ingredients or combustion catalysts, the resulting composite EMs can often be used as solid propellants. Nearly all energetic nanomaterials and composites based on GO andrGO have been reported in the past few years [25].

In relation to the stability of primary explosives, the use of small quantities of graphene as an intermediate can be used to desensitiz high-energy propellants of high explosive strong charge. GO and rGO will significantly increase hypergolic ionic liquids (EILs) inflammation and burning properties. GO (or rGO), for example, can be a lubricant that can significantly improve hypergolic EIL's low temperature efficiency by growing their viscosity [74]. It was considered in practice very necessary for the optimum performance that the kind of graphene derivative was tailored to a certain ionic-liquid functionality [25].

1.6.2 Activated carbons as a technological additive in fuel mixtures

Activated carbons have unique properties in the form of high specific surface and adsorption capacity of gases and liquids. The total global production of AC is approximately 1.5-2 million tons per year [75,76].

Activated carbons are an amorphous form of carbon with a very high specific surface area and a developed porous structure (Fig. 7). Due to the high degree of micro porosity, they have a low density and are visualized as solid foam or powders with a relatively small bulk structure. Its chemical structure and high specific area make it possible to obtain adsorption or chemical reactions with organic materials and other non-polar compounds in the gas or liquid phase.

One of the important advantages of activated carbon is low cost. Activated carbon is a product of the processing of carbon-containing materials, widely distributed on the planet in the form of plant waste, by carbonization and demineralization of organic content.

There are two main methods of carbon activation: physical and chemical activation [77]. Physical activation is accomplished through the use of oxygen, carbon dioxide or water. When chemical activation of raw materials used highly active chemicals. Typically, the chemicals used to activate coal are acids, strong bases, and salts [78]. Basically, phosphoric acid, potassium hydroxide, sodium hydroxide, calcium chloride, zinc chloride, etc. are used as activators. The most commonly used industrial process is the chemical activation of peat, coal, bark, lignite, wood and plant materials, such as almond shell, coconut shells, rice hulls, etc.

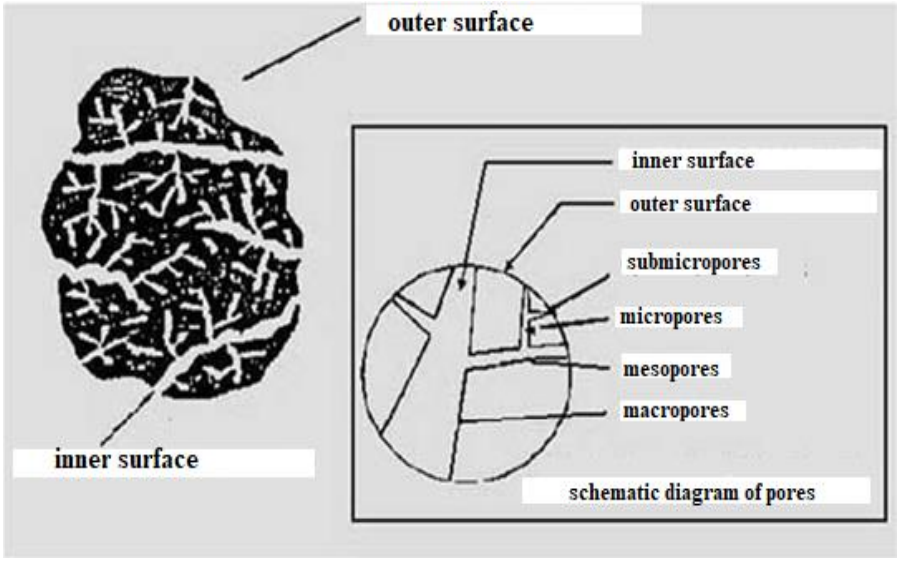

Figure 7 - Pore Size Classification (activated carbon) [79]

Activated carbon has a unique porous structure (Fig. 7), chemical activity compared with other forms of carbon and a large specific surface area, which are responsible for the effectiveness of the adsorption capacity of numerous substances [79]. The formation of the porous structure of activated carbon is achieved as a result of the oxidation of carbon-containing raw materials during the interaction of activating agents at constant high temperatures. During thermal carbonization of the

source material with chemical activating agents, as a result of burning out the organic part, the volume of existing pores increases and new pores form.

Activated carbon with a porous structure can be divided into three main groups:

- Macropores - Pores with a length of more than 50 nm;
- Mesopores - Pores with a diameter from 2 to 50 nm;
- Micropores - Pores with a diameter of less than 2 nm.

The pore size of activated carbons can range from 1000 to 0.0002 microns. Therefore, they have a wide pore size distribution.

The use of activated carbons (AC) as a technological additive to modify the burning rate of energetic materials is mainly investigated in two directions: the composition of metallized fuels and non-metallized fuels [80].

At present, quite a lot of unique physicochemical properties of activated carbon have been observed and disclosed. For example, the use of AC in the composition of non-metallized fuels becomes a very relevant subject of study in the field of combustion of energy materials. Published work on the positive effect of AC on the combustion process of composite fuels [81].

In work [82], it was noticed that the presence of activated charcoal in the composition of aluminum-containing solid fuels is an effective modifier for the burning rate. Later, on the basis of experimental results carried out in [83], it was shown that activated carbon has a good prospect for use as a potential modifier of burning rate for most non-metallized solid fuels. It was shown that the addition of a small amount (0.4%) of activated charcoal significantly increases the burning rate of aluminized composite fuels. Activated carbon together with transition metals and their oxides (Fe_2O_3) exhibit a synergistic effect and increase the burning rate by about five times to 54 mm/s at 70 atmospheres of initial pressure in comparison with the basic composition (11 mm/s at 70 atm.). These high burning rates were also accompanied by a higher burning pressure index (n).

Later works [84] reported a noticeable increase in the burning rate of aluminized composite fuels when activated charcoal was added in a mixture with copper chromite, but the burning rate was still comparatively lower with compositions where iron oxides were used [82]. It was also noted in work [83] that the burning rate of AC compositions is affected differently depending on the time of the experiments. This confusion was associated with a high absorption capacity of moisture from the environment. As it turned out, humidity can play a role in increasing the burning rate in composite solid fuels.

Removing the metal component from the fuel composition makes it possible to focus in more detail on the thermal effect of the reaction, thereby reducing the complexity of decoding the mechanism of fuel decomposition. Since in the military industry, non-metallized carbon-containing EM compositions are most often used to reduce the thermal signature (visibility in the thermal range). Thus, we can conclude that the introduction of even very low concentrations of activated carbon can affect the nature of the combustion of fuel systems. The goal was a more detailed study of the mechanism by which AC affects the combustion characteristics.

1.7 Setting tasks and objectives

In a number of previous works, the effect of metal oxide carbon material on the combustion characteristics of fuels was studied in detail. However, recently new allotropic carbon modifications have been obtained with unique properties: CNTs, graphenes, activated carbon, fullerenes. The study of their influence on combustion parameters as a technological additive to high-energy fuels has gained relevance over the past decade. Also, the mechanism of the influence of carbon on the combustion characteristics of high-energy fuels is not completely clear. The results published to date describe only the final outcome of the effect of carbon on the combustion characteristic of EM.

Based on the foregoing, the objectives of this work are:

1. To develop and create a metal-organic frame structure (MOF) based on waste plant materials and metal oxide nanoparticles;
2. To study the kinetics of thermal decomposition of a pyrotechnic composition based on ammonium nitrate in the presence of a metal-organic frame structure (MOF) with various metal oxides;
3. To determine the effect of a metal-organic frame structure (MOF) with various nanoparticles of metal oxides on the combustion conditions of pyrotechnic compositions at initial pressures from 1 to 3.5 MPa;
4. To study the possibilities of initiating the combustion process of a pyrotechnic composition by laser radiation with the addition of a metal-organic frame structure (MOF);
5. Determine the effect of the metal-organic frame structure (MOF) on the activation energy of the pyrotechnic composition AN/Mg/NC.

2 EXPERIMENTAL PART

2.1 Materials and initial reagents

In this work, the following reagents were selected as the main starting components:

- Activated CRH was obtained in the Laboratory of Functional Nanomaterials of the Institute of Combustion Problems, Almaty, Kazakhstan. Carbon has a high specific surface area around 3186 m^2/g and obtained from the carbonization of rice husk by the high– temperature pyrolysis in argon atmosphere followed by chemical activation with potassium hydroxide (KOH) at a temperature of 900°C around 40 min;

- AN was used as an oxidizer in the condensed mixture with a diameter of particles between 30-40 μm. AN (NH_4NO_3) from a commercially market with purity around ≥99% (without further purification). It was mechanical treated by planetary mill (15 min) and dried in own to remove water content;

- Magnesium powder (Mg) was used as a high energetic fuel with partial diameter around 30-40 μм and ≥ 99% purity. Melting point ~650°C and density 1.74 g/ml at 25°C (Sigma Aldrich);

- Copper oxide (and nickel oxide) black color powder with a purity of at least 99,7% (Sigma-Aldrich), acted as a catalyst mechanically included on the surface of activated CRH by the mechanical method in the planetary mill (10 min) [85,86]. The diameter of the basic metal oxide particles was in 50 nm range. Deposition of particles on the surface of activated CRH;

- A polymer used as an efficient binder was nitrocellulose (NC). It is a core component in missiles, flares, bombs, explosive mines, etc., that are widely distributed. The NC (12.6% N) used as a 5% ethanol solution (purity rating 96%) was given in study [17].

2.2 Obtaining of activated carbon with a high specific surface

Carbon materials from RH was obtained by crushing, pre-carbonation, desilication (for rice husks) and their chemical activation, respectively (Fig. 8).

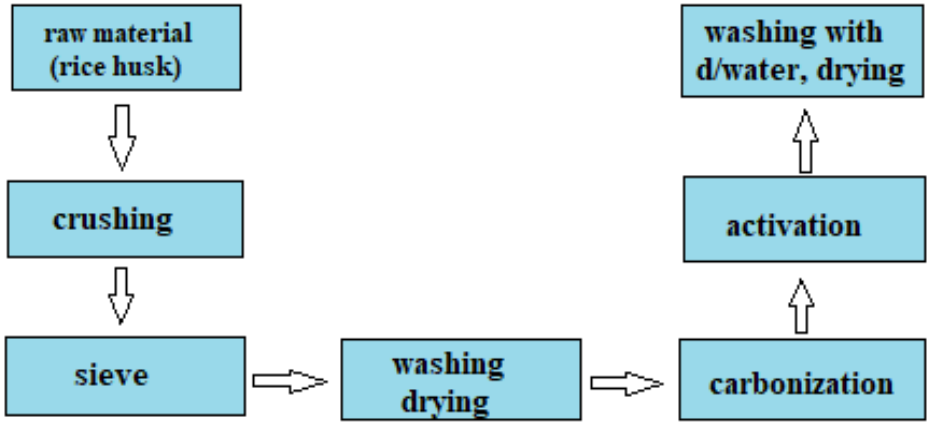

Figure 8 - Illustration of the process of obtaining activated carbon (graphene layers)

RH was washed several times with distilled water to remove impurities, and dried at 110°C for 1 h. The method of preliminary carbonization of RH was performed in an iron reactor at a temperature of 250-500°C with a heating rate of 10°C/min at a rate of supply of argon ~5 cm^3/min, dwell time 60 min. The obtained RH samples were desilicated in 1 M KOH solution and heated to 80°C for 3 h to remove SiO_2. After that, the sorbent was washed with distilled water to a neutral environment, by repeated boiling and decantation. The sorbent was dried for 2 hours at 1100°C, weighed, and the product yield was determined. Then the dried samples were mixed with crushed KOH in a ratio of 1:5 and warmed to melt KOH. The mixture was transferred to a stainless-steel reactor and activated at 850°C for 2 hours. After activation, the obtained samples were washed several times with distilled water by the above method. Fig. 9 shows a schematic diagram of the carbonization and activation system.

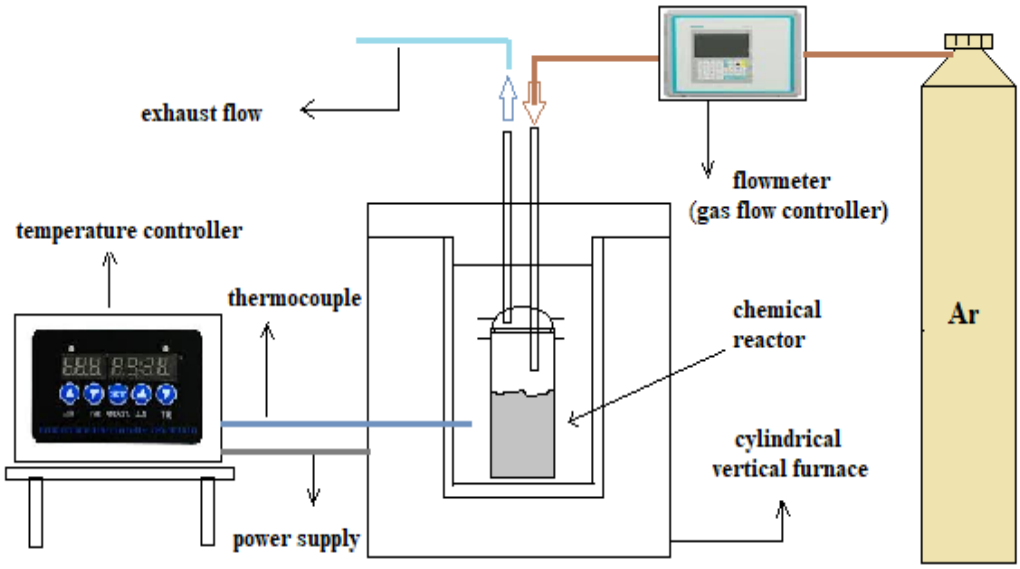

Figure 9 - Schematic diagram of the system of carbonization and activation

2.3 Physical and chemical research methods

2.3.1 The method of low-temperature nitrogen adsorption

Information on the texture of samples of activated carbon based on rice husk was obtained by low-temperature nitrogen adsorption on a SORBTOMETR device designed to determine the total specific surface area of meso and macroporous substances and materials by thermal desorption of an adsorbate gas by the BET method in accordance with State Standard 23401-90.

In sub-critical adsorption of adsorbates, their molecules are adsorbed on a solid surface, such as lamination process, and when the pressure is sufficiently large (about 0.1 relative pressure) is formed by several layers. Browner, Emmett, and Teller developed a theory to explain this multilayer adsorption. The field of applicability of this theory is approximately in the range of 0.05 and 0.35. The BET equation is still the most important equation for characterizing mesoporous solids, mainly because of its simplicity. The BET theory is based on the kinetic model of the adsorption process advanced by Langmuir, that is, the surface is energetically

uniform (the adsorption energy does not change during adsorption in the same layer) and there is no interaction between adsorbed molecules.

2.3.2 Scanning electron microscopy and energy dispersive analysis

The surface morphology of the obtained samples was studied using a QUANTA 3D 200i microscope (FEI, USA) with an accelerating voltage of 30 kV. A local analysis of the chemical composition of the sample was carried out on a microscope equipped with an EDAX energy dispersive X-ray spectrometer and equipped with a semiconductor detector with an energy resolution of 128 eV (polymer, window d = 0.3 mm).

2.3.3 X-ray phase analysis

An investigation of the X-ray process was carried out using cobalt K_a radiati, and the capper K_a radiation in the range 2θ=10°-70°. In this situation the analyser was treated with a DRON-4 M diffractometer. Determine the extending of the X-ray lines, the associated value of the crystallites of the substance and the deformation of crystal grid, the additive X-ray photos were taken from the low speed of 1-2 deg/min in the range of 40 to 800 q. Its values are defined as the width, measured in degrees, of the x-ray line at half height.According to the results of measuring the line width of quartz for an interplanar distance of 1.98 Å, where there is no influence of the preferred direction, the crystallite sizes (L) were calculated with an accuracy of ± (8-10%).

2.3.4 Adsorption studies of methylene blue

Model solutions with the necessary dye concentrations were prepared by successive dilution of the initial solution with a concentration of 1500 mg/dm^3. A sample of 0.1 ± 0.001 g of coal ground in an agate mortar was transferred into a glass container with a capacity of 50 ml, 25 ml of MB solution was added, covered with a Petri dish and stirred for 20 minutes on a magnetic stirrer. The carbon suspension was transferred into tubes and centrifuged for 15 minutes. 5 ml of clarified solution was taken to measure the optical density, in cuvettes with a distance between the working faces of 10 mm on a photoelectric colorimeter using a blue light filter. Using the optical density value, using the calibration curve, the residual of MB concentration was calculated in the solution. Based on the results of MB sorption on a carbon material, the values of equilibrium adsorption ability were calculated by the formula:

$$X = \frac{0{,}025 \cdot (C_1 - C_2 \cdot K)}{m} \cdot 0{,}025 \qquad (1)$$

where, C_1 - is the concentration of the initial dye solution, (1500 mg/dm^3)

C_2 - concentration of the solution after contacting with coal, mg/dm^3

K - is the dilution coefficient of the solution taken for analysis after contacting with the carbon material (the solution was diluted 10 times), K = 10

m - is the mass of a sample of activated carbon, g (≈0.1 g)

0,025 - the volume of a solution of methylene blue, taken for clarification, dm^3 [87].

2.4 Determination of particle size by method Scirocco Malvern Mastersizer 2000

To determine the particle size after mechanochemical activation and after burning solid fuels, the dry measurement method Malvern Mastersizer 2000 was used. A typical system with the main modules: an optical unit, a unit for dry and liquid samples, and a computer system. The optical unit is used to collect the source data, which is used to measure the particle size in the sample. The purpose of the unit is to prepare a sample and deliver them to the optical unit so that the measurement passes. Malvern Mastersizer can process various types of dispersion, including dry powders, as well as samples ground in a liquid. A computer system is a stand-alone computer that runs Malvern software. The software controls the optical unit and the powder collection units, and also analyzes the raw data from the optical unit to determine the particle size [88].

2.5 Synthesis of metal organic frameworks

A number of factors should be addressed during the synthesis of metal–organic frameworks. In the phase of synthesizing, for example, solvents and their quantities play an important role. Experimental design has established optimal conditions for the synthesis MOF (Fig. 10,11). Activated carbon and copper oxide have therefore been dissolved in pure methanol solvent for synthesis of MOF first. The mixed solution was then processed into a Teflon-lined autoclave and heated for 24 hours at 105°C to create a MOF like cubic crystals, after ample ripple at ambient temperature and dark-black precipitation was produced. We will remember that heating gradually breaks down the mixed solution and leads to the organic ligand decongestion. The dark-black crystals were repeatedly washed with methanol and anhydrous chloroformed during 72 hours followed with filtration on the reaction container wall. The resulting solid product was finally dried at 120°C under vacuum for 8 hours.

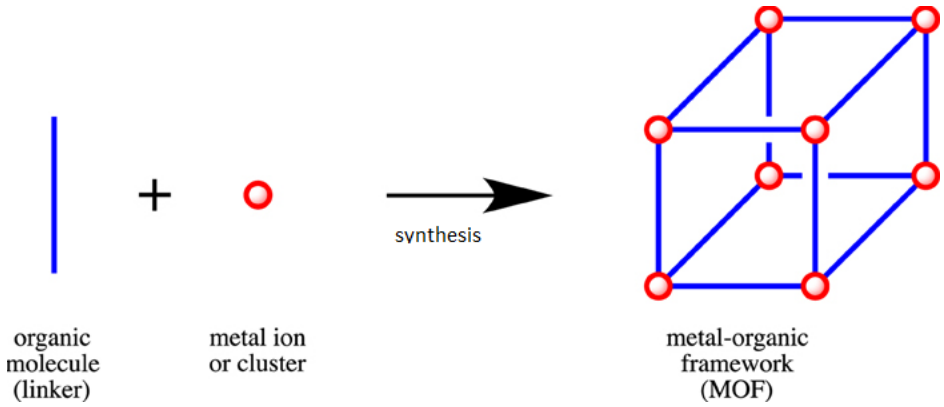

Figure 10 – Synthesis of MOF structure [116]

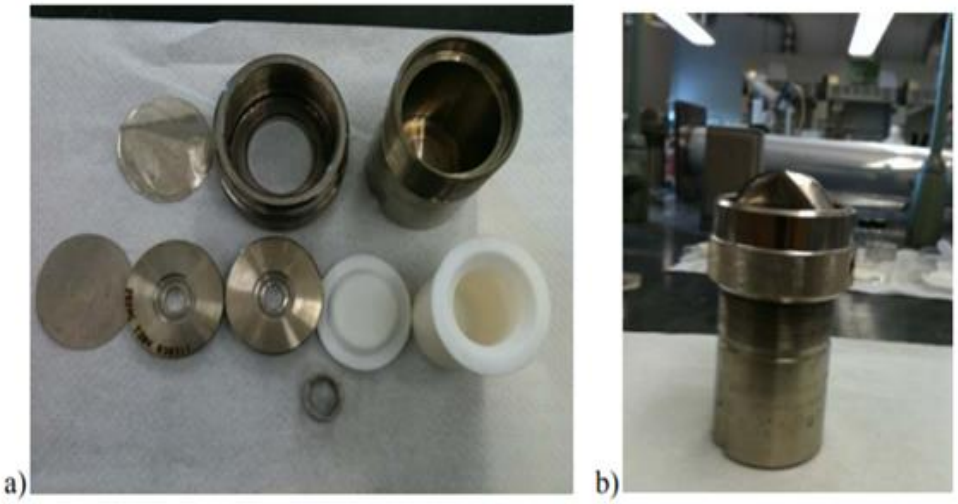

Figure 11 - (a) The parts of the autoclaves, (b) the entire setup the autoclave

2.6 Samples preparation for high-pressure chamber studying of burning rate

Activated CRH was obtained in the Laboratory of Functional Nanomaterials of the Institute of Combustion Problems, Almaty, Kazakhstan. In the planetary millet, the manually extracted nitrate (15 min) of ammonium (purity 99%) was carried out. In the design mixture with a diameter of 30-40 μm, ammonium nitrate was used as an oxidizer. As a source, magnesium (Mg) and a diameter of 30-40 μм were used. It was 50 nm in diameter and served as catalyst for the metal oxide pieces. Cellulose nitrate has been used as a binder. The diameter of compositions is 6 mm and the length is 10 mm. The compositions were in following ratios: AN/Mg/NC – 75/24.7/0.3; AN/Mg/NC/CRH – 75/21.8/0.3/2.9 and AN/Mg/NC/CRH-Me_xO_y – 75/21.7/0.3/3. All samples were pressed in a press form (Fig. 12,13).

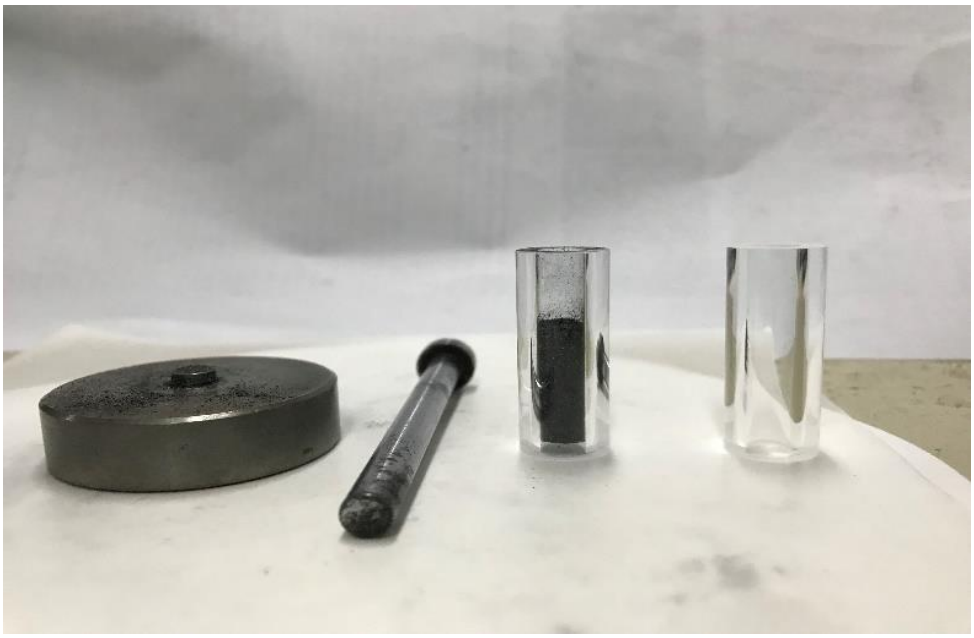

Figure 12 - Samples for research in solid form

Figure 13 – Pressed samples on a hydraulic press mold for research

2.7 The method of studying the linear burning rate

The combustion cycle was studied in the combustion chamber under nitrogen gas pressure. The nichrome wire inflamed the sample. The initial pressure from 1 to 3.5 MPa is added to each sample. The combustion chamber has a glass window that allows a high-speed video camera (MotionXtraHG-100 K) to display and film the burning process with a duration approaching 1000fps, with a resolution of 1504×1128pixels.

The linear burn rate is a significant ballistic feature of the energy materials and the captured high-speed camera videos were used for calculating the burning intensity. This system facilitates the monitoring in a dynamic mode of the combustion speed of the sample from the start to the full combustion stage. The linear regression rate in mm/s^{-1} was reported. Accuracy of calculation was roughly ±0.01 mm. Both tests have been replicated three times and the overall burn rate is calculated. The practical work machinery is shown in Fig. 14 [17].

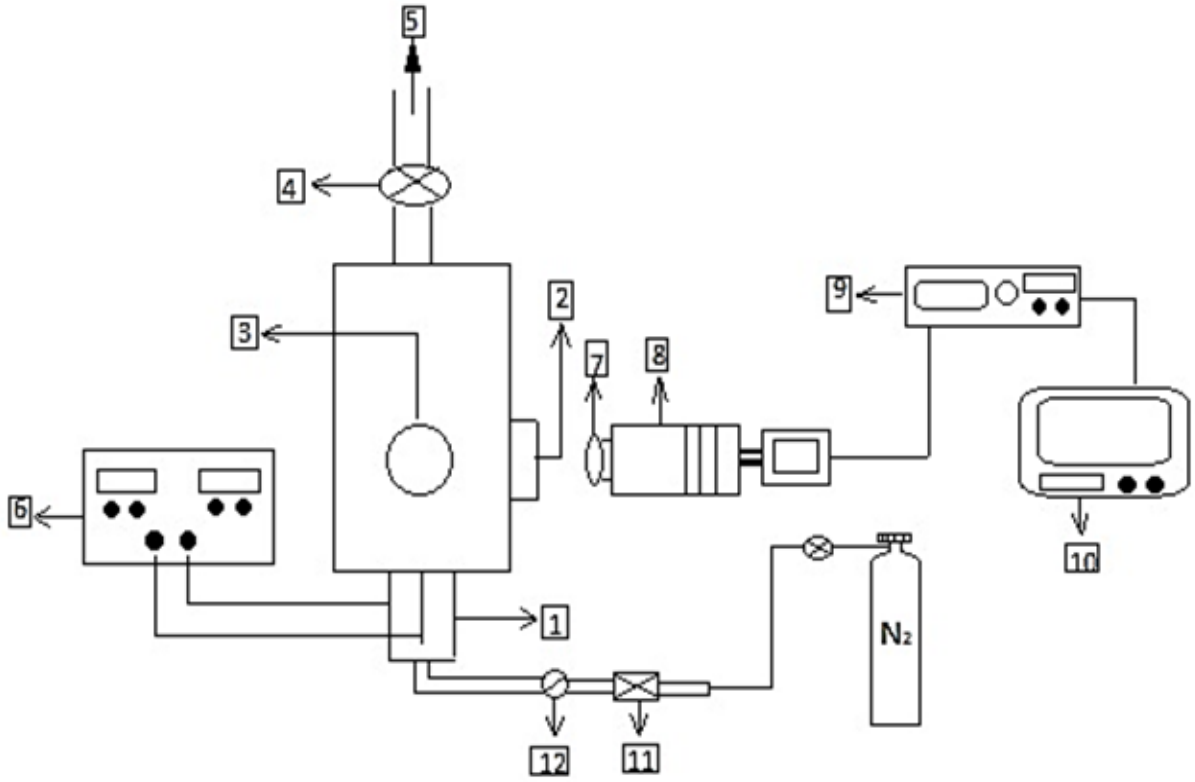

Figure 14 - Scheme of the combustion chamber under pressure: 1 – sample holder; 2 – window to capture of a video; 3 – window for the light source; 4 – exit valve; 5 – exhaust line (combustion gas); 6 – power supply; 7 – lens; 8 – high–speed video camera; 9 – video recorder; 10 – PC (monitor); 11 – pressure manager; 12 – pressure gauge

Burning rate is strongly affected by the value of initial pressure. The pressure dependence on linear burn rate is described by the Saint Robert's Law expression (Vieille's Law):

$$r_b(\text{mm/s}^{-1}) = r_0 + a[P(\text{MPa})]^n \quad (2)$$

where r_b is the linear burn rate, r_0 is constant (initial burning rate), a is the burn rate coefficient, n is pressure exponent. The values of a and n are analytical concepts and can not be anticipated logically. This term tends to compare the linear burning intensity with the pressure value in a number of operating conditions for an application [17, 89].

To calculate the burning rate, the samples were placed on a strand burner (Fig. 15) which is equipped with an igniter and parallel contacts for measuring linear rate. The strand burner is a removable part of the high-pressure chamber (Fig. 16).

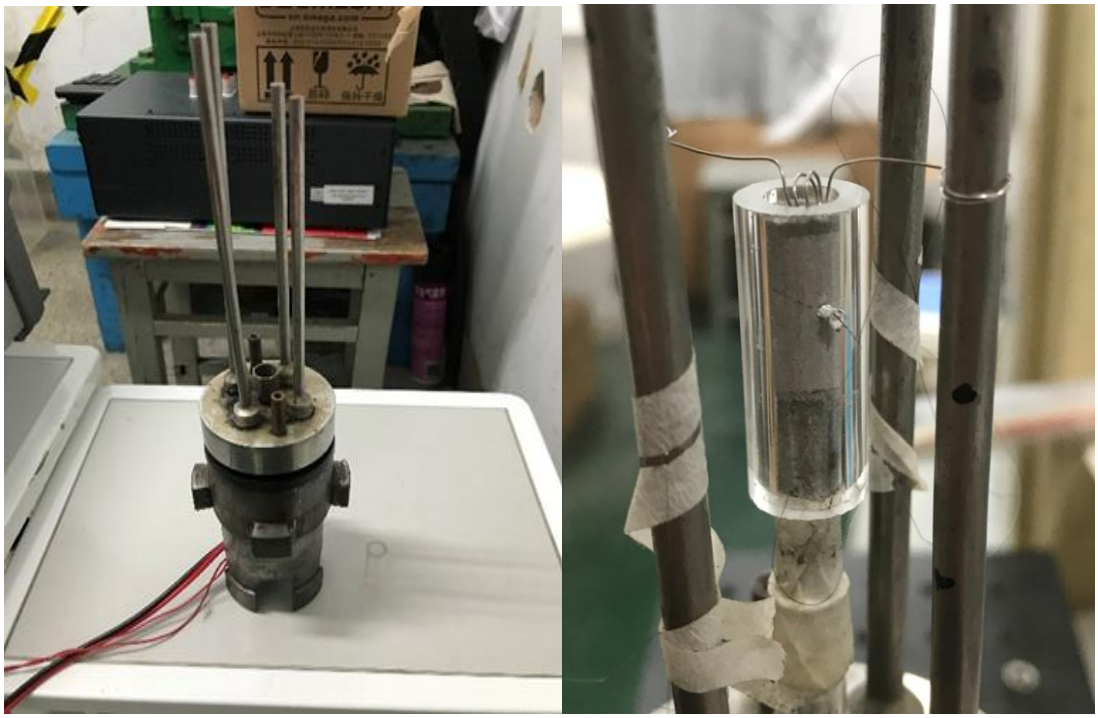

Figure 15 – Strand burner

Figure 16 - High-pressure chamber

Combustion of the samples was initiated using a nichrome wire, which was heated by applying current when the required level of excess pressure was reached. The accuracy of the pressure sensor is ± 0.5% FSO (Full Scale Output), equal to 0.077 MPa.

2.8 Methods for determination of thermal characteristics

2.8.1 Differential thermal analysis

The differential thermal research (Fig. 17) performed kinetic study. A mass loss versus temperature map for the defined temperature range (up to 2000°C) is given by the thermogravimetric analysis (TGA). This method for evaluating the failure of volatile materials or thermo-stability is used extensively in material research, inorganic chemistry, fuel and geology and can also be used to detect explosives. Experiments may typically be performed using a temperature ramp of 5-10°C min^{-1} in inert areas such as nitrogen or in the oxidizing environment to test oxidative decomposition in the thermal stability or variability. In case of mass losses, the TGA method will give quantitative data on the path of a decomposition, and if the losses are in discrete stages. The TGA can also be operated in an isothermal mode, where the weight loss rate is measured at a fixed temperature. This form of analysis can be used to estimate unpredictable failure levels or substance degradation rates [20].

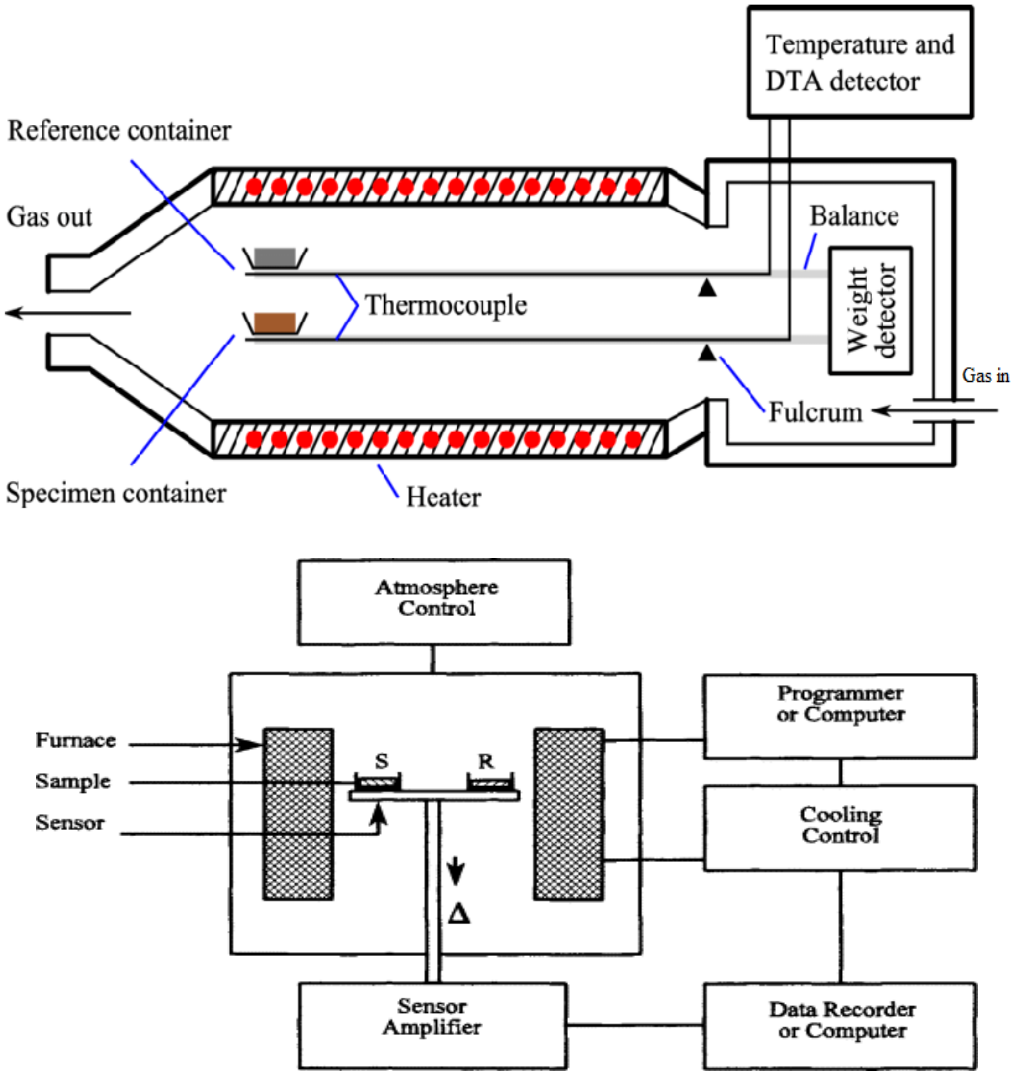

Figure 17 – The scheme of the differential thermal analyzer (DTA-TG)

This technique defines a general TGA experiment whose measurements different from this method are specified: TGA analysis was performed on the open Al_2O_3 cranks with a thermogravimetric analyzer of 30°C at a pace of 5°C min^{-1}, at a sample weight of ~1−5 mg. The samples had been dried in vacuum for 24 hours at 40°C for the moisture reduction, as far as practicable [20].

2.8.2 Differential scanning calorimetry analysis

The average exthermic state of the measured compositional behavior can be assessed by a differential calorimetric scan (DSC) and it may lead to the estimation of possible reactive risks. A sample and a comparison in a DSC are continuously lifted and heat is applied to the reference to retain it as a sample at the temperature. The incorporation of heat makes up for the missing or regained heat as a consequence of an average endothermic or exothermic reaction. When the heat production (Watts) in the sample reaches a certain amount, the samples heat supply is cut off, which is due to the exothermic behavior within the sample [20].

It depends on the quality of the instrument in question. A peak in DSC thermal is observed in the case of an exothermic (endothermic) reaction. The initial heating mode constructs the base line, and the exotherm is drawn to coincide with the initial increase. At the intersection of the two lines the temperature is called the initial temperature of a chemical reaction which corresponds to a detectable level of heat. The energy released(-ΔH) was calculated as the area under the heat (Watts) and the time curve during the process. DSC is a popular screening tool, because it is safe because it includes a small quantity of samples (less than 1 mg of energy material is suitable). Fig. 18 shows the general configuration of DSC facilities.

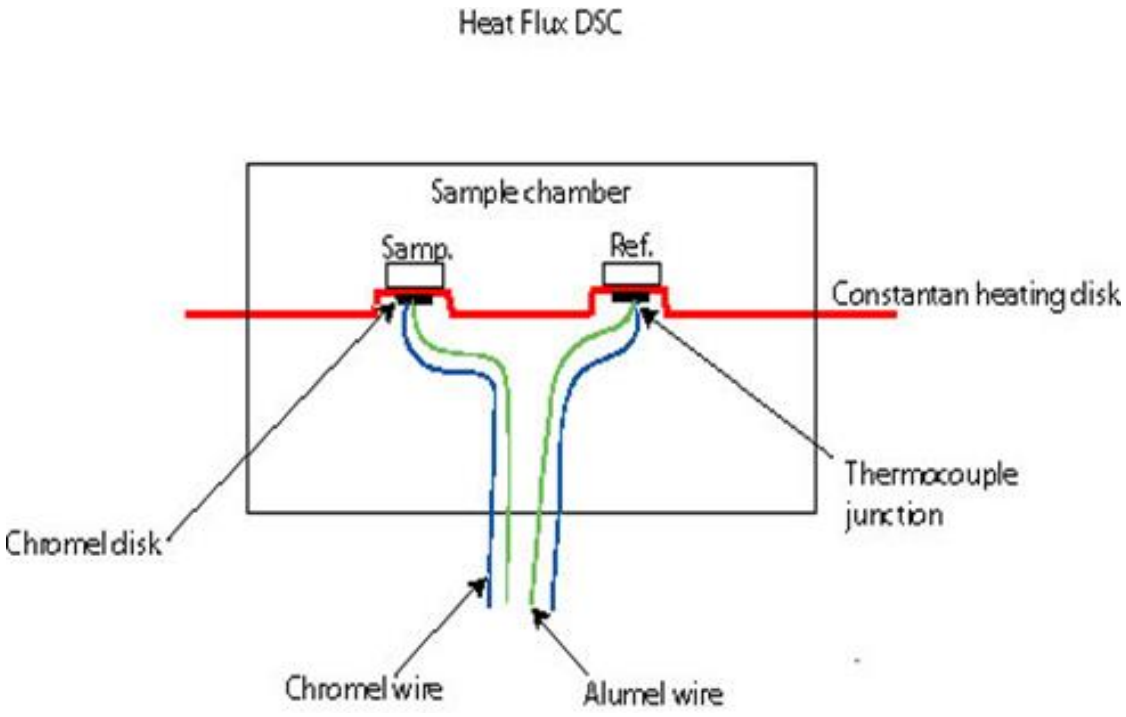

Figure 18 – The scheme of the differential scanning calorimetry (DSC)

2.9 Determination of activation energy

Exothermic kinetics are critical to determine the ability of thermal explosion materials and systems. For eg, these parameters are accessible from DSC-determined starting temperature (T_{onset}), which implies a chemical reaction rate. The initial temperature detected is therefore a measure of the kinetics of the reaction. There has been extensive consideration of such interpretation [80], and we agreed in compliance with ASTM Protocol E 698-99 to use the Standard Test Method to test parameters including activation energy (E_a), for Arrhenius Kinetic Constants for thermally unstable substance from the U.S. Society for Testing and Materials (ASTM) [91]. The study of Ozawa [92] and Kissinger [83] offers the theoretical context of this technique [20].

In the kinetics of thermal decomposition, the activation energy is important and the Kissinger approach is evaluated by the DSC analysis. This approach is widely used and involves no detailed model of reaction. The activation energy (E_a) is derived from the total physical energy and the cumulative amount of energy from the initiation of the chemical reaction, with some researchers operating with Kissinger approach to analyze the energy from the composite rocket and solid high energy materials [94,95].

According to the Kissinger method, E_a is expressed by the following equation:

$$\frac{E_a}{R} = \frac{dln(\beta T_p^{-2})}{dT_p^{-1}} \quad (3)$$

where T_p - is the peak temperature of the DTA curve. E_a - can be calculated from the slope of the plot of $ln(\beta T_p^{-2})$ against T_p^{-1}. E_a can be expected to vary when T_p on the DSC curve changes with the addition of the catalyst.

Professor Ozawa suggested that the degree of reaction is a constant value independent of the heating rate. Thus, proposing the following formula:

$$ln(\beta) = const - 1.052(-\frac{E_a}{R}) \quad (4)$$

where, β - is the heating rate; E_a - is the activation energy; R - is the gas constant;

2.10 Laser ignition method

Laser beam ignition is an alternative ignition mechanism that provides several benefits over other ignition processes. A non-exhaustive list involves high specific time and space, reduced ignition latency, no need for pre-existing, simultaneous ignition of numerous combustion chambers by optical fiber communication, an increased chance for ignition for a wider array of mixing ratios (vacuum to high pressure), and electromagnet interference (EMI) which is the product of a non-exhaustive list of interference. The laser and electric spark ignition tests for fuel-rich blends have shown that laser ignition has a higher chance of ignition at lower pressures, regardless of the initial chamber pressure (CCP) [96]. Laser ignition can be performed in many cases explicitly, through which propellants consume the laser energy directly when the laser beam has been applied, or indirectly through which

laser energy is transferred via another means, such as metal particulates, from the laser beam into the propellants.

Materials and Samples. Activated carbon based on rice husk was obtained in the Laboratory of Functional Nanomaterials of the Institute of Combustion Problems (Almaty, Kazakhstan). Mechanical treatment (15 min) of ammonium nitrate (purity 99%) powder was carried out in a planetary mill. Ammonium nitrate was used as an oxidizer in the condensed mixture with a diameter of 30-40 μm. Magnesium (Mg) was used as a fuel, and its diameter was 30-40 μм. The metal oxide particles had a diameter of 50 nm and they acted as a catalyst. Cellulose nitrate has been used as a binding agent. The formulations were respectively diameter and duration of 3 mm and 10 mm (Fig. 19,20).

Figure 19 – Press form of samples for laser ignition test

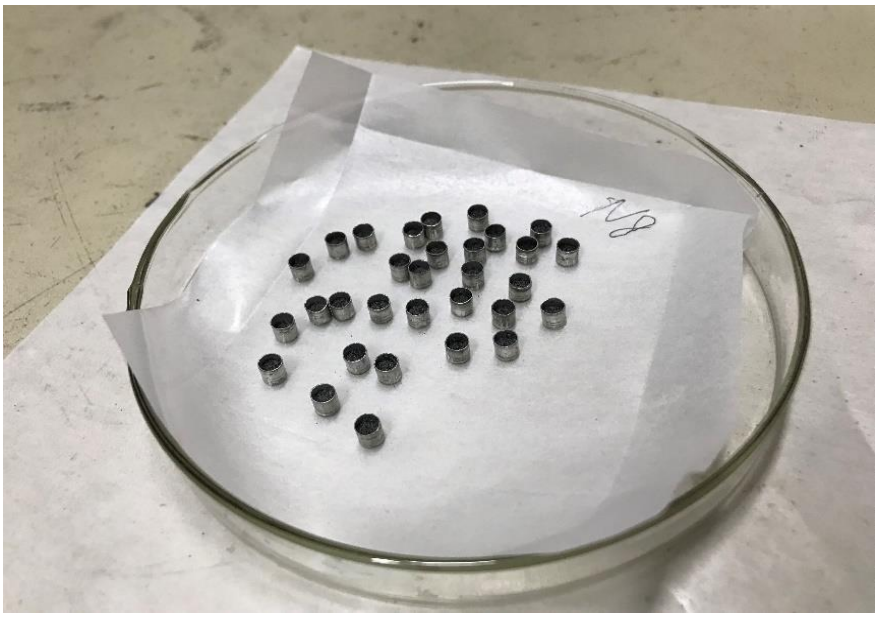

Figure 20 – Samples for initiation

Measurement of Laser Ignition Characteristics

The scheme graph shown in Fig. 21 indicates the setup used for laser sample ignition. The ignition was supplied with a 974 nm long fibre-connected laser diode, a 300 ms pulse width and laser power was determined by a lazer diode controller (up to 40 W with a resolution of ~6 mW and the laser was triggered using an external generator (RS Components 610–629). The laser beam performance was concentrated on a sample material surface with a focal lens (50 mm diameter and 50 mm focal length). The incident beam diameter of the lens was about 50 mm. Sample field measurements vary from 0.7 and 3.5 mm in diameter (± 0.05 mm mistake). For a beam driver to rest on for initiation, a glass block was used. 30 samples have been prepared and burned in each composite to activate laser initiation [26].

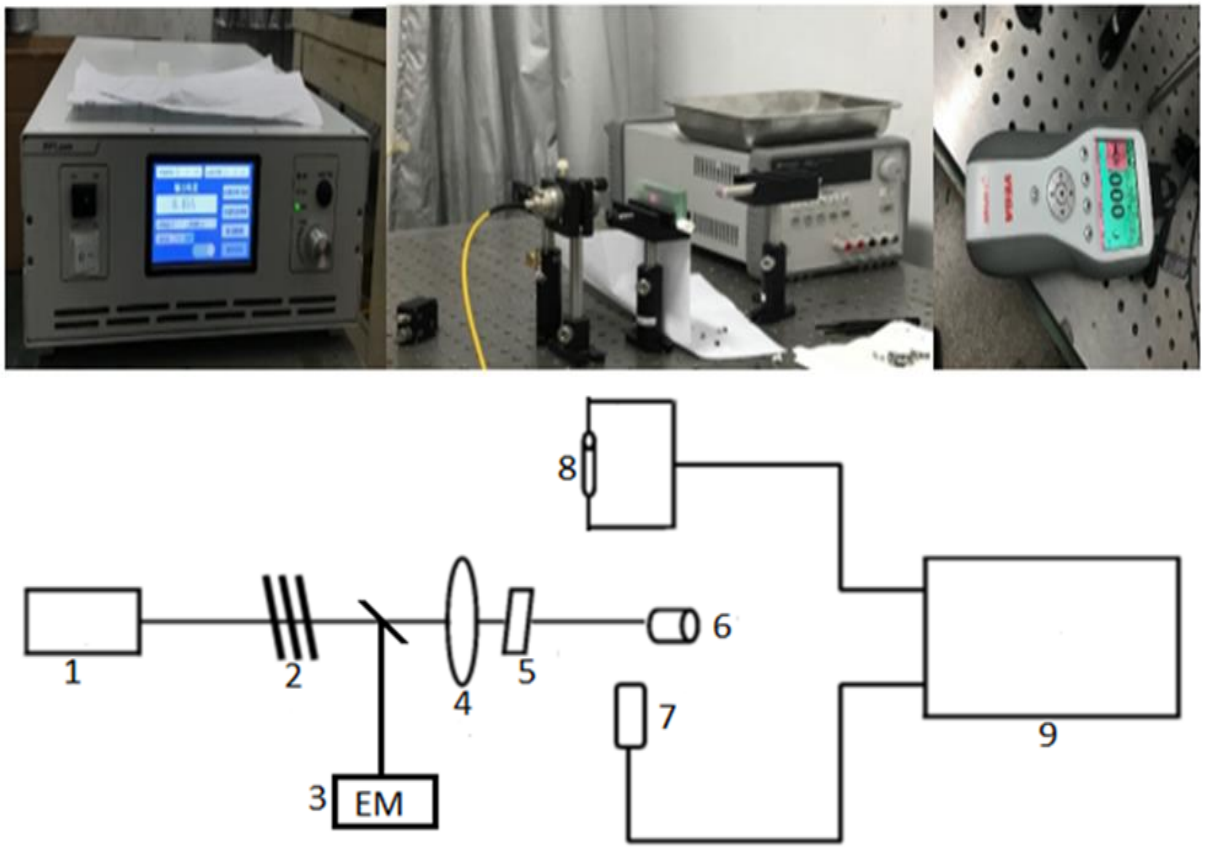

Figure 21 – Experimental set up for laser ignition: 1 – laser diode; 2 – attenuator split; 3 – energy meter; 4 – focusing lens; 5 – glass plate; 6 – sample; 7 – optic detector; 8 – sampling resistance; 9 – data analysis system

When the equipment has been properly set up, a sample holder containing the propellant content has been mounted under the focal lens on a height adjustable point, and laser concentrate has been put on the sample sheet. The sample material would be heated and encountered with enough laser power following exposure to the laser beam. In analyzing the pause, increase, and burn times shifts across a variety of beam widths, laser intensity and pulse durations, the ignitive properties of the propellant were examined [26].

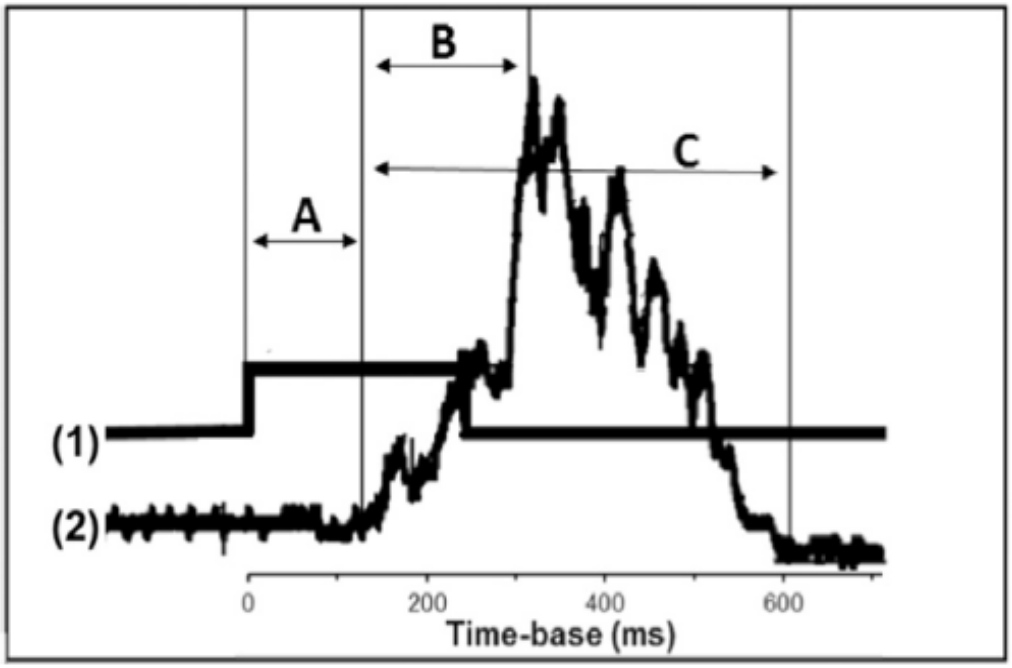

Figure 22 - Oscilloscope traces of (1) laser pulse and (2) the ignited flame with measures: (A) delay time, (B) rise time and (C) burn time

The wait period, time increase and time burn metric concepts display graphically in Fig. 22. The time between the start of the laser pulse and the onset of the propellant deflagration is taken to take delay time (a), the time between onset of deflagration and ignition is taken to take up the time between onset of deflagration and burn time (c) to take the time between start and end of deflagration [26].

2.11 The method of thermodynamic calculations using the NASA-CEA program

A software kit is used, NASA, Glenn Research Center – Chemical Balance and Application (CEA) [97]. The study of the thermodynamics is performed by means of a comprehensive database, which includes computational measurements for high temperature procedures (high temperature) and research for rocket fuel combustion and their thermodynamic characteristics (Fig. 23).

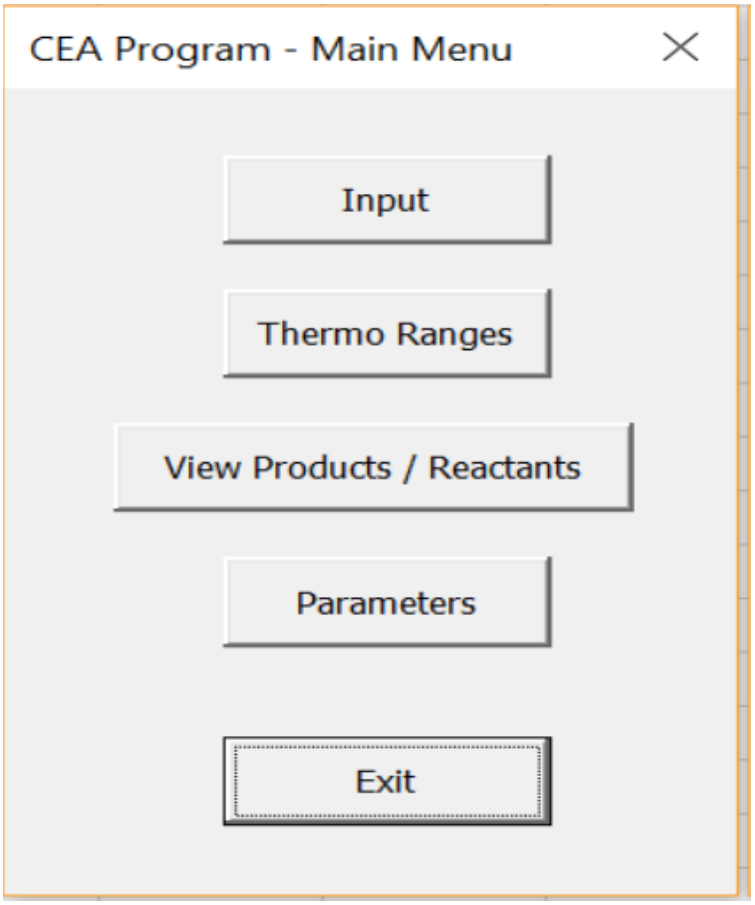

Figure 23 - Interface of NASA-CEA program

The NASA CEA programme, for the composition of species within a user-specified mixture, uses two thermodynamic state functions. The compositions of the chemical equilibrium are calculated by using a descent iteration method for Newton-Raphson, on the basis of Gibb's energy or Helmholtz power which describes the thermodynamic state. Until convergence criteria are reached, the program will use this Iteration process. Gaseous products are only required for integration at first, and then the software tests whether the simplified phases of the goods have to be included in the method [97].

3 RESULTS AND DISCUSSION

3.1 The studying of the physicochemical properties of the obtained activated CRH

3.1.1 Investigation of the structural characteristics of activated CRH by Scanning electron microscopy and Energy Dispersive X-Ray Spectroscopy

Activated carbon obtained from rice husk was studied in the present work by a technique combining two methods of estimating micro- and nanostructured objects: scanning electron microscopy (SEM) and Raman spectroscopy, which allowed us to estimate the topology of the carbon structure being formed, number of sheets in graphene particles, presence of chemical impurities, and structural defects.

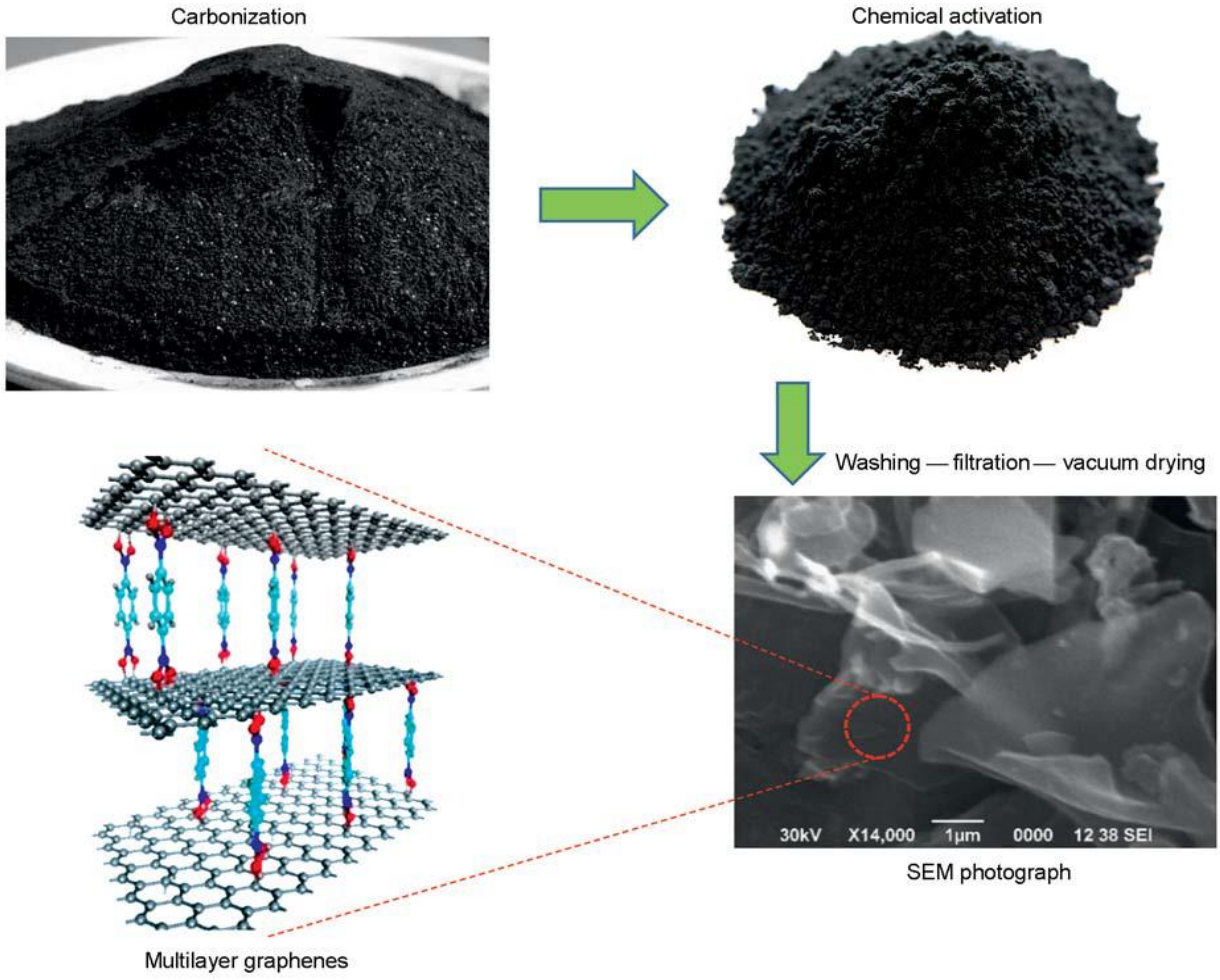

Figure 24 - Diagram of the process of obtaining activated carbon with graphene layers

The SEM photograph of activated CRH in Fig. 24 shows the particles with a typical graphene structure, which has a crumpled semitransparent surface. The sheets contain defects and inclusions of solid carbon components, but there are also some defectless regions with a homogeneous surface structure. The elemental composition of activated CRH testifies to effective removal (by means of chemical activation and washing) of silicon-based impurities, which suggests that the carbon

component has an extremely high concentration. It can be concluded that the activated carbon has a typical surface morphology defined by the raw material (RH) and possesses amwell-developed specific surface (3000 m^2/g) with a large number of micro- and meso-pores.

It is known that the Raman spectroscopy is one of the most informative methods for studying carbon structures with a high degree of graphitization [98-101]. The present study was performed with a wavelength of 473 nm at 6–7 points of the specimen. As is seen from the spectra in Fig. 25, the resultant carbon material consists of anisotropic disordered carbon structures and a large number of multilayer graphene structures.

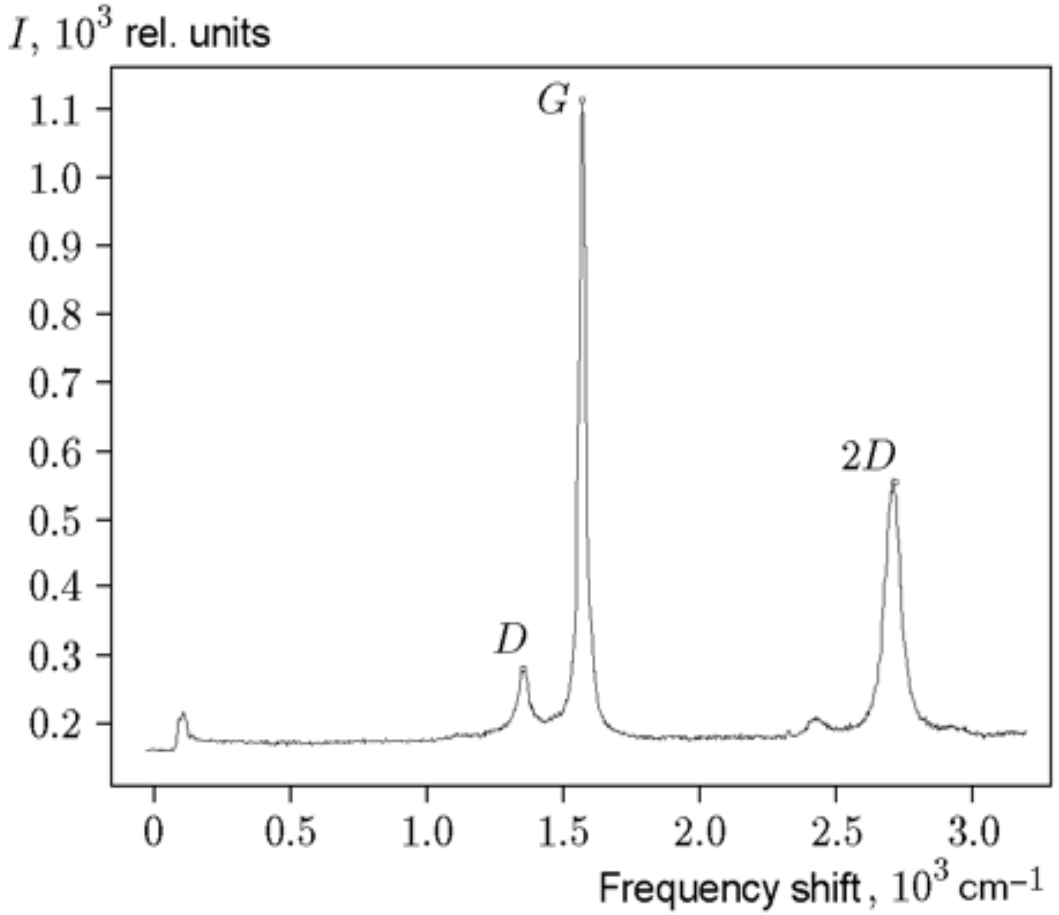

Figure 25 – Raman spectra of activated carbon obtained from rice husk

The intensity of the peaks *G* and *2D* allows us to conclude that the graphene film consists of three or more sheets (I_{2D}/I_G = 0.63). All spectra contain the peaks *D*, *G*, and *2D*, which testifies to the presence of deformations in the crystal structure of the graphene film and also to the presence of mechanical stresses. A detailed study of the Raman spectroscopy results showed that the CRH-based specimen consists of multilayer graphene with amorphous carbon components.

Physicochemical characteristics of AC based on rice husk

According to scanning electron microscopy data presented in Fig. 26, a developed porous structure is observed, which has multilayer graphene layers, which show the presence of defects, but there are areas without defects with a homogeneous structural surface.

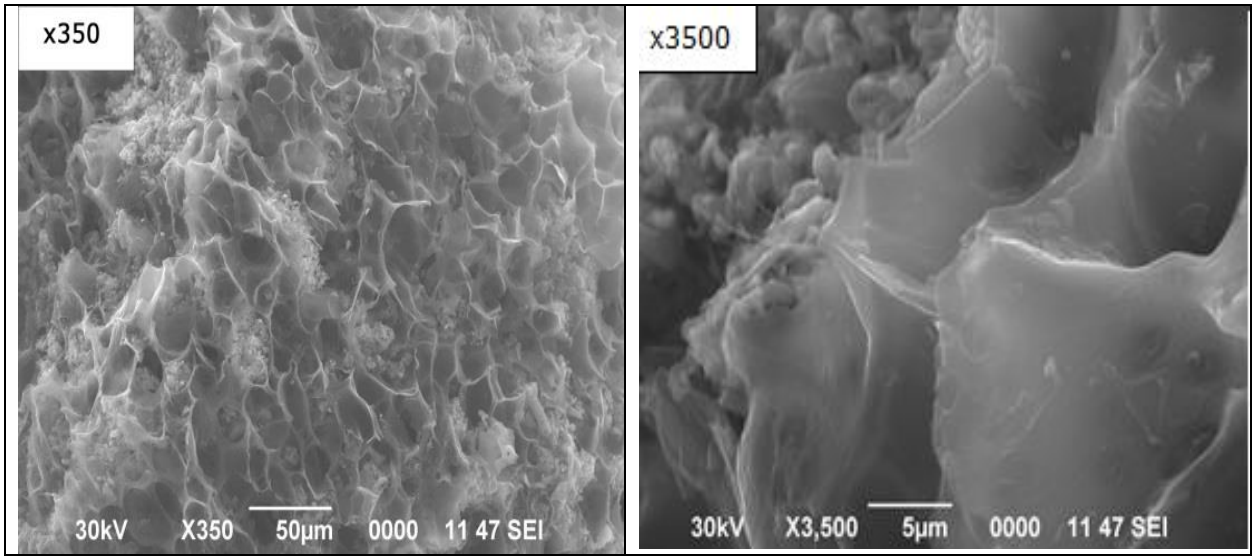

Figure 26 - SEM analysis of a sample of activated carbon based on rice husk

Elemental analysis of the sample was determined using the energy dispersive X-ray microanalysis (EDAX) method shown in Fig. 27.

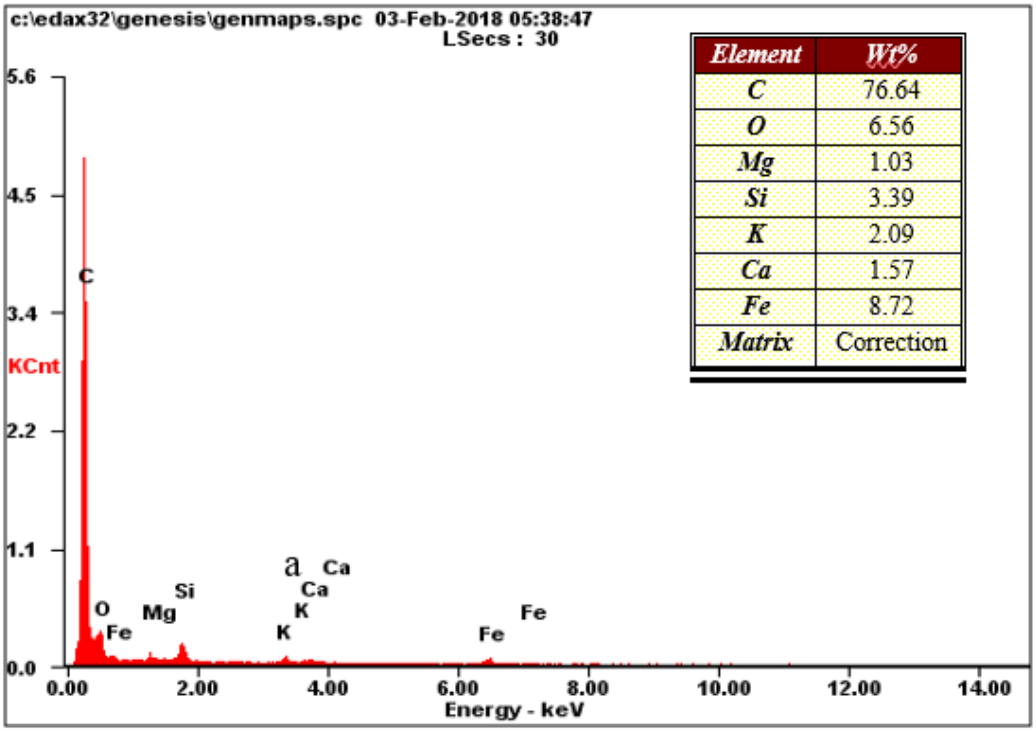

Element	Wt%
C	76.64
O	6.56
Mg	1.03
Si	3.39
K	2.09
Ca	1.57
Fe	8.72
Matrix	Correction

Figure 27 - The elemental composition of the activated carbon sample obtained from rice husk

The results of elemental analysis are presented in Table 4. The samples contain a high carbon content, which indicates a sufficient depth of carbonization. The higher the degree of carbonization, the higher the carbon content and the smaller the other components. In addition, there are various impurities of salts and oxides.

Physicochemical characteristics of CRH based CuO particle additives

AC has a high surface area of around 3,000 m^2/g, with a high absorption capacity of approximately 371 ml/g, as shown in table 1. Table 1. The existence of metal contaminants depends on the manufacturing CRH equipment (chemical activation with several active reagents, walls of the stove) in Fig. 29 Elemental Analysis (EDAX) of CuO doped AC. The amplitude of the G and 2D peaks (I_{2D}/I_G = 0.63) was shown in the study of the Raman spectrum, in Fig. 30, which helps us to infer the graph-structure (three or more layers) of the CRH. Scan electron microscopy (SEM) was used to study the morphology of CRH doped with CuO particles. Fig. 28 shows the results [17].

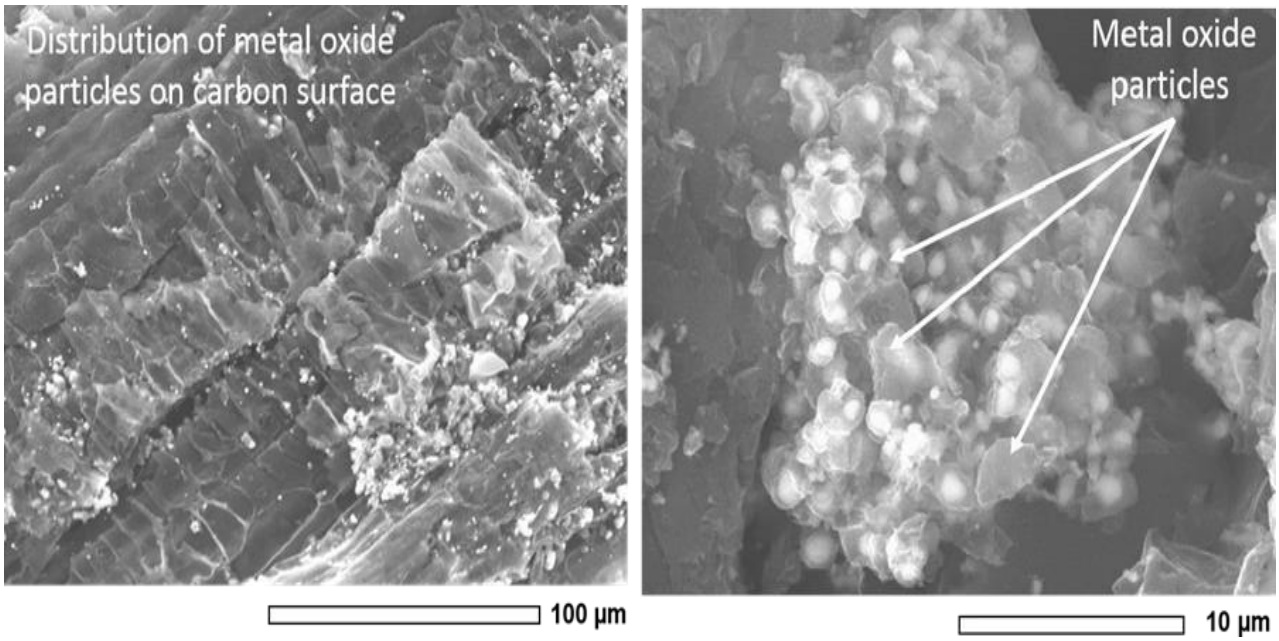

Figure 28 - SEM images of copper oxide particles on the surface of activated CRH

Two SEM micrographs with a morphological characteristic and elemental study from the high surface region of CRH with embedded copper oxide particles of different sizes were shown in Fig. 28,29. AC based on rice husk carbohydrate has a developed start material macro–and microstructure. The AC produced from a rice huck has an elastic, cell and round shaped framework with a scale of 3×3 µm. The AC is a wave system with a formed pore. In the SEM photograph of CRH with CuO, shows particles with a characteristic graphene structure, having crumpled translucent surface. The layers contain defects and inclusions of solid carbon components; however, there are areas without defects, with a homogeneous surface structure.

CRH is perfect for various metal oxide catalysts due to its high-surface area, porosity, adhesiveness and mean inertness. The intensity of the G-2D peaks (I_{2D}/I_G=0.63) is indicated in Fig. 30, and the AC consists of graph-structure (three or more layers) can be found in Fig. 30 (analyze of spectrum of Raman spectra).

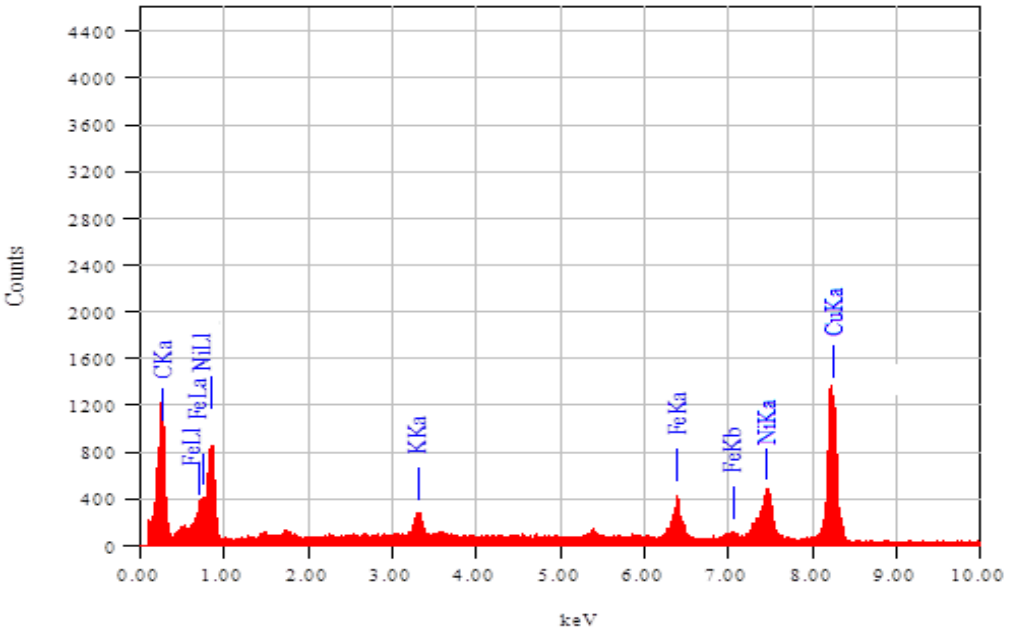

Figure 29 - EDAX analysis of the MOF (CRH-CuO) surface

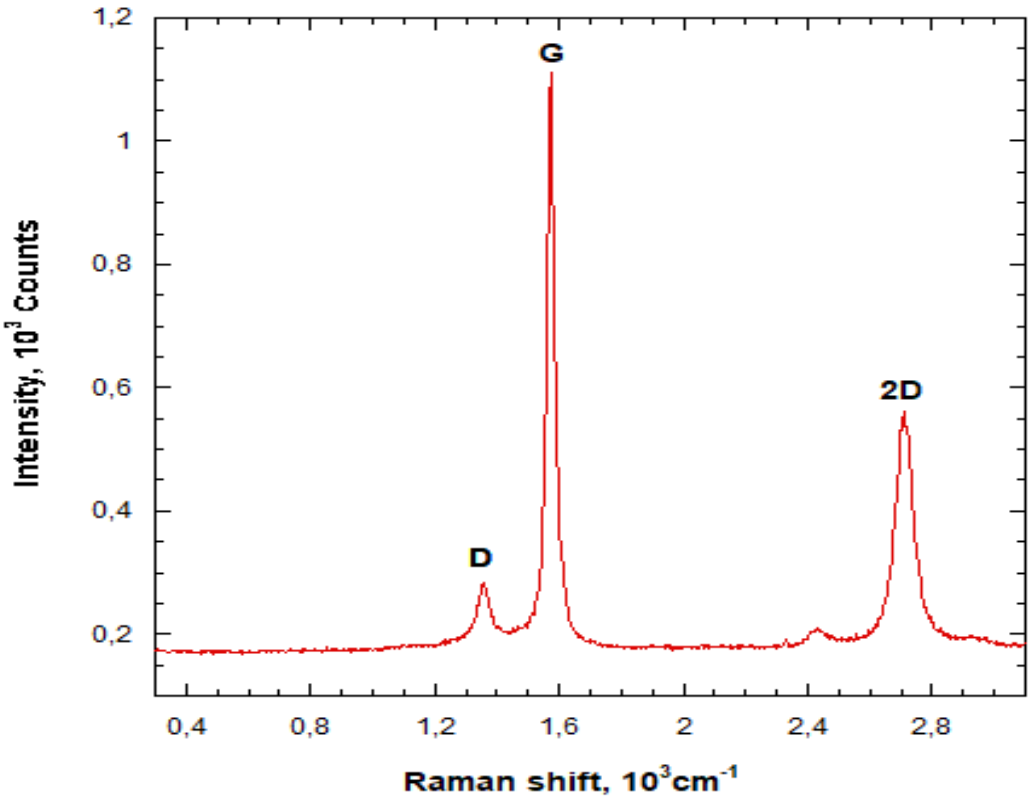

Figure 30 - Raman spectra of the surface of activate CRH with CuO

Table 1 - Summary of the physico-chemical properties of activated CRH

Properties	*Value*
Mass, %	0.1
Initial concentration of indicator (by methylene blue C1), mg/dm^3	1500
Optical density, *D*	0.062
The volume of the indicator solution, dm^3	0.025
Spectrometer transmittance, *T* %	96.6
Adsorption activity, mg/g	371
Specific surface, m^2/g	3186

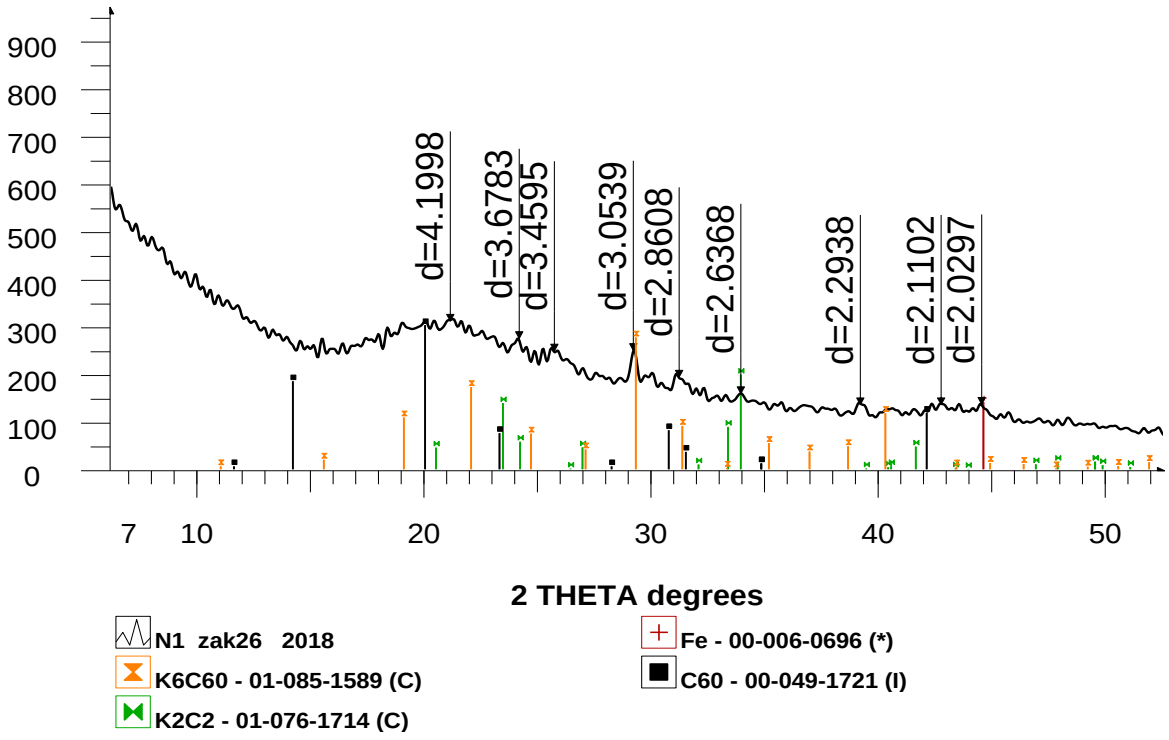

Figure 31 - X-ray pattern of a sample of carbon material obtained on the basis of RH

X-ray phase analysis was performed on activated carbon based on rice husk with chemical activation in the presence of potassium hydroxide. The X-ray diffraction pattern of this material is shown in Fig. 31. As follows from the X-ray diffraction pattern, the main phase of the sample is the X-ray amorphous phase, possibly C_{60} carbon. In addition to the halo with a maximum d=4.1998 Å, characteristic of C_{60} carbon, a number of diffraction lines weak in intensity are

present in the X-ray diffraction pattern. Some of these lines can be attributed to K_6C_{60}, K_2C_2 and to reduced iron.

3.2 Adsorption capacity of activated CRH in methylene blue

The sorption capacity of activated CRH was determined by standard methods, including sorption of methylene blue. In accordance with the values on the calibration graph, if we take the value K = 10, the concentration C = 60 along the x axis will correspond to a value of adsorption activity equal to 225 mg/g. So, in accordance with GOST, the value of adsorption activity for the tested activated CRH should lie above the value of C = 60.

Fig. 32 demonstrates the advantage of sample a in AC based on RH using the alkaline agent KOH in adsorption capacity (371 mg/g, respectively) by methylene blue over AC based on RH and without activation (82 mg/g, respectively). To obtain carbon material based on chemically activated rice husk, an alkaline agent KOH was used, which promotes the formation of a porous structure by leaching the mineral part contained in the initial precursor and opening new pores.

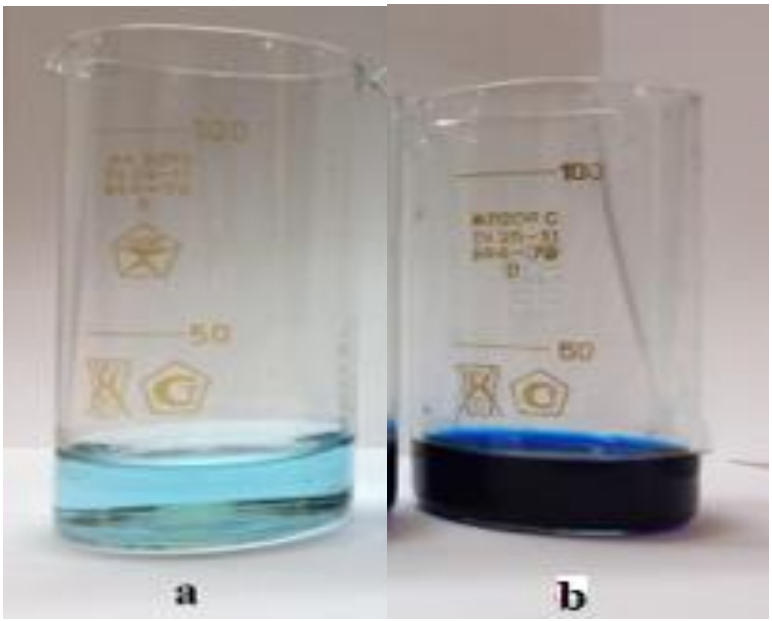

Figure 32 - The residual concentration of methylene blue in solutions:
a - AC based on RH with activation; g - AC based on RH without activation;

Table 2 - The results of test of activated CRH

D			<D>	C, mg/dm^3	X, mg/g
0,135	0,135	0,135	0,135	15	371,25
0,140	0,140	0,140	0,140	18,5	370,375
0,136	0,136	0,136	0,136	15,5	371,125
0,139	0,139	0,139	0,139	18	370,5
0,141	0,141	0,141	0,141	19	370,25

Table 3 - The results of test non-activated CRH

D			<D>	C, mg/dm^3	X, mg/g
0,360	0,360	0,360	0,360	120	75
0,361	0,361	0,361	0,361	121	72,5
0,359	0,359	0,359	0,359	119	97,5
0,358	0,358	0,358	0,358	118	80
0,356	0,356	0,356	0,356	116	85

Tables 2,3 show the results obtained during the experiment. For each optical density value on the calibration graph, the corresponding solution concentration value after contacting with activated carbon is determined along the X axis. Further, based on the obtained values, the adsorption capacity of coal is determined by the formula (1). The mass of the samples is 0.1 g, the volume of methylene blue is 25 ml, the volume of distilled water is 50 ml, and the volume of the clarified solution is 5 ml.

3.3 The specific surface area of activated CRH determination by BET method

Table 4 shows the values of the texture properties of the studied samples of activated CRH from isotherms of the BET model based on low-temperature nitrogen adsorption (N_2).

Table 4 - Specific surface values and elemental composition of activated CRH

Sample	S_{BET}, m^2/g	SC by MB, X, мg/g	C, %	O, %	Mg, %	Si, %	K, %	Ca, %	Fe, %	Yield, %
AC based on CRH	3186	371	76,64	6,56	1,03	3,39	2,09	1,57	8,72	42

The high sorption capacities of the MB monolayer (Table 4) for sample also indicate high mesoporosity, since MB is known to be available for pores with diameters greater than 1.5 nm. In addition, knowing the number of MB molecules in the monolayer, one can also estimate the specific surface area. Thus, according to adsorption studies, the samples are highly porous materials with a developed specific surface.

3.4 Size distribution of powder particles after mechanical activation

The distribution of particles in a powder or granular or particulate matter scattered in a liquid is a list of values or a mathematical function, which determines the relative amounts of particles, usually by weight, present according to the size.

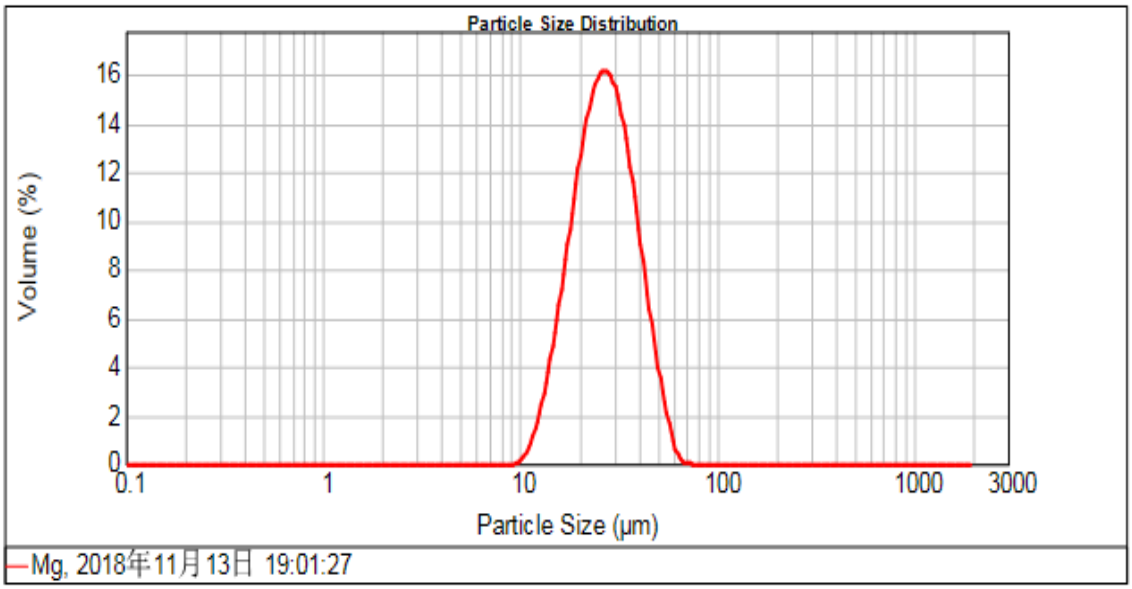

Figure 33 – Particle size distribution of Mg

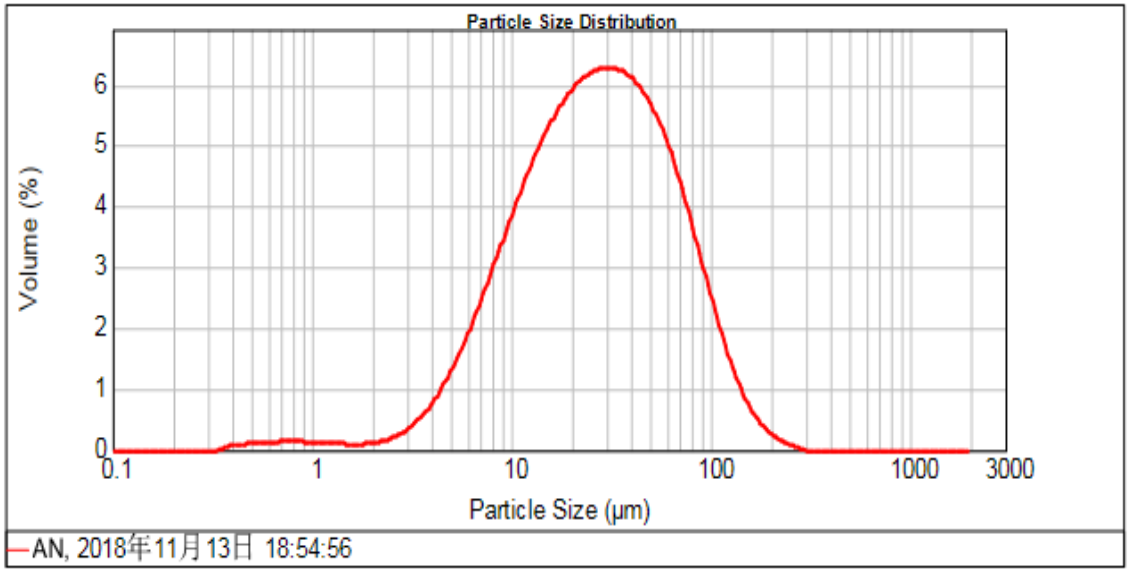

Figure 34 – Particle size distribution of AN

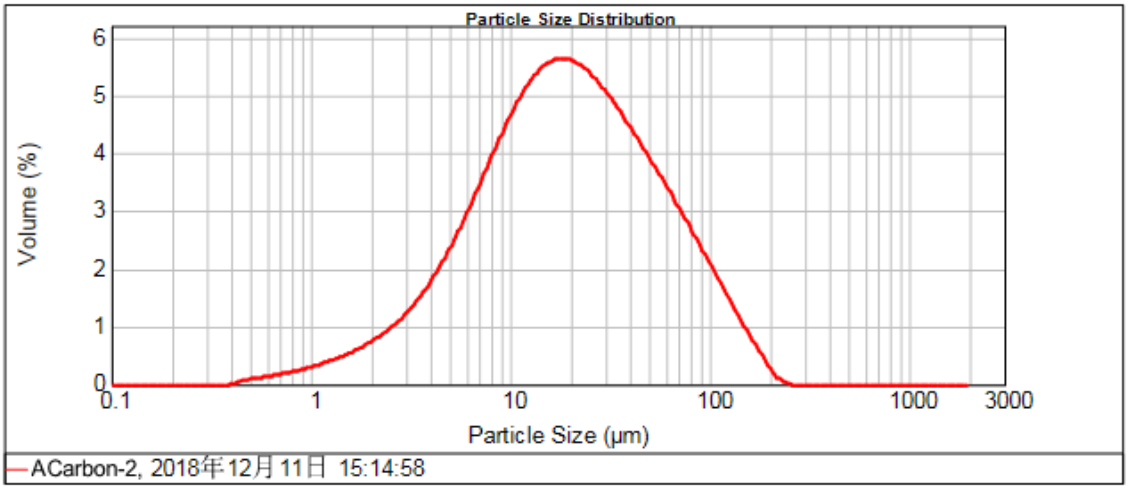

Figure 35 – Particle size distribution of activated CRH

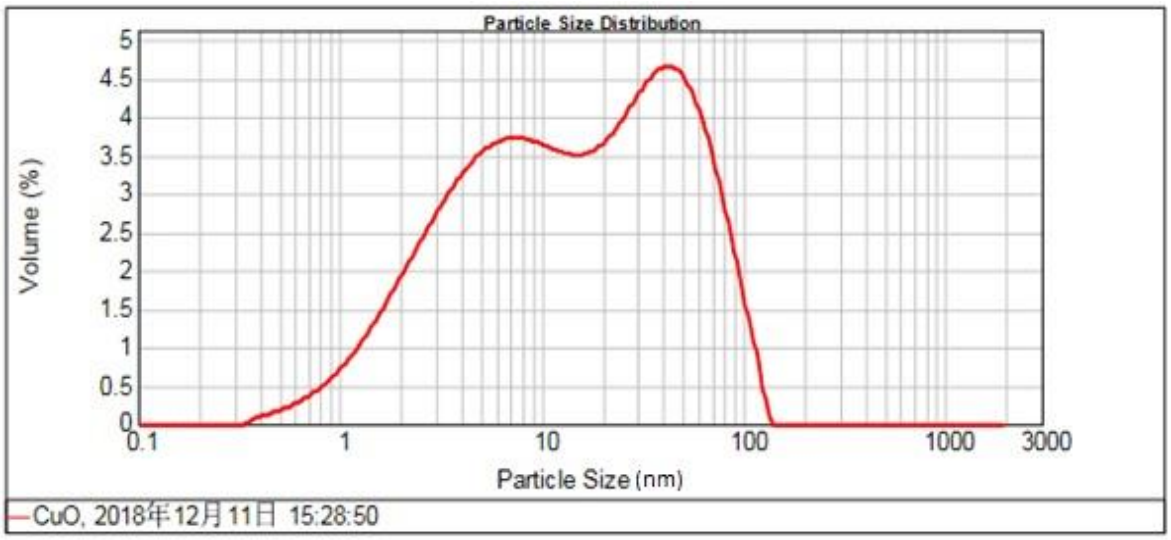

Figure 36 – Particle size distribution of CuO

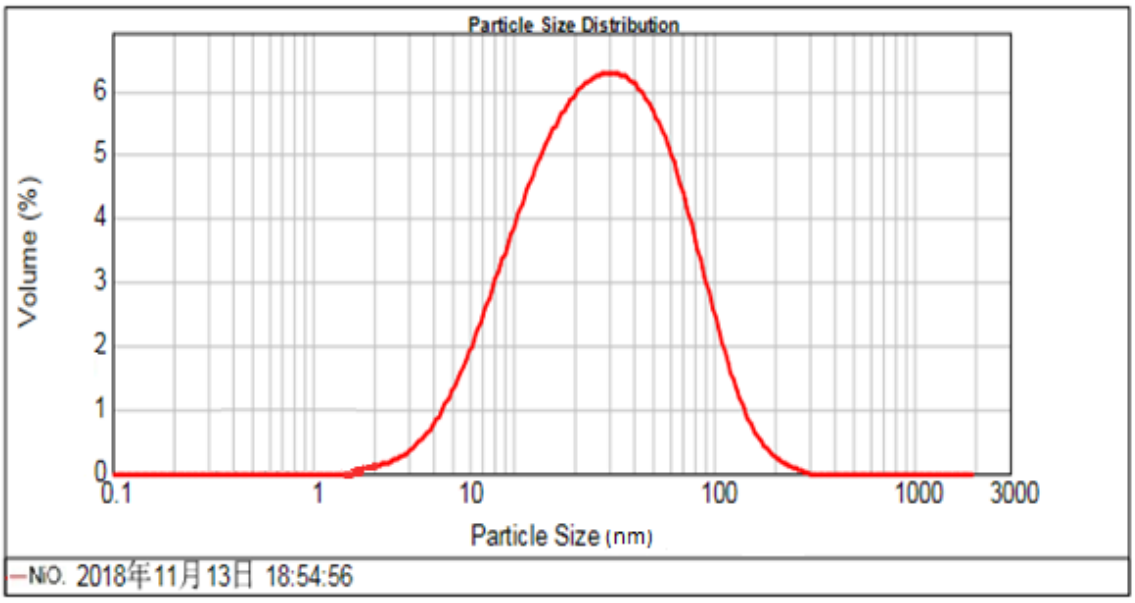

Figure 37 – Particle size distribution of NiO

The particle size distribution of the powders and the composite after mechanical activation was determined using the Malvern Mastersizer 2000 equipment (Fig. 33-37). For example, in Fig. 35 shows the results of the analysis of the distribution of particles of the source magnesium. The average particle size of the powder is 30 μm. The specific surface area is 0.24 m^2/g.

3.5 Investigation of the effect of energy materials on laser initiation

Finding the ignition energy threshold of the propellant was important as this benchmarked the minimum energy requirements for subsequent testing. In each case, a «Go/No-Go (+/-)» result was recorded for whether or not the ignition took place. Table 5 shows the results of the spent laser energy and ignition delay time to initiate for each composition [101].

Table 5 - The results of the spent laser energy and ignition delay time to initiate for each composition

№	Compositions	Ignition energy, J	Ignition delay, ms
1	AN/Mg/NC	25.97	902
2	AN/Mg/NC/**CRH**	9.31	810
3	AN/Mg/NC/**CRH-NiO**	6.88	688
4	AN/Mg/NC/**CRH-CuO**	4.35	506

According to the results, we can see that the energy spent on laser initiation of the composition decreases (Fig. 38). As seen for the initiation of the basic composition (AN/Mg/NC) which does not contain MOF (CRH-CuO) was spent 25.97 J of energy. And for the initiation of the composition AN/Mg/NC/CRH-CuO used 4.35 J of energy, almost four times less energy was spent.

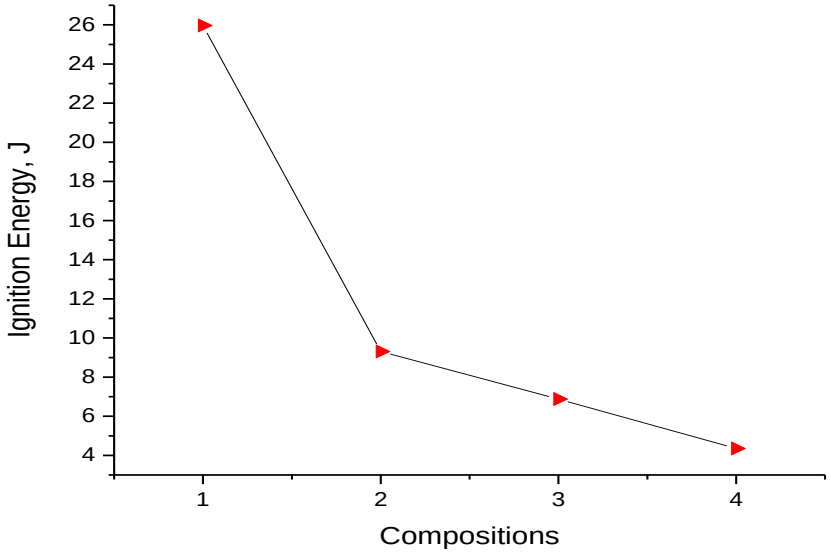

Figure 38 - Ignition energy dependencies on the compositions

The thermal properties of the energetic material play an important part in addition to the laser energy. This is due to the fact that the activated CRH itself in the form of as a fuel contains a large amount of energy. Metal oxides (CuO/NiO) can be the catalyst for our AN-based propellant system. Ignition by a low-medium laser energy of continuous wave is a complicated process, which includes transfer and dissipation of the heat generated by laser and also the energetic material decomposition in a long-time scale.

The ignition delay time is of particular interest as it can affect both system safety and system response times. Fig. 39 presents the dependencies of the ignition delay time on the compositions. As shown, to initiate the compositions with a

decrease in energy expended, the delay of the ignition time was also reduced. Ignition delay of basic AN/Mg/NC composition was 902 ms and for the AN/Mg/NC/CRH-CuO composition reduced to 506 ms. It could be said that the composition with activated carbon based on metal oxides reacts quickly to inflammation and is sensitive to initiation.

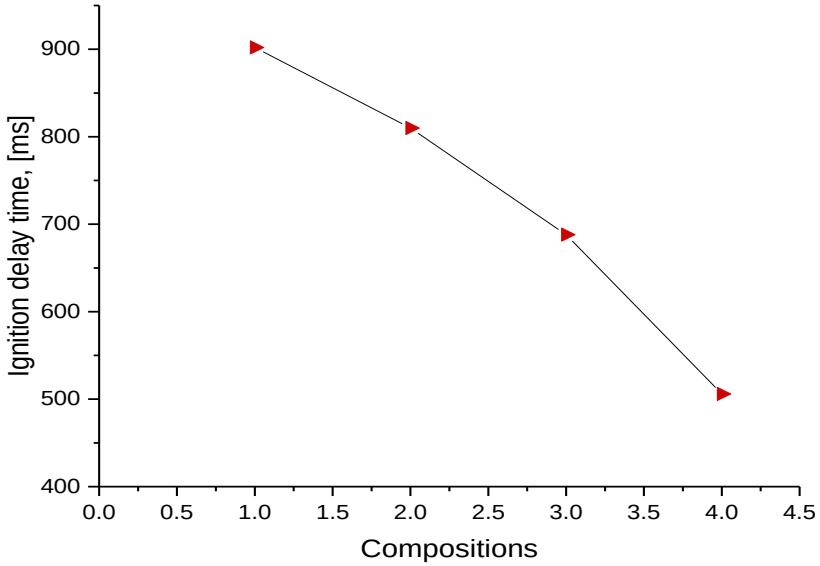

Figure 39 - Dependencies of the ignition delay time on the compositions

The study shows that the propellant laser ignition limit is dependent on laser energy and inflammatory period and suggests AN/Mg/NC/CRH-MeO as a successful laser inflammation candidate for several purposes. First, to produce efficiently and sustainably inflammatory results, the propellant does not need the introduction of optical sensitizers to maintain the chemical properties. The results of the study support the development of a laser diode propellant ignitor based on direct ignition of propellant load without the need for sensitive or primary pyrotechnic. secondly, the propellant burned sustainably with a laser energy of ~4.35 J provided an ignition delays of 506 ms [26].

3.6 The calculation of the thermodynamic theoretical burning products

The calculation of the burning of AN/Mg/NC, AN/Mg/NC/CRH and AN/Mg/NC/CRH-CuO pyrotechnic compositions was performed on a computer using the chemical equilibrium and application (CEA) program for calculating the chemical equilibrium of NASA.

The calculations were carried out according to the effect of graphitized carbon, which is the closest in characteristics to the activated CRH used in the work, on the combustion characteristic of AN, to analyze the increase in the productivity of the monofuel under study. The pressure in the combustion chamber varies from a minimum value of 0 to 80 MPa per square inch. This operating pressure range was selected as a typical operating pressure for energy fuels.

Table 6 - Distribution of combustion products of AN/Mg/NC composite (NASA-CEA) as a function of pressure

THERMODYNAMIC PROPERTIES								
P, BAR	1.0000	2.0000	3.0000	4.0000	5.0000	6.0000	7.0000	8.0000
T, K	2831.36	2898.68	2937.51	2964.68	2985.49	3002.30	3016.35	3028.40
MASS FRACTIONS								
*H	8.0678-4	6.9249-4	6.2710-4	5.8168-4	5.4712-4	5.1940-4	4.9634-4	4.7669-4
HO2	2.3179-5	3.0136-5	3.4971-5	3.8776-5	4.1954-5	4.4703-5	4.7136-5	4.9327-5
*H2	4.1862-3	3.9503-3	3.7945-3	3.6762-3	3.5800-3	3.4987-3	3.4282-3	3.3658-3
H2O	2.9408-1	2.9677-1	2.9848-1	2.9974-1	3.0075-1	3.0159-1	3.0231-1	3.0294-1
*Mg	6.8017-3	4.9657-3	4.0457-3	3.4630-3	3.0509-3	2.7397-3	2.4940-3	2.2940-3
*MgO	8.4960-3	7.7600-3	7.2228-3	6.8024-3	6.4582-3	6.1673-3	5.9161-3	5.6955-3
MgOH	3.2796-3	3.4482-3	3.4925-3	3.4961-3	3.4821-3	3.4594-3	3.4323-3	3.4030-3
Mg(OH)2	8.6367-3	1.1628-2	1.3721-2	1.5367-2	1.6737-2	1.7915-2	1.8953-2	1.9883-2
*NO	1.0622-2	1.1225-2	1.1555-2	1.1776-2	1.1939-2	1.2067-2	1.2170-2	1.2256-2
NO2	4.7058-6	6.4762-6	7.7877-6	8.8667-6	9.7993-6	1.0629-5	1.1383-5	1.2076-5
*N2	2.7502-1	2.7474-1	2.7458-1	2.7448-1	2.7440-1	2.7434-1	2.7429-1	2.7425-1
*O	7.0462-3	6.1788-3	5.6751-3	5.3217-3	5.0510-3	4.8324-3	4.6497-3	4.4933-3
*OH	3.4024-2	3.3022-2	3.2292-2	3.1708-2	3.1218-2	3.0794-2	3.0420-2	3.0083-2
*O2	4.4261-2	4.1316-2	3.9630-2	3.8453-2	3.7553-2	3.6825-2	3.6217-2	3.5694-2
MgO(cr)	3.0271-1	3.0425-1	3.0483-1	3.0507-1	3.0517-1	3.0518-1	3.0515-1	3.0509-1

As you can see, all components have a weak, but noticeable dependence on the value of the initial pressure. Tables 6,7,8 shows detailed data on the calculation of the distribution of combustion products by molar concentration during combustion of AN/Mg/NC, AN/Mg/NC/CRH and AN/Mg/NC/CRH-CuO compositions with and without MOF (CRH-CuO) (fig. 40,41).

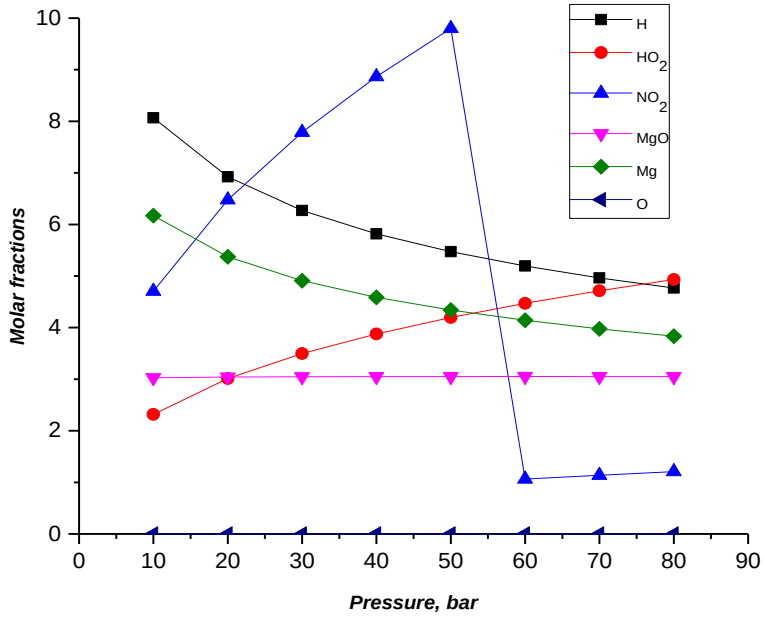

Figure 40 - The distribution of combustion products AN/Mg/NC composite (NASA-CEA) depending on the pressure

Table 7 - Distribution of combustion products of AN/Mg/NC/CRH composite (NASA-CEA) as a function of pressure

THERMODYNAMIC PROPERTIES								
P, BAR	1.0000	2.0000	3.0000	4.0000	5.0000	6.0000	7.0000	8.0000
T, K	2833.81	2901.50	2940.57	2967.92	2988.87	3005.79	3019.95	3032.09
MASS FRACTIONS								
*CO	1.0872-2	1.0658-2	1.0496-2	1.0364-2	1.0252-2	1.0153-2	1.0064-2	9.9839-3
*CO2	1.7814-2	1.8151-2	1.8405-2	1.8612-2	1.8789-2	1.8945-2	1.9084-2	1.9210-2
*H	8.0982-4	6.9746-4	6.3326-4	5.8869-4	5.5479-4	5.2759-4	5.0498-4	4.8570-4
HO2	1.9463-5	2.5021-5	2.8816-5	3.1765-5	3.4201-5	3.6288-5	3.8122-5	3.9760-5
*H2	4.4647-3	4.2427-3	4.0957-3	3.9839-3	3.8931-3	3.8162-3	3.7494-3	3.6903-3
H2O	2.9297-1	2.9559-1	2.9725-1	2.9847-1	2.9944-1	3.0025-1	3.0095-1	3.0156-1
*Mg	6.8779-3	5.0580-3	4.1438-3	3.5635-3	3.1522-3	2.8409-3	2.5948-3	2.3941-3
*MgO	7.8384-3	7.1587-3	6.6661-3	6.2819-3	5.9679-3	5.7029-3	5.4744-3	5.2737-3
MgOH	3.1929-3	3.3686-3	3.4216-3	3.4335-3	3.4271-3	3.4116-3	3.3911-3	3.3679-3
Mg(OH)2	8.2396-3	1.1090-2	1.3086-2	1.4657-2	1.5966-2	1.7094-2	1.8089-2	1.8980-2
*NO	9.4913-3	9.9580-3	1.0201-2	1.0356-2	1.0467-2	1.0550-2	1.0615-2	1.0667-2
*N2	2.7555-1	2.7533-1	2.7521-1	2.7514-1	2.7509-1	2.7505-1	2.7502-1	2.7499-1
*O	6.1721-3	5.3724-3	4.9105-3	4.5878-3	4.3412-3	4.1426-3	3.9770-3	3.8354-3
*OH	3.1635-2	3.0586-2	2.9836-2	2.9241-2	2.8746-2	2.8319-2	2.7942-2	2.7605-2
*O2	3.6239-2	3.3338-2	3.1660-2	3.0480-2	2.9572-2	2.8835-2	2.8215-2	2.7681-2
MgO(cr)	2.8780-1	2.8936-1	2.8994-1	2.9018-1	2.9028-1	2.9030-1	2.9027-1	2.9021-1

Table 8 - Distribution of combustion products of AN/Mg/NC/CRH-CuO composite (NASA-CEA) as a function of pressure

THERMODYNAMIC PROPERTIES								
P, BAR	1.0000	2.0000	3.0000	4.0000	5.0000	6.0000	7.0000	8.0000
T, K	2843.77	2912.01	2951.34	2978.84	2999.89	3016.86	3031.05	3043.20
MASS FRACTIONS								
*CO	1.0649-2	1.0426-2	1.0260-2	1.0124-2	1.0009-2	9.9079-3	9.8176-3	9.7357-3
*CO2	1.7821-2	1.8170-2	1.8432-2	1.8644-2	1.8825-2	1.8984-2	1.9126-2	1.9255-2
*Cu	1.5548-3	1.5445-3	1.5368-3	1.5303-3	1.5246-3	1.5195-3	1.5148-3	1.5105-3
CuO	2.0948-5	2.7419-5	3.2041-5	3.5755-5	3.8908-5	4.1673-5	4.4150-5	4.6402-5
CuOH	1.3131-5	1.9480-5	2.4568-5	2.8982-5	3.2954-5	3.6605-5	4.0011-5	4.3218-5
*H	7.8980-4	6.7909-4	6.1593-4	5.7213-4	5.3884-4	5.1216-4	4.8999-4	4.7109-4
HO2	1.9565-5	2.5177-5	2.9014-5	3.1999-5	3.4468-5	3.6586-5	3.8447-5	4.0111-5
*H2	4.3431-3	4.1201-3	3.9729-3	3.8612-3	3.7706-3	3.6939-3	3.6275-3	3.5687-3
H2O	2.9085-1	2.9348-1	2.9514-1	2.9637-1	2.9734-1	2.9815-1	2.9884-1	2.9945-1
*Mg	6.5894-3	4.8296-3	3.9484-3	3.3901-3	2.9950-3	2.6965-3	2.4607-3	2.2685-3
*MgO	7.6196-3	6.9442-3	6.4579-3	6.0799-3	5.7717-3	5.5120-3	5.2883-3	5.0922-3
MgOH	3.0905-3	3.2530-3	3.2992-3	3.3071-3	3.2982-3	3.2808-3	3.2591-3	3.2350-3
Mg(OH)2	8.0927-3	1.0882-2	1.2833-2	1.4368-2	1.5646-2	1.6747-2	1.7717-2	1.8587-2
*NO	9.4902-3	9.9630-3	1.0210-2	1.0369-2	1.0483-2	1.0568-2	1.0636-2	1.0690-2
*N2	2.7278-1	2.7255-1	2.7244-1	2.7236-1	2.7231-1	2.7227-1	2.7224-1	2.7221-1
*O	6.1479-3	5.3515-3	4.8918-3	4.5707-3	4.3254-3	4.1278-3	3.9631-3	3.8223-3
*OH	3.1422-2	3.0379-2	2.9634-2	2.9044-2	2.8552-2	2.8128-2	2.7755-2	2.7420-2
*O2	3.6845-2	3.3960-2	3.2291-2	3.1118-2	3.0215-2	2.9482-2	2.8865-2	2.8334-2
MgO(cr)	2.8557-1	2.8708-1	2.8763-1	2.8787-1	2.8796-1	2.8797-1	2.8793-1	2.8787-1

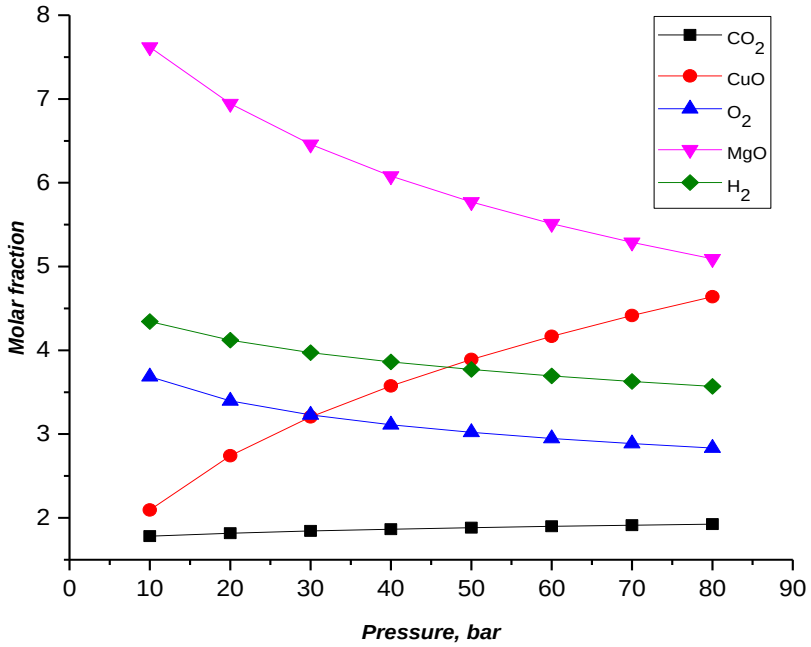

Figure 41 - The distribution of combustion products AN/Mg/NC/CRH-CuO composite (NASA-CEA) depending on the pressure

Table 9 shown the parameters used to thermodynamics calculate the theoretical combustion products.

Table 9 – Calculation parameters

Reagents	Mass, %	Education enthalpy kJ/Kg-mol	The initial temperature, K
Fuel, Mg	0.9529515	45.964	298.15
Fuel, CRH	0.0471480	15.836	298.15
Fuel, CuO	0.0099010	306336.048	298.15
Oxidizer, AN	0.9900990	-365342.184	298.15
The ratio of oxidizer and fuel O/F=4.00000 The amount of fuel, %=20 Equivalence ratio = 0.981014 Chemical equivalence ratio = 0.942792			

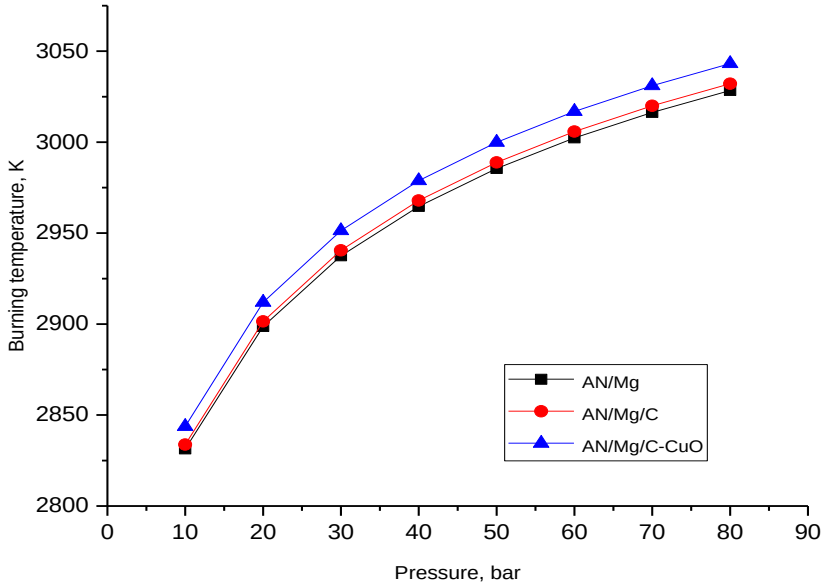

Figure 42 - Theoretical burning temperature of AN/Mg/NC, AN/Mg/NC/CRH and AN/Mg/NC/CRH-CuO compositions depending on the pressure

Fig. 42 shows the result of comparing theoretical burning temperature the performance of AN/Mg/NC, AN/Mg/NC/CRH and AN/Mg/NC/CRH-CuO compositions depending on the pressure. As a result, of the calculations shown with the increasing pressure of chamber showed increased on the adiabatic temperature of pyrotechnic compositions. Increase of pressure values is explained by the influence of composite on dissociation of products.

3.7 Studies of MOF (CRH-CuO) addition effect to AN/Mg/NC composite on the thermal decomposition of AN by Differential scanning calorimetry analysis

The measured DSC curves are presented in Fig. 43 and the detailed parameters of AN/Mg/NC energetic mixture thermal decomposition are listed in Table 10. The Thermal data in terms of DSC onset temperature *(T_{onset})*, offset temperature *(T_{offset})* and peak for maximum thermal decomposition *(T_{max})* are listed in Table 10.

Table 10 – Thermal data in terms of T_{onset}, T_{offset} and T_{max} obtained from DSC thermograms of an AN/Mg/NC, an AN/Mg/NC/CRH and an AN/Mg/NC/CRH–CuO (3%) mixtures

		1st step (180–230 °C)			2nd step (230–300 °C)		
sample	β (K min^{-1})	T_{onset}	T_{offset}	T_{max}	T_{onset}	T_{offset}	T_{max}
AN/Mg/NC	5	173.0	211.3	199.2	232.5	269.1	276.4
	10	176.3	223.5	203.9	243.0	287.4	279.0
	15	187.1	223.9	206.9	245.1	292.8	283.5
	20	186.2	223.5	206.2	252.9	307.5	294.5
		1st step (100–180 °C)			2nd step (210–270 °C)		
sample	β (K min^{-1})	T_{onset}	T_{offset}	T_{max}	T_{onset}	T_{offset}	T_{max}
AN/Mg/NC/AC	5	107.6	172.3	123.1	214.3	225.1	219.3
	10	116.8	176.5	128.1	230.8	245.0	240.6
	15	117.5	179.1	137.0	234.0	254.3	242.6
	20	117.9	186.8	140.5	239.5	261.9	248.5
		1st step (100–200 °C)			2nd step (200–260 °C)		
sample	β (K min^{-1})	T_{onset}	T_{offset}	T_{max}	T_{onset}	T_{offset}	T_{max}
AN/Mg/NC/AC-CuO	5	105.3	174.9	126.4	202.7	217.1	209.1
	10	111.8	171.4	131.9	215.3	228.5	222.1
	15	113.0	186.2	136.2	223.8	240.0	229.2
	20	114.5	188.1	134.6	225.1	250.5	237.9

Fig. 43 shows the DSC traces of AN/Mg/NC mixture decomposition in the presence of various additives (pure and MOF (CRH-CuO) at β = 5 K/min heating rate in a nitrogen atmosphere. Fig. 43a shows the DSC traces of AN/Mg/NC (in the ratio: 75/24.7/0.3) energetic mixture without any additives. Decomposition of the mixture during on three stage exothermic reactions. First, exothermic peak held at 137°C, second at 199°C and third exothermic peak at 276°C.

The DSC curve indicates that initially, there is small heat absorption, accompanied by the soft an endothermic peak of water evaporation respectively. Starting from the 19 minute at a temperature of ≈120°C first exothermic peak held on. At the 25 minute at a temperature of ≈170°C complete decomposition begins which corresponds to a sharp increase in the heat release (the second exothermic peak), at the 41st minute at the temperature range 230–270°C the last decomposition peak of the system is occurs.

The modification of thermal decomposition of an AN/Mg/NC mixture can be observed when adding 2.9% pure activated CRH (Fig. 43b: curve 1). There was a significant decrease in the third peak decomposition temperature in comparison with the basic mixture, approximately 50°C (from 276 to 219 °C). There is no endothermic peak due to water evaporation since with strong adsorption properties of activated CRH [92, 93]. When pure activated CRH was added, an increase of the heat flow (max) a range 4 times during a third exothermic reaction is observed (1.2 mW vs. 6.4 mW).

The same pattern of thermal decomposition of an AN/Mg/NC mixture can be observed when adding 3% MOF (CRH-CuO) (Fig. 43b: curve 2). One can see a significant decrease in the initial decomposition temperature in comparison with basic AN/Mg/NC mixture decomposition begin approximately at 126 °C. There is no endothermic peak due to water evaporation respectively (as in Fig. 43a). The DSC analysis shows that the addition of the MOF (CRH-CuO) leads

to the disappearance of the three-stage character of the decomposition of AN/Mg/NC mixture and the appearance of two exothermic peaks in the DSC curve with a strong shift toward low temperatures: the decomposition begins at a temperature of ~100°C and the maximum temperature is ~209°C. A decrease of exothermic peak maximum temperature in comparison with the basic mixture approximately 60°C (from 276 to 209°C) is observed.

The thermal decomposition of an AN/Mg/NC energetic mixture has a three-stage character. The catalytically effect of the transformed triple stage mechanism into two stage [104,105]. All investigations were studied at the same heating rate β = 5 K/min^{-1}, but the heat flow higher than other mixtures. The MOF (CRH-CuO) an increase in the heat flow rate (max) from 1.2 mW (in comparison with Fig. 43) up to 7.2 mW. The DSC curves did not show a unimodal curve. Inclusion of carbon particles in the composition impact on strong curves transformations. Necessary to note that increasing the heating rate (until β = 20 K/min^{-1}) did not tend to eliminate secondary decomposition peaks.

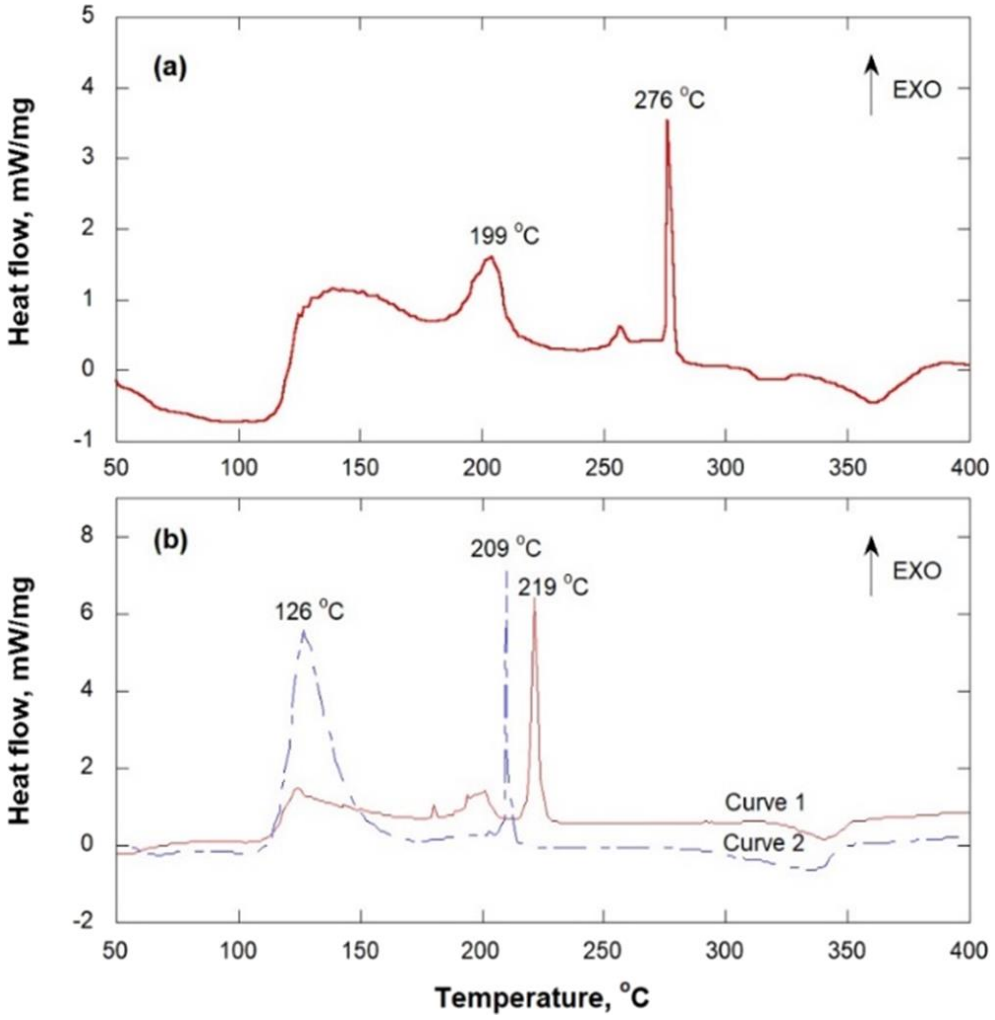

Figure 43 – DSC curves measured at β = 5 K min^{-1} for AN/Mg/NC, AN/Mg/NC/CRH and AN/Mg/NC/CRH–CuO mixtures

The effects of additives on combustion/decomposition characteristics of AN and AN-based compositions have been widely studied by many authors. Recently, researchers have reported that transition-metal oxides such as MnO_2, Fe_2O_3, TiO_2, and CuO could well catalyze the thermal decomposition of AN-based propellants [105].

To perform the kinetic analysis, an AN/Mg/NC/CRH-CuO energetic mixture was decomposed at four different heating rates (β = 5, 10, 15 and 20 K/min^{-1} in the nitrogen media). Fig. 44 shows that with increasing the heating rate, the onset temperature of all DSC trace peaks do not shift to higher temperatures. However, the location of the decomposition peaks on the temperature axis are shifted to higher values.

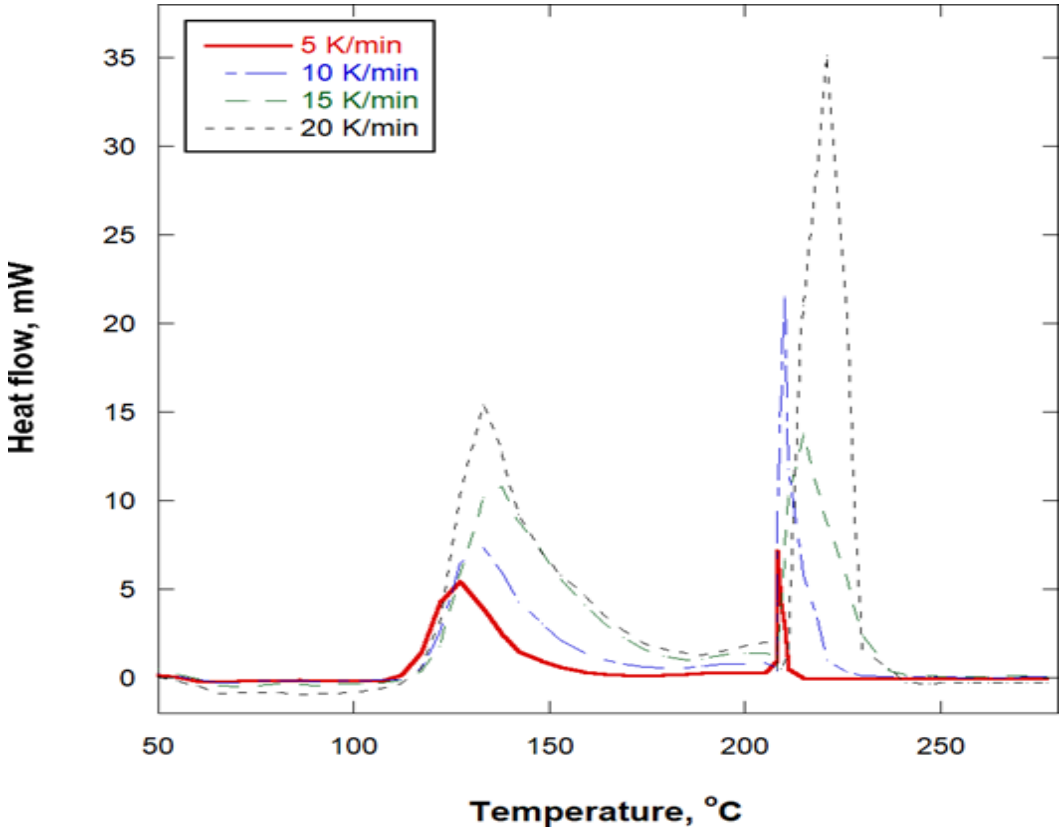

Figure 44 – Effect of heating rate on the decomposition of AN/Mg/NC/CRH–CuO mixture in nitrogen with flow rate of 300 cm^3/min^{-1} in alumina crucibles

Because of the complicated and multicomponent structure, the DTG curves found have a dynamic multistype decomposition process with more than 3 processes. The resulting catalyst, unreacted metal (Mg) and diluted decomposition products of NC and AN could be the main reason for the contamination at the end of the test TG. Furthermore, the TG curves for the AC and AC-CuO samples vary from the blank reference sample with comparatively less residue because of the more complete breakdown.

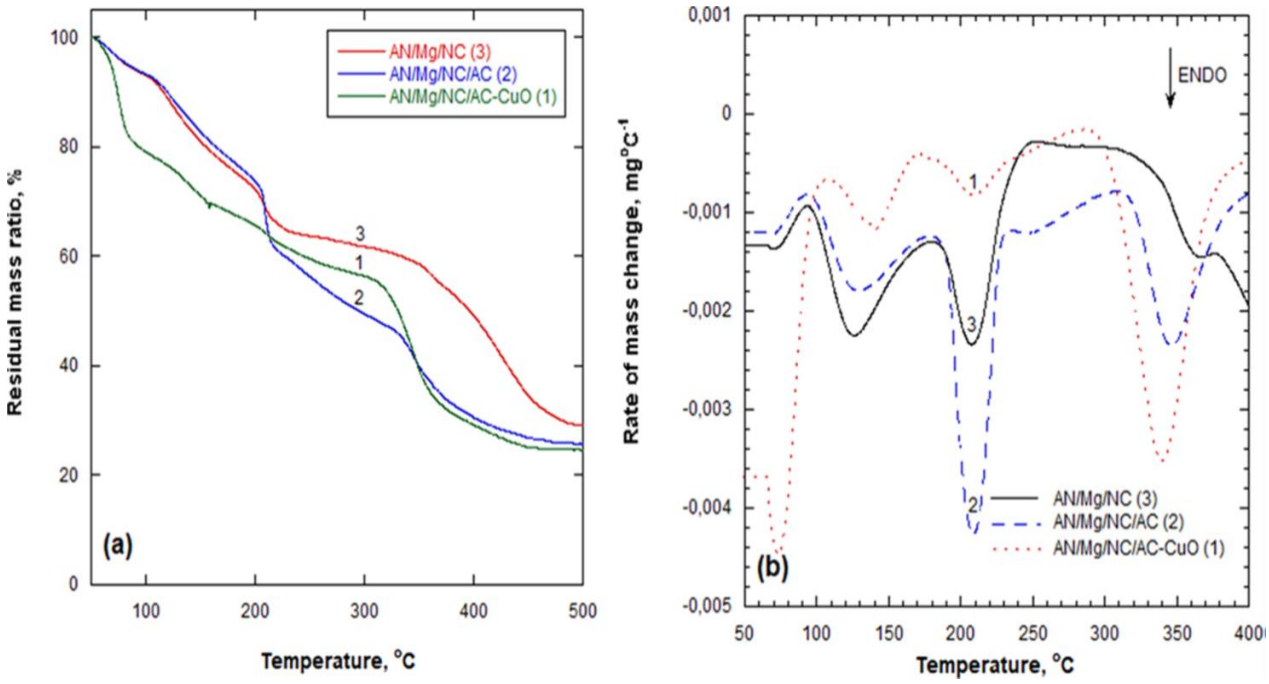

Figure 45 - (a) TG and (b) DTG curves of the three samples (AN/Mg/NC, AN/Mg/NC/CRH, and AN/Mg/NC/CRH-CuO) in a nitrogen medium (β = 10K·min^{-1})

Fig. 45 shows the TG (thermogravimetry) and DTG (derivative thermogravimetry) profiles obtained for the three samples in a nitrogen medium at β = 10 K·min^{-1} heating rate. The TG curves showed a continuous mass loss in the temperature range from 60 to 500°C. The total mass losses measured by TG analysis were around 71, 74, and 76% w/w of AN/Mg/NC (3), AN/Mg/NC/CRH (2), and AN/Mg/NC/CRH-CuO (1), respectively.

3.8 Studies of the effect of MOF (CRH-NiO) to AN/Mg/NC composite on the thermal decomposition of AN by Differential scanning calorimetry analysis

The characteristics of the heat discharge of composites prepared by different methods at different heating rates by the DSC method were measured. Fig. 46a show two exothermic peaks at 196.95ºC and 261.43 ºC, in Fig. 46b at 206.22ºC and 294.56ºC, starting from 165 to 267ºC the main ammonium nitrate decomposition occurred:

$$NH_4NO_3 \rightarrow N_2O + 2H_2O + Q \quad (1)$$

When activated CRH was added, a sharp decrease in heat absorbed from 261.43 to 220.35ºC and 248.52 ºC by the sample was noticeable (Fig. 47c, 47d). With the addition of MOF (CRH-NiO), the thermal decomposition temperature decreased by 15-20ºC. (Fig. 48e, 48f). The addition of MOF (CRH-NiO) to AN may affect as a catalyst to AN.

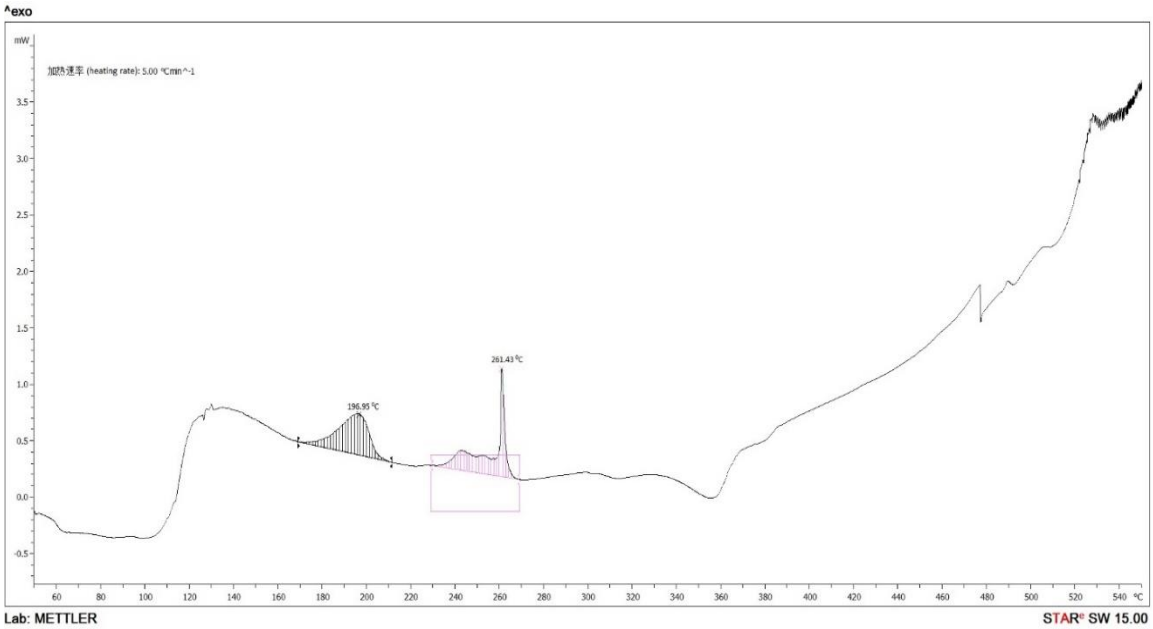

a

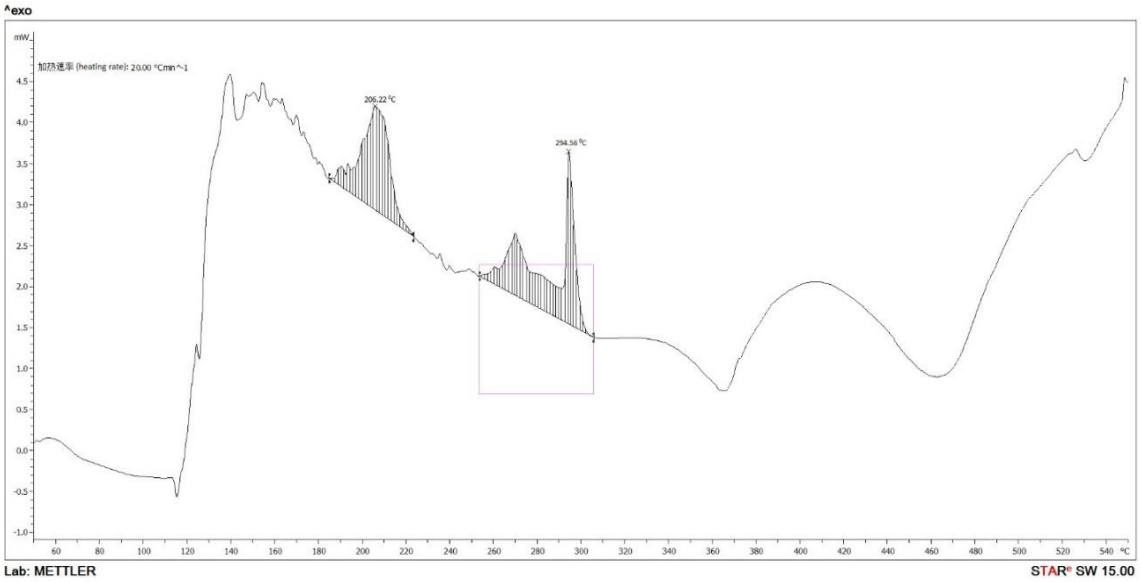

b

Figure 46 - DSC curves measured at (a) β = 5 and (b) β = 20 K min^{-1} for AN/Mg/NC

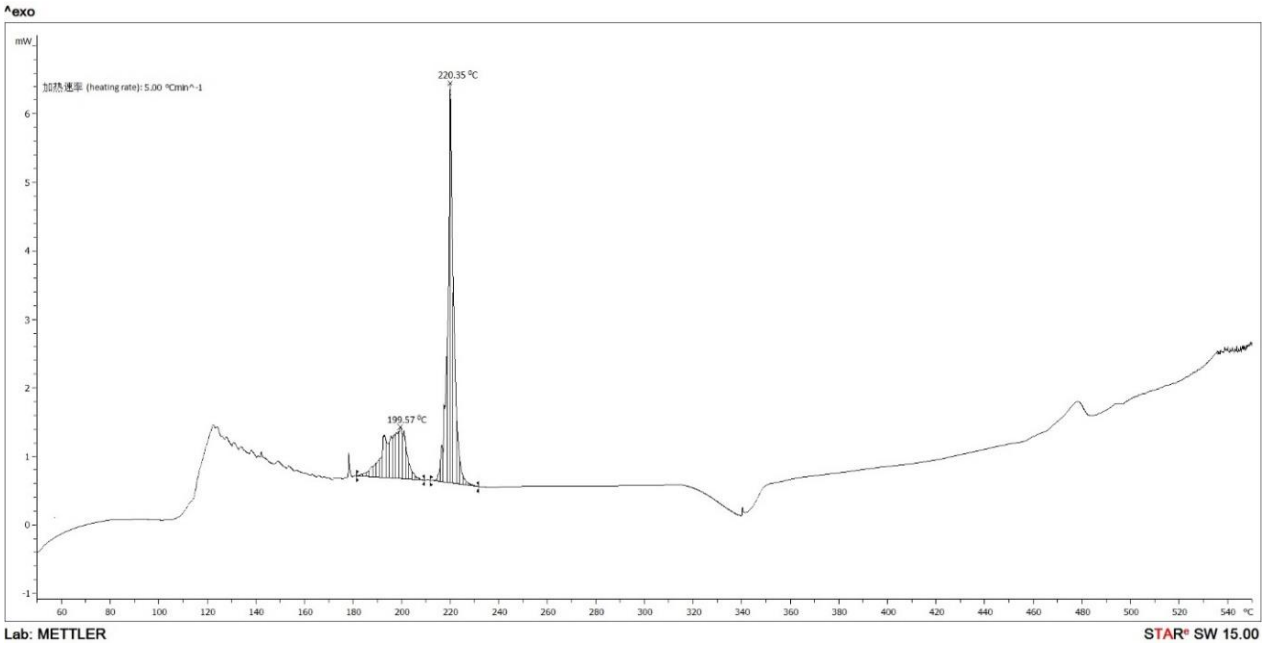

c

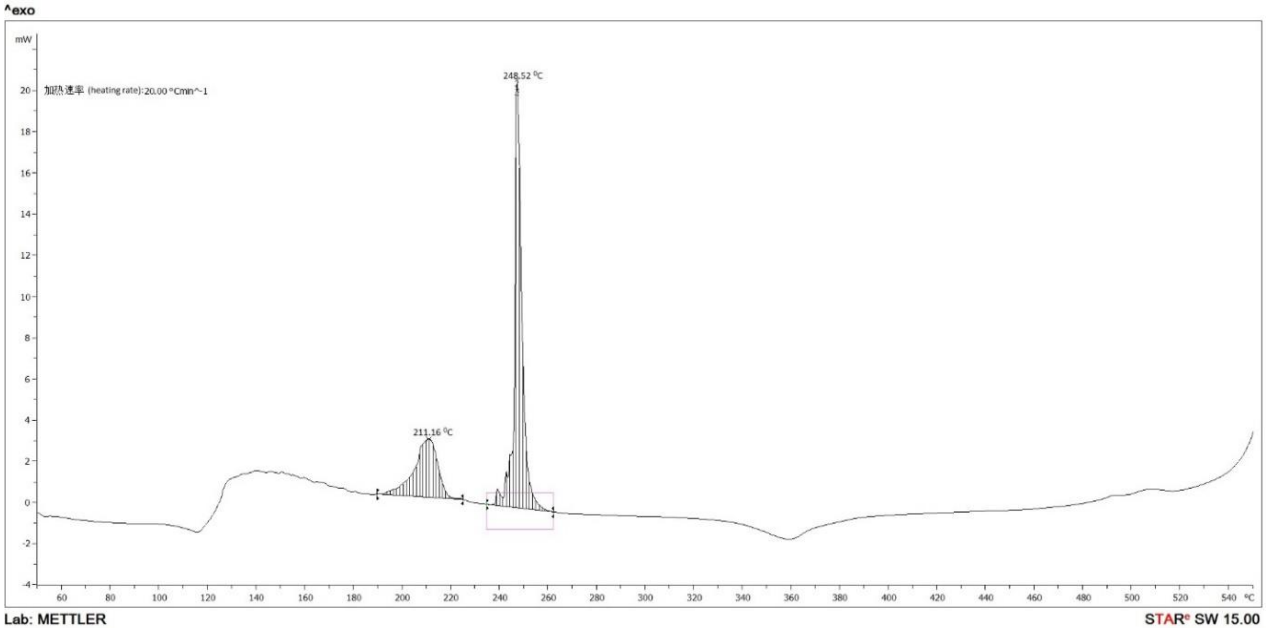

d

Figure 47 - DSC curves measured at (c) β = 5 and (d) β = 20 K min^{-1} for AN/Mg/NC/CRH

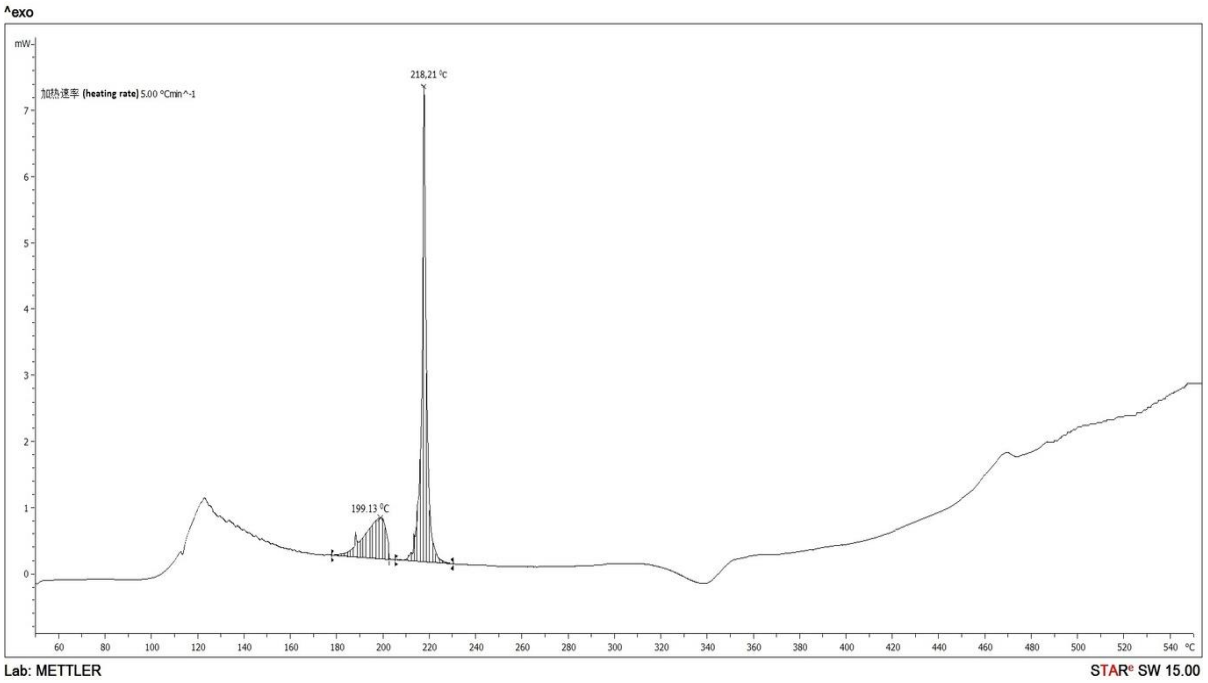

e

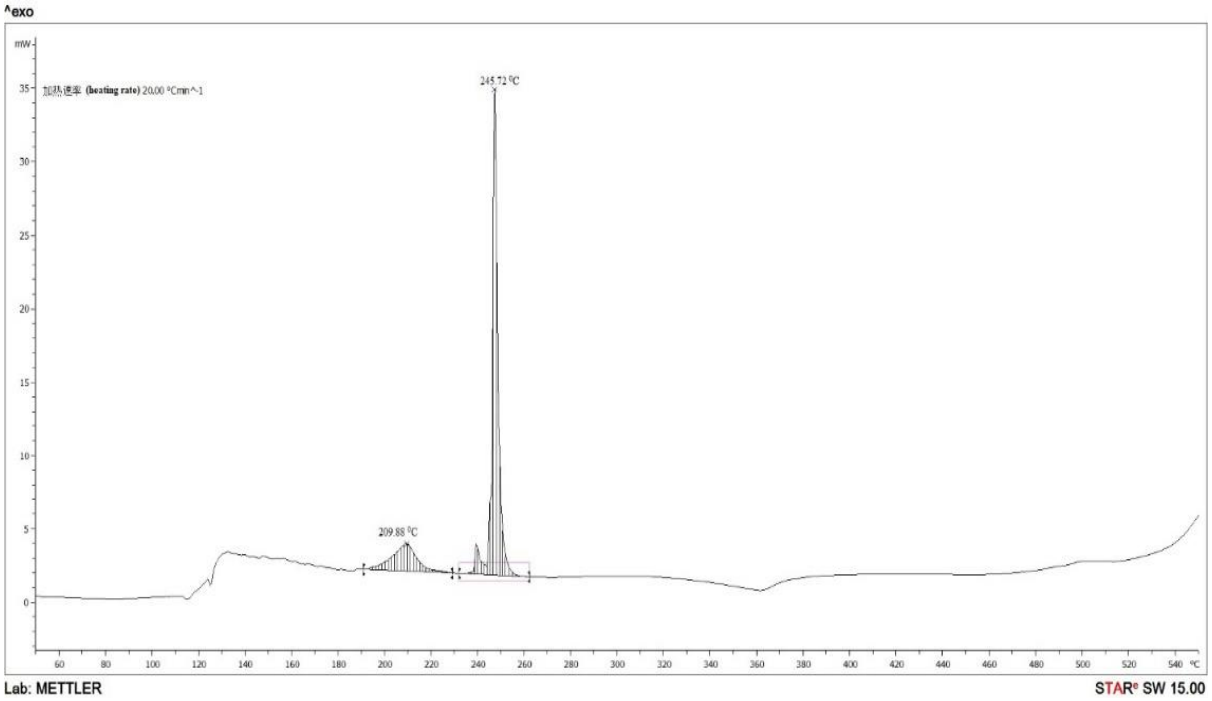

f

Figure 48 - DSC curves measured at (e) β = 5 and (f) β = 20 K min^{-1} for AN/Mg/NC/CRH-NiO

Based on the obtained DSC results, it can be concluded that activated CRH and MOF (CRH-NiO) has a direct impact on the process of AN thermal decomposition, reducing the complete decomposition temperature and the reaction rate. It was established that the addition of activated CRH affects the temperature change of phase transitions during the AN decomposition [17].

3.9 Investigation of the MOF (CRH-FeO) effect on thermal characteristics of AN/Mg/NC composite

Thermogravimetric analysis (TGA) is a thermal analysis technique that consists in measuring mass changes in a sample in a regulated atmosphere at the same time as increasing temperature. Weight loss-time and mass loss-temperature measurement (for analysis at continuous heating speed) were recorded. The findings were shown as weight lowering. TGA Q5000 IR, TA Universal Test, the molten crucible was constructed of titanium, the gas was 5.0 pure air, the temperature range 40-900°C, and the heating intensity was 10°C/min (Fig. 49). The device was used for the test of thermography.

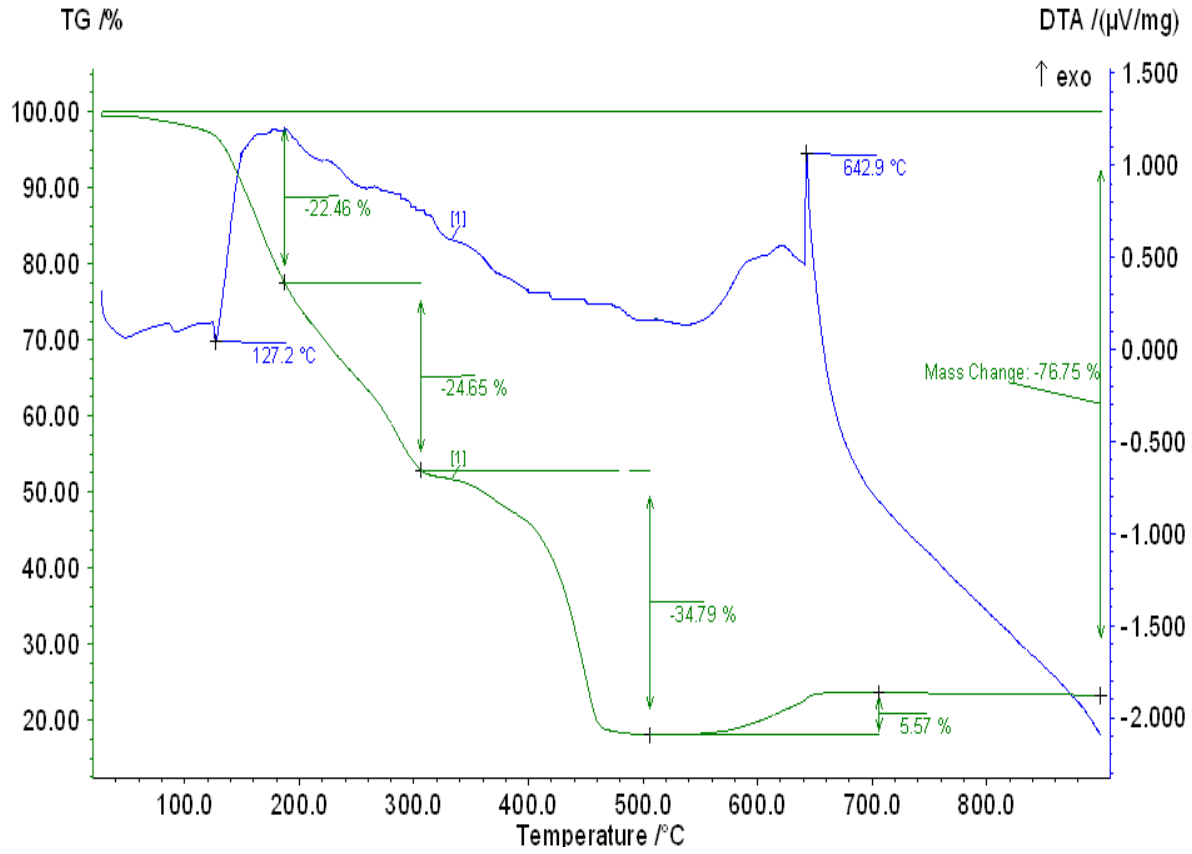

a)

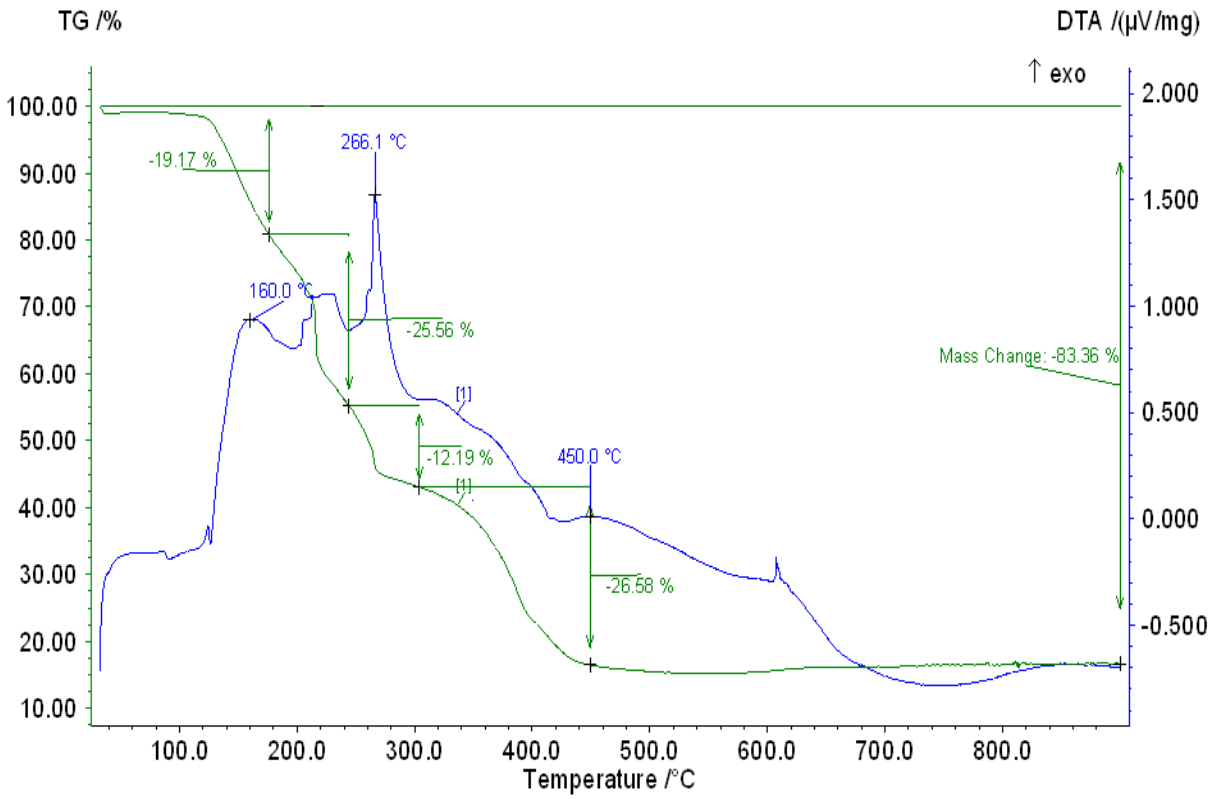

b)

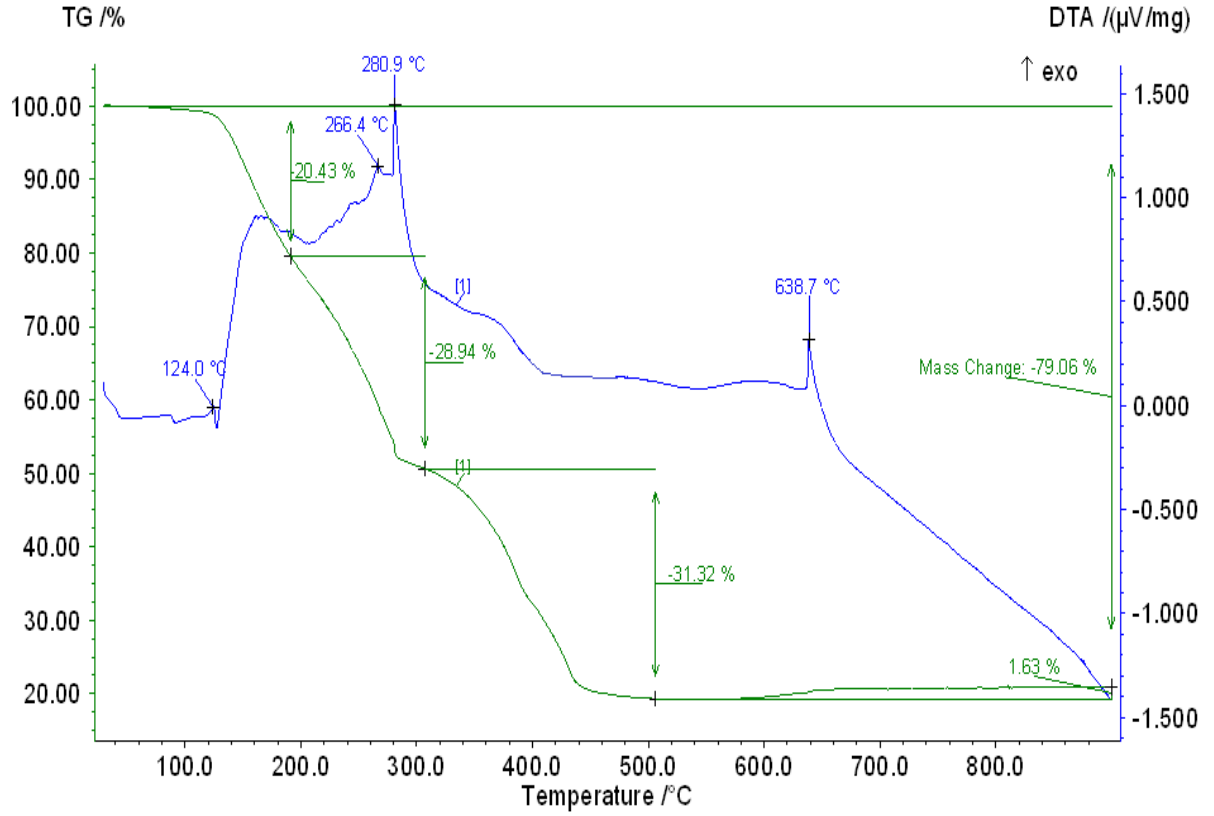

c)

Figure 49 - The results of thermogravimetric and differential thermal analysis of the composite materials: a) AN/Mg/NC, b) AN/Mg/NC/CRH, c) AN/Mg/NC/CRH-FeO

In the Fig. (49a), we investigated the condensed system AN/Mg/NC. Here, the use of ammonium nitrate as an oxidant has affected the melting point of the fuel. The melting point of magnesium decreased from 659 to 642°C. Thus, it improved the ignition system. In the Fig. (49b) AN/Mg/NC/CRH, adding activated carbon (C) to this condensed system reduces the phase exchange, melting and decomposition temperatures of ammonium nitrate. The phase exchange of ammonium nitrate ranges from 127 to 122°C, the melting point reduced from 169 to 160°C, and the decomposition temperature increased from 200 to 280°C. At the same time, carbon oxidation (266°C) occurs. Fig. 49c shows AN/Mg/NC/CRH-FeO system, in this figure, the condensed system is often used for pyrotechnic compounds (for example in colorful scale pyrotechnics) [106, 107] and detonation. To accelerate the operation of the system and its stabilization, various transition metal oxides were used. The combination of FeO with the condensed system stabilized the composition of the system. This is very effective for pyrotechnic compounds [108].

3.10 Activation energy (E_a) calculation for AN/Mg/NC/CRH-CuO and AN/Mg/NC/CRH-NiO compositions according to the Kissinger method

Fig. 50 shows such plots for 3 different samples of AN/Mg/NC/CRH mixtures decomposition with and without additives of activated CRH. The correlations of the plots *of* $ln(\beta/Tp^2)$ vs. $1/Tp$ are shown in Fig. 50 to obtain the kinetic parameters of AN/Mg/NC/CRH mixtures decomposition. As can be seen, a plot of $ln(\beta/T^2)$ against $1/T_p$ gives straight lines throughout the all investigated decomposition points for the approximation of $-E_a/R$ and A values from fitted curves. In other words, the result of the determination of basic kinetic parameters for AN/Mg/NC energetic mixture decomposition in the form of graphical plots, reflecting the slope of the heating rate constant as a function of the obtained as the maximum decomposition temperature of the system.

The determined kinetic parameters of the observed thermal decomposition of AN/Mg/NC mixtures are detailed in Table 11. All kinetic data are calculated by the Kissinger method. Based on the data shown in Table 11 there are three exothermic peaks during the decomposition of AN/Mg/NC and AN/Mg/NC/CRH mixture. As for the total amount of all exothermic peaks, the E_a of AN/Mg/NC determined by DSC data is about 90.06 kJ/mol with log A of 1.5×10^9, whereas E_a for the second mixture AN/Mg/NC/CRH is 82.8 kJ/mol with log A of 1.6×10^9 In the presence of involved MOF (CRH-CuO) additive, the values of E_a decreased lower. In particular, E_a of the AN/Mg/NC decomposition under the effects of MOF (CRH-CuO) is 81.8 kJ/mol, which were close in comparison to AN/Mg/NC/CRH mixture, respectively. Addition of activated CRH and CRH with copper oxide particles reduced the energy barrier for decomposition of AN/Mg/NC mixture up to ~10 kJ/mol. Thus, the obtained value for E_a at the addition of CRH is significantly lower than the E_a for the initial stage of the basic AN/Mg/NC mixture. Results of E_a calculations allow

concluding that copper oxides doped nonporous activated CRH as catalytic additives allowed to reduction of kinetic barrier of AN/Mg/NC mixture thermal decomposition, which is finally leads to a significant acceleration of reaction rate as a whole and shifting of initial decomposition temperature value to the low temperature areas.

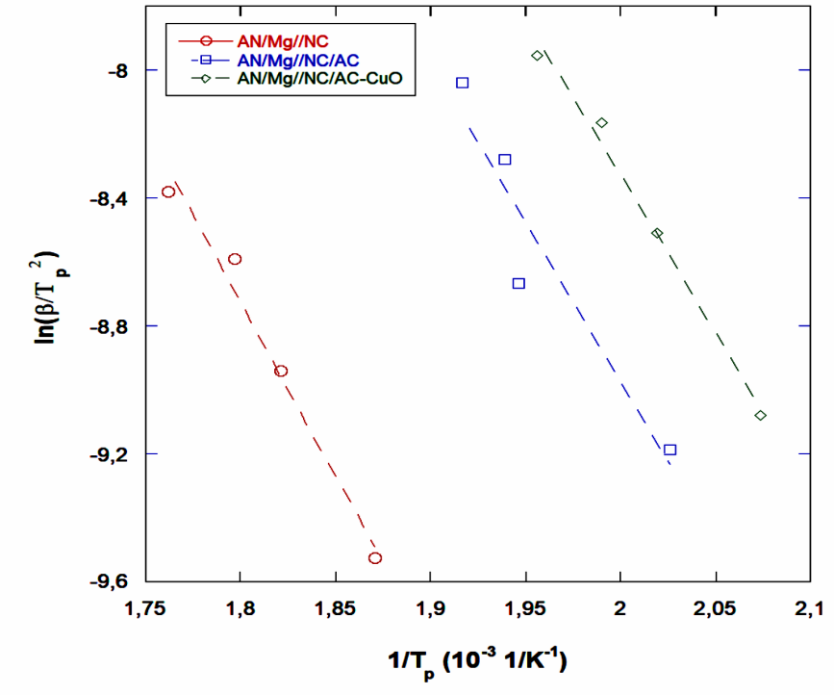

Figure 50 - Kinetics plots *(ln(ß/Tp^2)* vs. 1/*T*p) for the non-isothermal decomposition of AN/Mg/NC mixtures with and without additives of activated CRH

Table 11 - The kinetic parameters for thermal decomposition of an AN/Mg/NC, an AN/Mg/NC/AC and an AN/Mg/NC/CRH–CuO (3%) mixtures according to the Kissinger method

Sample	*Q*, J g−1	*T*max, °C (*β*=5K/min)	R^2	ln(*β*/*Tp*^{2}) vs 1/*T*	*A* (s^{-1})	*E*a, kJ/mol
AN/Mg/NC *This work*	48.4	261.43	0.90	–10.8327	$1.5*10^9$	90.06
AN/Mg/NC/CRH *This work*	54.1	220.35	0.98	–9.9587	$1.6*10^9$	82.80
AN/Mg//NC/CRH–CuO *This work*	126.14	209.05	0.97	–9.8467	$1.3*10^9$	81.87
Pure AN *Gunawan et al.* [5]	-	293.05	0.99	-12.8335	$4.55*10^7$	102.6
AN and CuO (PSAN) Simoes *et al.* [54]	-	242	-	-	$5.6*10^5$	81.4 ± 3.5
Pure AN *Koga et al.* [55]	-	260	-	-	$2.4*10^6$	90.8 ± 0.7
Pure AN *Xu et al.* [56]	-	278.92	09996	-11.22203	$3.02*10^6$	93.3
Pure AN *Brower et al.* [57]	-	260	-	-12.5001	$4.1*10^4$	118

Kinetics by Friedman Method. A more detailed kinetic assessment approach, such as the Friedman isoconversion model, could be utilized to define the decomposition process more specifically. This method has led to a different heat output of the fundamental kinetic decomposition parameters of AN/Mg/NC composites. In the presence of AC or AC-CuO determined by the isococonversional method Fig. 51 shows a comparison between E_a dependency on the conversion rate (α) for AN/Mg/NC composite.

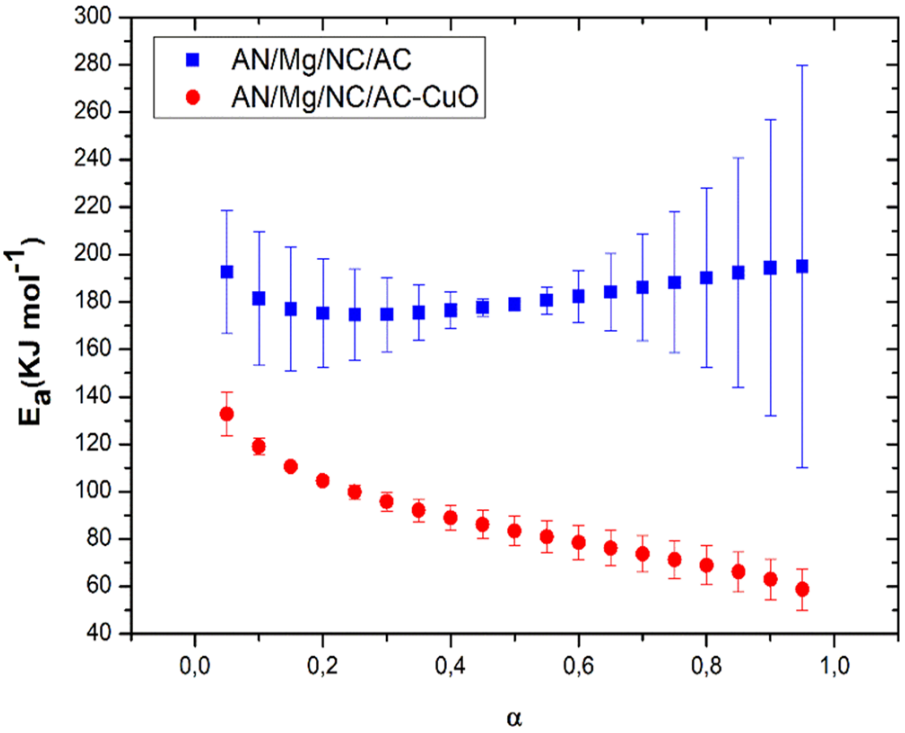

Figure 51 - Dependence of E_a on conversion rate for involved materials. (a) DSC curves of AN/Mg/NC composite with pure activated CRH. (b) DSC curves of AN/Mg/NC composite with MOF (CRH-CuO)

The initial decomposing process Ea decreases significantly under the effect of the AC-CuO catalyst (compared to pure AC). The trend line from α (132 kJ mol^{-1}) to α= 0,05 (57 kJ mol^{-1}) showed a significant decrease in Ea of AN/Mg/NC with AC-CuO, suggesting the catalytic activity of CuO particles. Specimens with pure AC show a constant trend in all points in the Ea of AN/Mg/NC calculated from DSC curves, and E_a is nearly independent of the change. The pure AC samples have a consistently high E_a value roughly 192 kJ mol^{-1}. The inert AC can be justified and it makes a small contribution to thermal release of composite thermal breakdown. The amount of E_a has a large size (25.8 kJ mol^{-1}) at the beginning and the end of the reaction (84.7 kJ mol^{-1}) in the decomposition of AN/Mg/NCs with pure AC. In comparison the Ea spread in the induction period is approximately less (3.2 kJ mol^{-1}) and only increases when it is close to decomposition (8.7 kJ mol^{-1}) in the presence of the AC-CuO catalyst during AN/Mg/NC decomposition. Fig. 51 and Table 2 indicate that the addition of pure AC definitely showed lowering of E_a for

AN/Mg/NC composite descomposition for both kinetic strategies (Kissinger and Friedman) used to evaluate E_a.

The values of composites can be determined by the DSC values measured at each heating rate in determining the activation (E_a) of AN/Mg/NC/CRH-NiO compositions with β=5, 10, 15 and 20 K·min^{-1}. Tables 12,13,14 shows the calculated activation energy (E_a) according to the Kissinger method [109-111].

Table 12 - Calculation of the activation energy (E_a) according to the Kissinger method for the composition AN/Mg/NC

T_{max}, ^{0}C	$1/T_{max}$	Heating rate, K/min	ln(β/T^2)
261.43	1.870627	5	-9.52688
276.05	1.820830	10	-8.94216
283.52	1.796396	15	-8.58991
294.56	1.761463	20	-8.37838
	slope	-10.8327	
	E_a	90062.32	J/mol
		90.06	kJ/mol

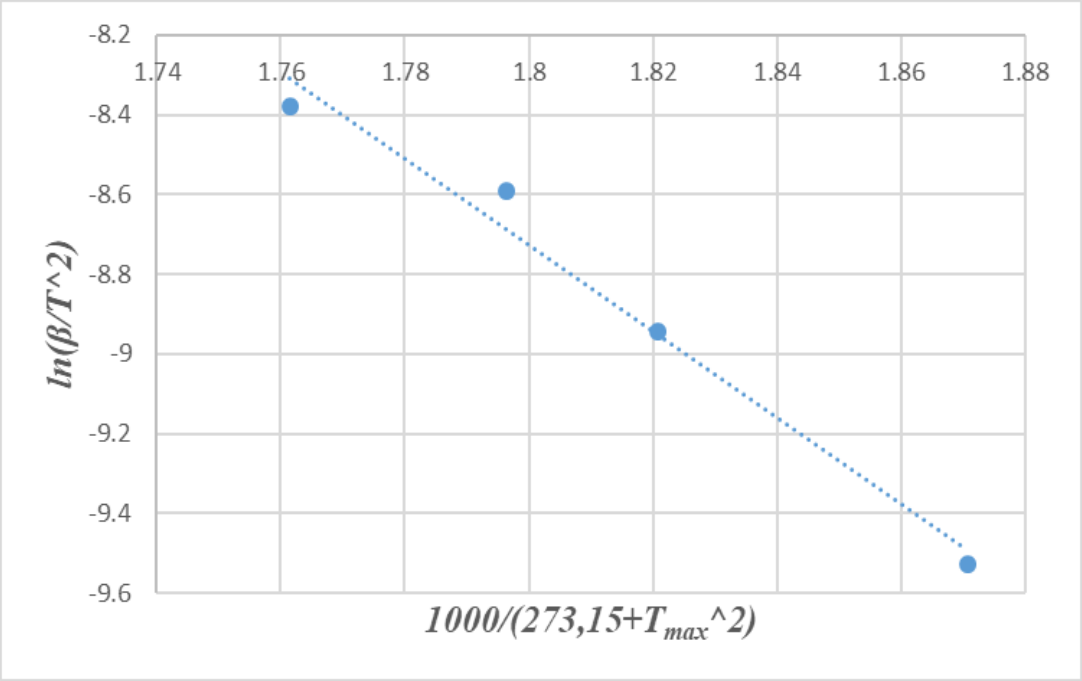

Figure 52 - Kissinger plot of AN/Mg/NC composition

Fig. 52 presents the results of calculations in the form of graphs reflecting the slope of the heating rate constant as a function of the variable obtained as the maximum decomposition temperature. As shown by the results of calculations, obtained experimental data, the activation energy of the composition AN/Mg/NC was 90.06 kJ/mol according to the Kissinger method.

Table 13 - Calculation of the activation energy (E_a) according to the Kissinger method for the composition AN/Mg/NC/CRH

T_{max}, °C	$1/T_{max}$	Heating rate, K/min	ln(β/T^2)
220.35	2.026342	5	-9.18661
240.60	1.946472	10	-8.66839
242.61	1.938886	15	-8.27949
248.52	1.916921	20	-8.03973
	slope	-9.9587	
	E_a	82795.65	J/mol
		82.80	kJ/mol

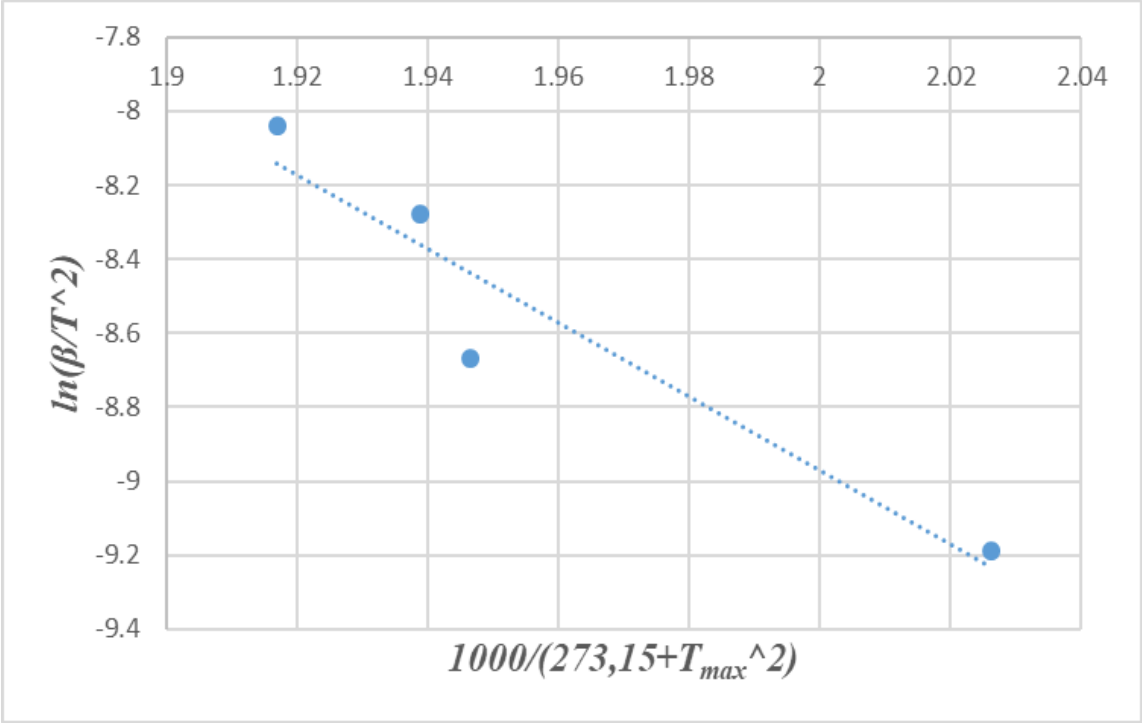

Figure 53 - Kissinger plot of AN/Mg/NC/CRH composition

In Fig. 53, as shown by the results of calculations obtained from experimental data, the value of the activation energy of the composition of AN/Mg/NC/CRH according to the Kissinger method was 82.80 kJ/mol.

Table 14 - Calculation of the activation energy *(E_a)* according to the Kissinger method for the composition AN/Mg/NC/CRH-NiO

T_{max}, °C	$1/T_{max}$	Heating rate, K/min	ln(β/T^2)
218,21	2,035167	5	-9,1672
239,82	1,949431	10	-8,66193
238,95	1,952743	15	-8,24923
246,72	1,923557	20	-8,02525
	slope	-9,52882	
	E_a	79221,62	J/mol
		79,22	kJ/mol

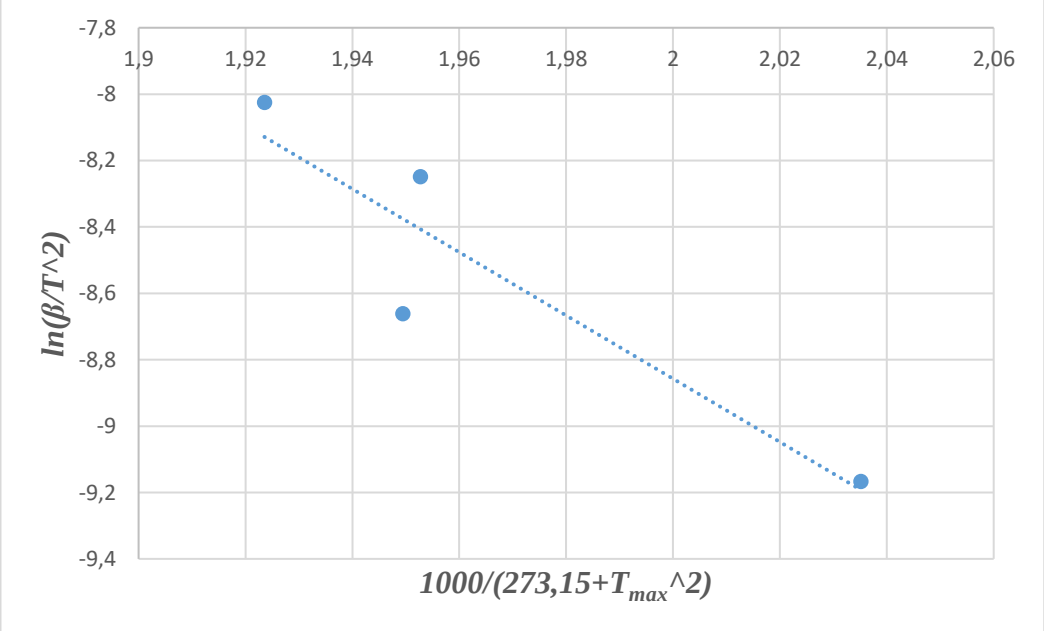

Figure 54 - Kissinger plot of AN/Mg/NC/CRH-NiO composition

Fig. 54 shows the results of calculations obtained from experimental data, the value of the activation energy of the AN/Mg/NC/CRH-NiO composition according to the Kissinger method was 79.22 kJ/mol.

The activation energy of composition AN/Mg thermal decomposition was reduced by adding activated carbon and NiO. These results show that the thermal decomposition of AN/Mg/NC gas generator can be improved by activated carbonized rice husk and NiO.

CRH and NiO additives reduce the activation energy of the AN/Mg/NC composition from 90.06 kJ/mol to 82.80 kJ/mol and 79.22 kJ/mol, respectively. Also they improve the decomposition reactions in the condensed phase, however, the main effect with the addition of NiO to the AN/Mg/NC/CRH-based propellants can be assumed to take place in the gas phase reaction zone. NiO can be the catalyst for our AN-based propellant system.

3.11 Combustion characteristics

3.11.1 The combustion–wave temperature profile of self–deflagrating an AN/Mg/NC/CRH mixture

Fig. 55 shows the combustion–wave temperature profile of an AN/Mg/NC/CRH mixture based on the experimental results in the ambient air. The combustion model of concern, a temperature profile of self–deflagrating AN/Mg/NC/CRH mixture in the ambient air. The temperature was measured by the K-type thin (50µm) thermocouple – Chromel/Alumel (Chromel: 90% nickel and 10% chromium/Alumel: 95% nickel, 2% manganese, 2% aluminum and 1% silicon). The thermocouple grade wire: 200°C to +1260 °C and limits of error: ± 1.1°C or 0.4%. The entire temperature profile is conveniently segmented into three working zones.

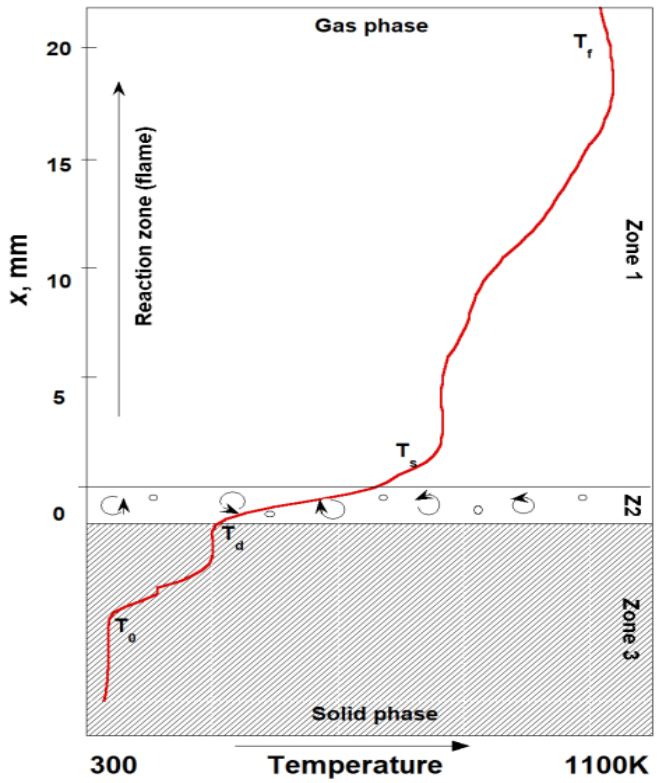

Figure 55 - The combustion–wave temperature profile of self–deflagrating an AN/Mg/NC/CRH mixture (in ratio:75/21.8/0.3/2.9)

Zone 1 shows the solid phase where chemical reactions do not occur, the temperature of the sample in slowly increases depending on the approach the boundary of Zone 2. The temperature value increase from the initial temperature (T_0 = 300 K) of the sample to the decomposition temperature (T_d = 570 K).

Zone 2 shows an intermediate zone (gas-liquid layer) where the already molten solid phase partially transfers into the gaseous phase. The combustion temperature rises from the decomposition temperature T_d to the combustion surface temperature Ts, gas-liquid layer zone temperature in a range of 570–770 K. The thickness of the gas-liquid layer (zone 2) is very small [113], because the sample burns without visible foaming as in the case of RDX burning [114].

The decomposition products which are formed in zone 2, are ejected from the surface and react to each other or react with molecules in the ambient air (zone 3) [115,116]. Zone 3 shows the gases reaction zone with a temperature value between 800 – 1100 K. In this area held the main process of oxidation and dissociation of products takes place with the formation of a flame.

3.11.2 AN/Mg energetic mixture combustion with/without MOF (CRH–CuO) and MOF (CRH-NiO)

To the successful application of an EMs, there are linear burning rate and the value of pressure exponent should be easily controllable. The value of *n* must be less than 0.6, for rocket propellants, and higher than 1.0, for gun propellants applications [112]. In the process of burning composites, the following reaction may occur:

$$NH_4NO_3 + Mg \rightarrow MgO + N_2 + 2H_2O \quad (2)$$

$$NH_4NO_3 + Mg + C \rightarrow MgO + N_2 + NO_2 + NH_3 + CO_2 + H_2O \quad (3)$$

$$NH_4NO_3 + Mg + C + CuO \rightarrow MgO + N_2 + NO_2 + NH_3 + CO_2 + H_2O \quad (4)$$

In Fig. 56 shown the results of experiments on combustion of: (a) an AN/Mg/NC mixture (in ratio: 75/24.7/0.3); (b) an AN/Mg/NC/CRH mixture (in ratio: 75/21.8/0.3/2.9); (c) an AN/Mg/NC/CRH–CuO mixture (in ratio: 75/21.7/0.3/3.0), at initital pressure p_0 = 3.5 MPa under N_2 atmosphere.

Fig. 56a demonstrates the combustion wave propagation in the AN/Mg/NC without any additives. The burning rate (r_b) of mixture r_b = 10.27 mm/s^{-1} at initial pressure p_0 = 3.5 MPa. Combustion occurs with bright light emission related to magnesium burning behavior. The addition of pure AC (Fig. 56b) showed an approximately small effect on the AN/Mg/NC energetic mixture combustion behavior, but despite this, the linear burning rate is increased about r_b=17.53 mm/s-1 at initial pressure p_0 = 3.5 MPa.

It is obvious, that the activated CRH promotes the combustion reaction of this energetic mixture. The combustion propagated with intensive light emission and the release of a small number of visible gases. The highest r_b result was achieved in the presence of CRH–CuO. Inclusion of CRH with nanosized metal oxide (CuO) had shown a significant enhancement of AN/Mg/NC mixture combustion character, the burning rate is increased about 2 times (r_b =20.46 mm/s) at initial pressure p_0=3.5 MPa.

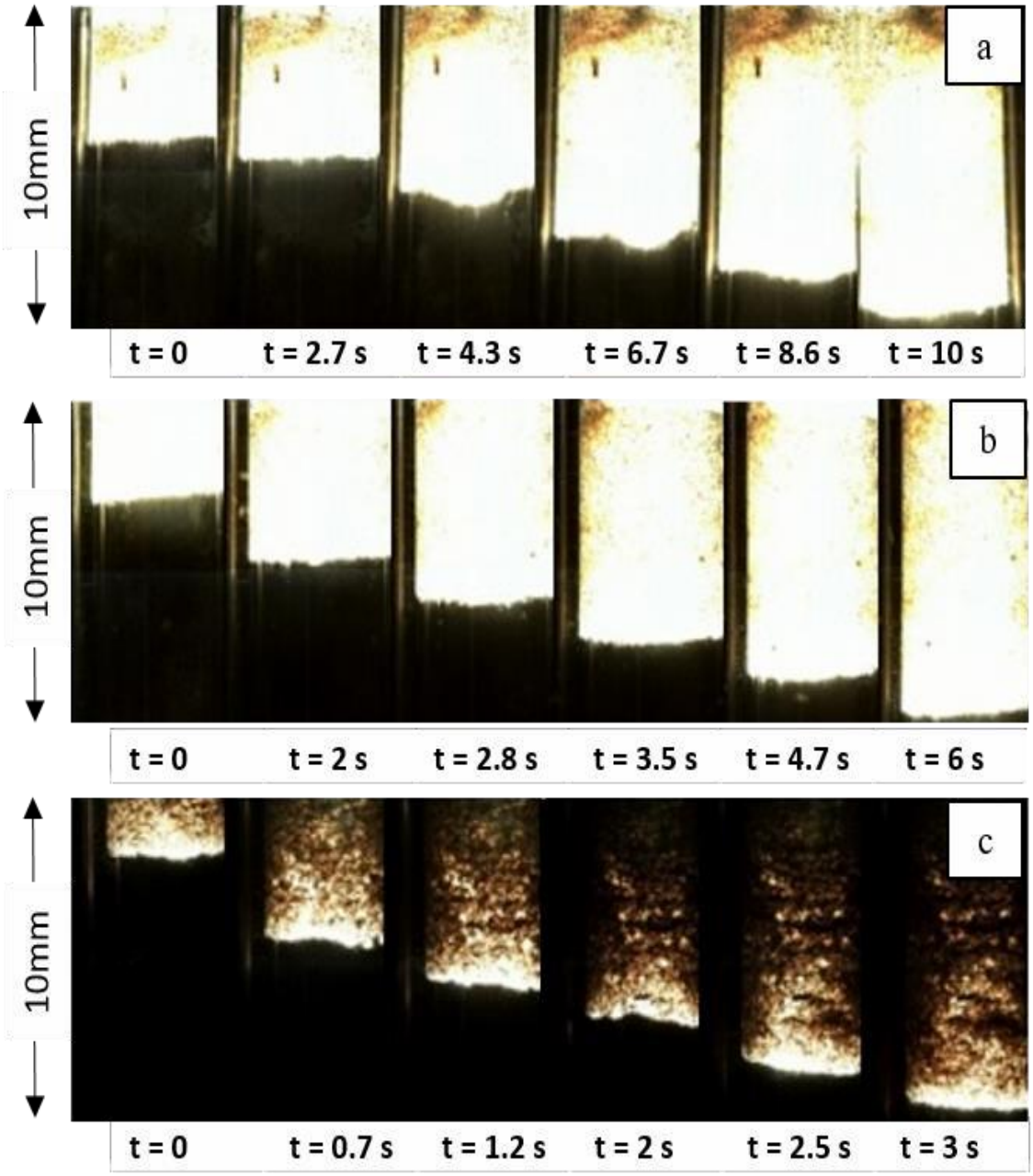

Figure 56 - The flame propagation processes of AN/Mg/NC/CRH–CuO (a), AN/Mg/NC/CRH (b) and AN/Mg/NC (c) energetic composites in the combustion chamber at an initital pressure of p_0 = 3.5 MPa

Fig. 57 shows the propagation of combustion wave at the AN/Mg/NC/CRH–CuO mixture burning in the high-pressure chamber at the initial pressures: 1 MPa, 2 MPa and 3 MPa under N_2 atmosphere. It is seen that as increasing the initial pressure enhances the propagation velocity of the combustion wave. At an initial pressure p_0 = 1 MPa (Fig. 57a), there is a slowest (r_b = 11 mm/s^{-1}) uniform combustion with the release of a small amount of visible gas. Increasing the initial pressure to p_0 = 2 MPa and 3 MPa (Fig. 57b and 57c) enhances the burning rate of AN/Mg/NC/CRH–CuO mixture to r_b = 14.96 mm/s^{-1} and r_b = 17.67 mm/s^{-1} respectively.

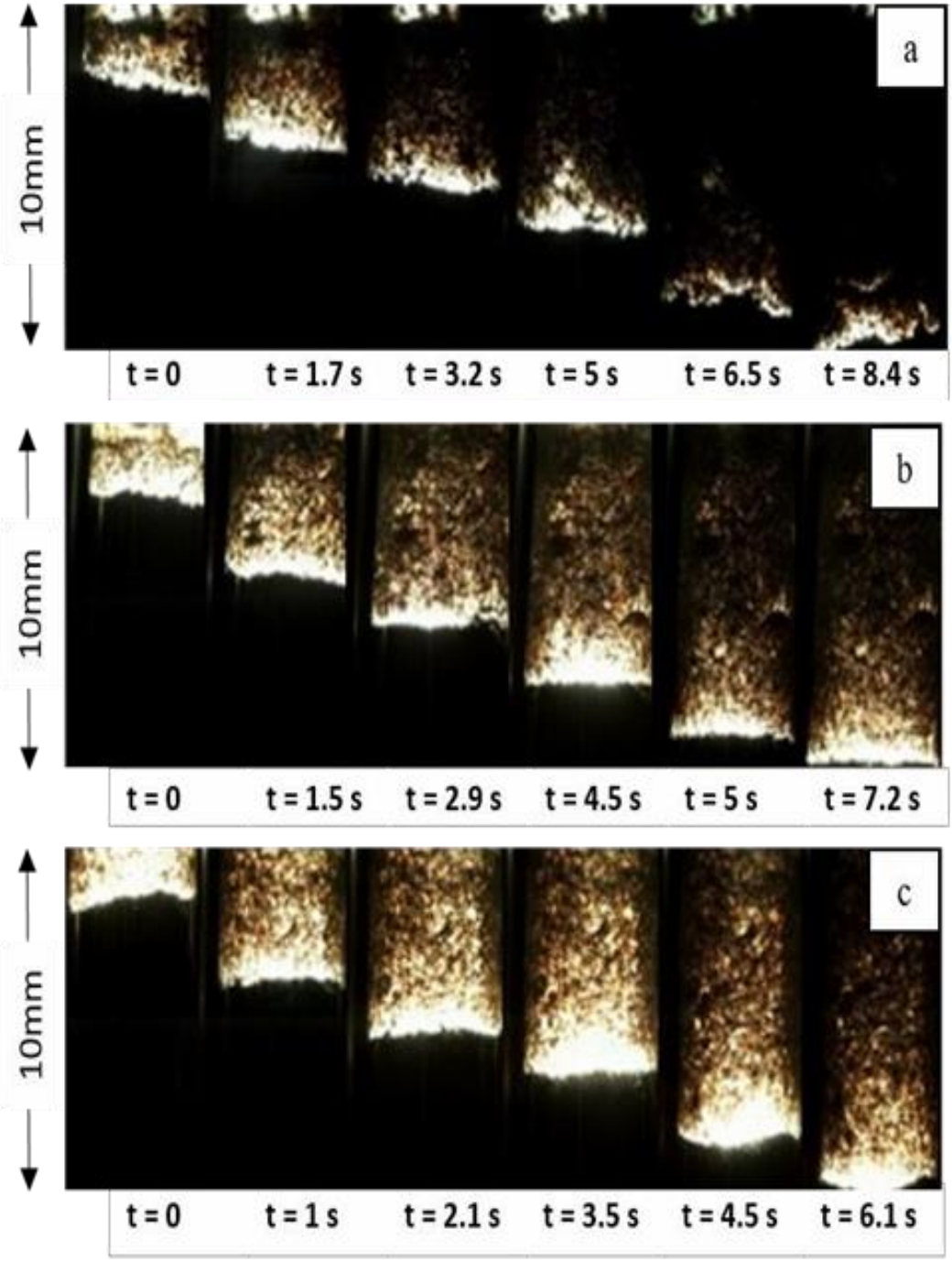

Figure 57 - Combustion wave propagation in the AN/Mg/NC/CRH–CuO mixture in the solid phase: (a) initial pressure p0 = 1 MPa; (b) initial pressure p0 = 2 MPa; (c) initial pressure p_0=3 MPa

Fig. 58 shows a comparative data on the linear burning rate as a function of the initial pressure (MPa) for an AN/Mg/NC, AN/Mg/NC/CRH and AN/Mg/NC/CRH–CuO mixtures under N_2 atmosphere. In comparison with the basic mixture, AN/Mg/NC with CRH additives burns 2 times higher within the whole pressure interval (Fig. 58). The highest burning rate result (r_b=20.46 mm/s^{-1} at initial pressure p_0=3.5 MPa) was achieved in the mixture with the presence of CuO contain CRH. The addition of pure CRH is also provided a significant enhancement of AN/Mg/NC mixture burning rate. Based on the results, there is a

question concerning the role of MOF (CRH–CuO) on combustion behavior of AN/Mg/NC mixture. However, the combustion of mixtures with or without adds has a low burning rate and pressure exponent (n = 0.53-0.42), which is responsible for the low sensitivity to mechanical and shocks impacts. A combination of CRH with copper oxide can make the AN/Mg/NC mixture burn at a speed of over 20 mm s^{-1} show high value of burning rate coefficient (a=11.46) and low value of pressure exponent n = 0.42).

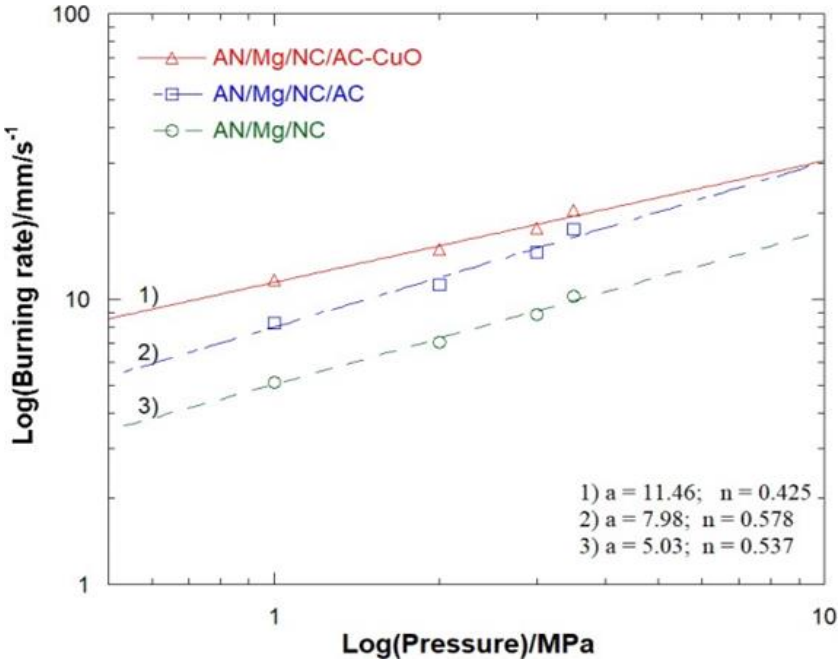

Figure 58 - Dependencies of the burning rates of composites AN/Mg/NC, AN/Mg/NC/CRH and AN/Mg/NC/CRH–CuO on the pressure

In summary, it can be assumed that the inclusion of the MOF (CRH–CuO) in the system of the energetic mixture based on AN/Mg/NC has improved many combustion characteristics. The effect of copper oxide on the combustion of composition has a catalytically combustion behavior. The catalyst CuO can increase the oxidation reaction velocity of fuel (magnesium) by the impact on the oxidizer decomposition character, and in the final, reached the high combustion velocity of energetic mixture. It can be concluded that the addition of CRH allows controlling the linear burning rate and pressure exponent values of the investigated energetic mixture.

AN/Mg energetic mixture combustion with/without MOF (CRH–NiO)

Fig. 59 shows the mechanism of AN/Mg composites combustion in the chamber at 1 MPa, 2 MPa, 3 MPa and 3.5 MPa pressures and depending on the increase in pressure, the burning rate also increased in the form of a line.

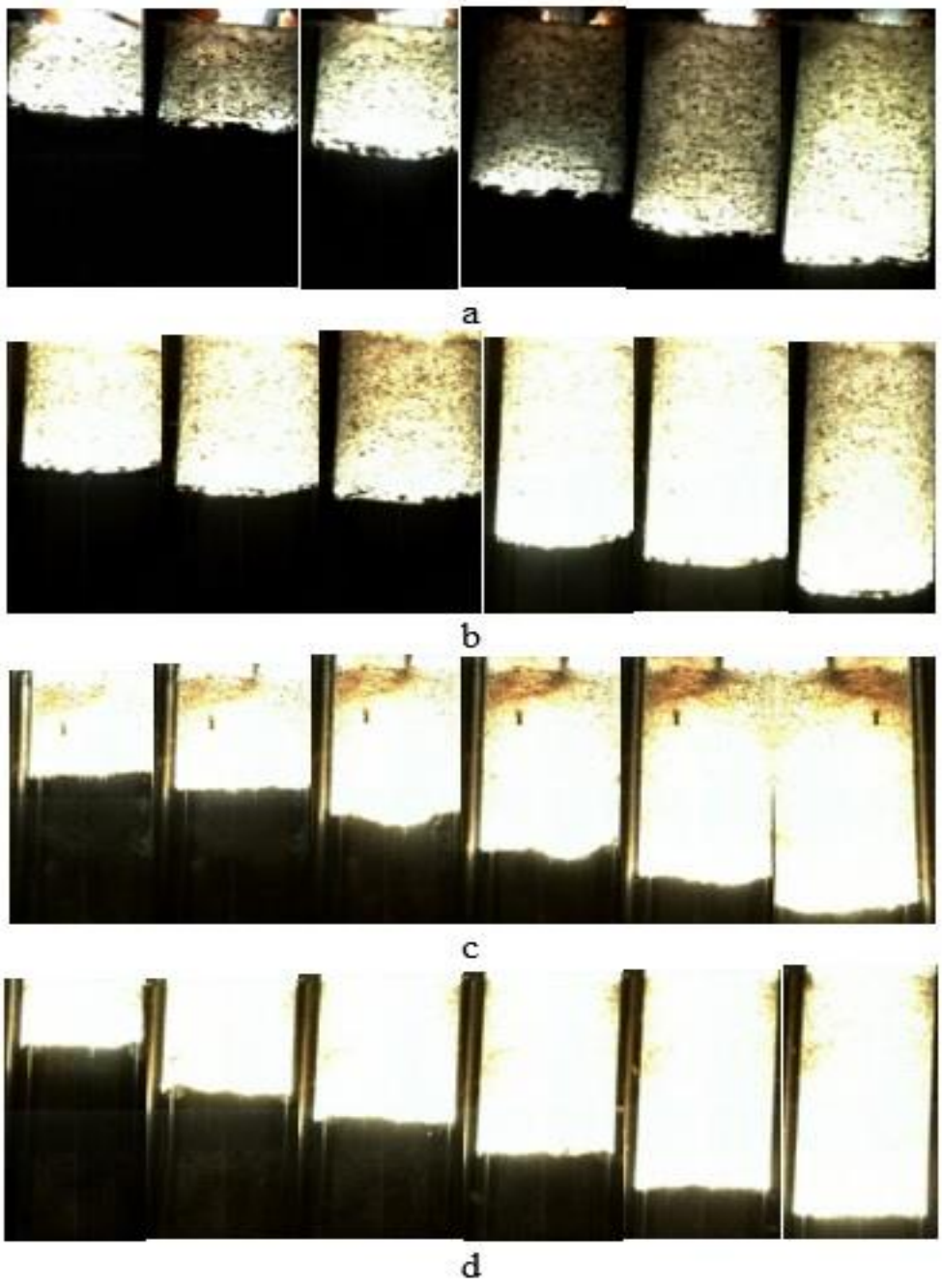

Figure 59 - Burning images of AN/Mg composites at pressures (a) - 1 MPa, (b) - 2 MPa, (c) - 3 MPa and (d) - 3.5 MPa

Fig. 60 shows the mechanism of AN/Mg/CRH composites combustion in the chamber at pressure of 1 MPa, 2 MPa, 3 MPa and 3.5 MPa.

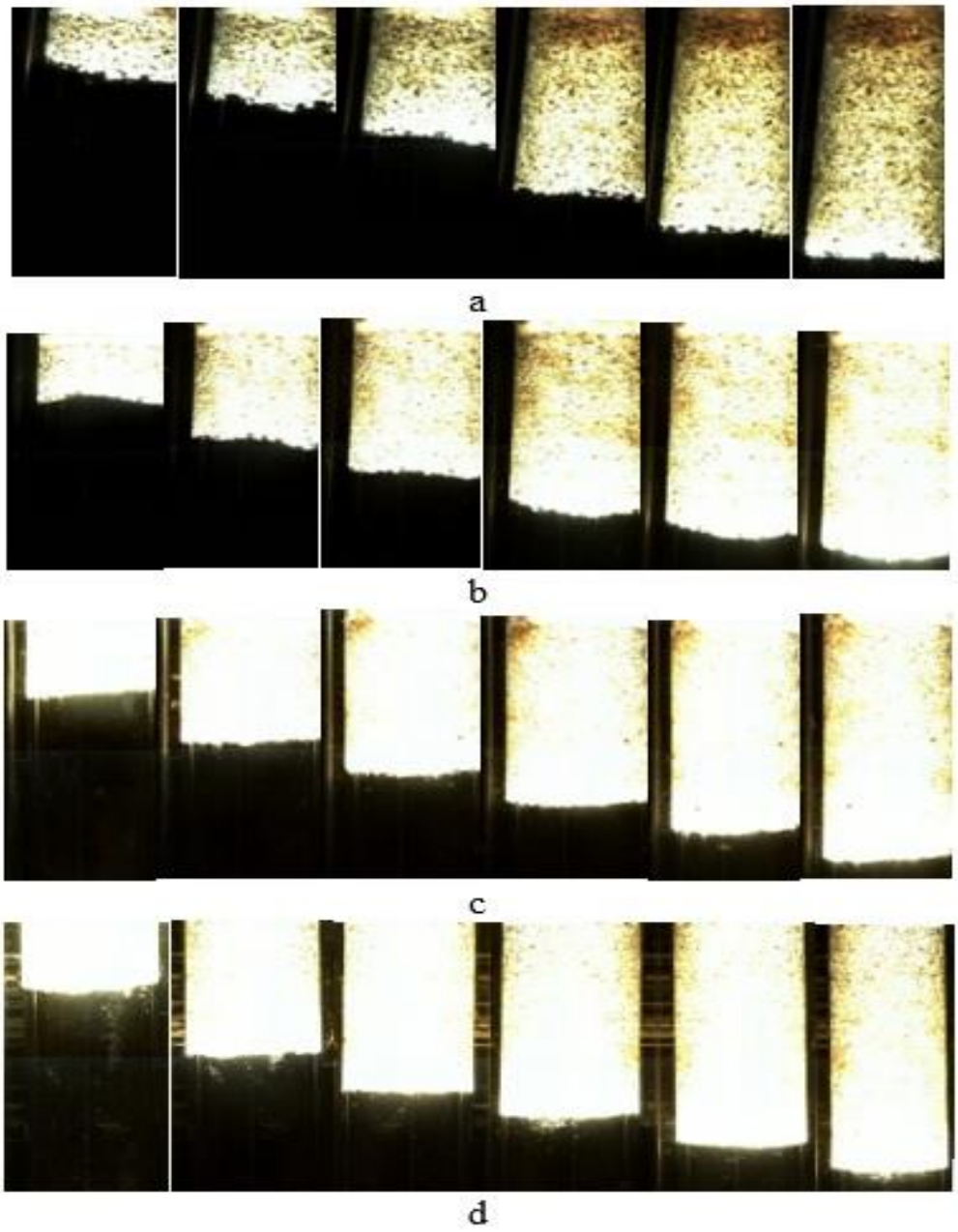

Figure 60 - Burning images of AN/Mg/CRH composites at pressures (a) 1 MPa, (b) 2 MPa, (c) 3 MPa and (d) 3.5 MPa

Fig. 60 shows a linear increase in combustion rates due to a linear increase in pressure on AN/Mg/CRH composites. Compared to the AN/Mg/NC system, the lower pressure limit was reduced, and the burning rates increased the catalytic effect of activated carbon. According to the experimental results, it can be seen that the propellants were completely burned at high combustion rates.

Fig. 61 shows the mechanism of AN/Mg/NC/CRH-NiO composites combustion in the chamber at a pressure of 1 MPa, 2 MPa, 3 MPa and 3.5 MPa.

In Fig. 61 also increases in burning rate due to increases in pressure for AN/Mg/NC/CRH-NiO. Compared with the AN/Mg system, the pressure deflagration limit was lowered and the burning rates increased by the catalytic effect of NiO.

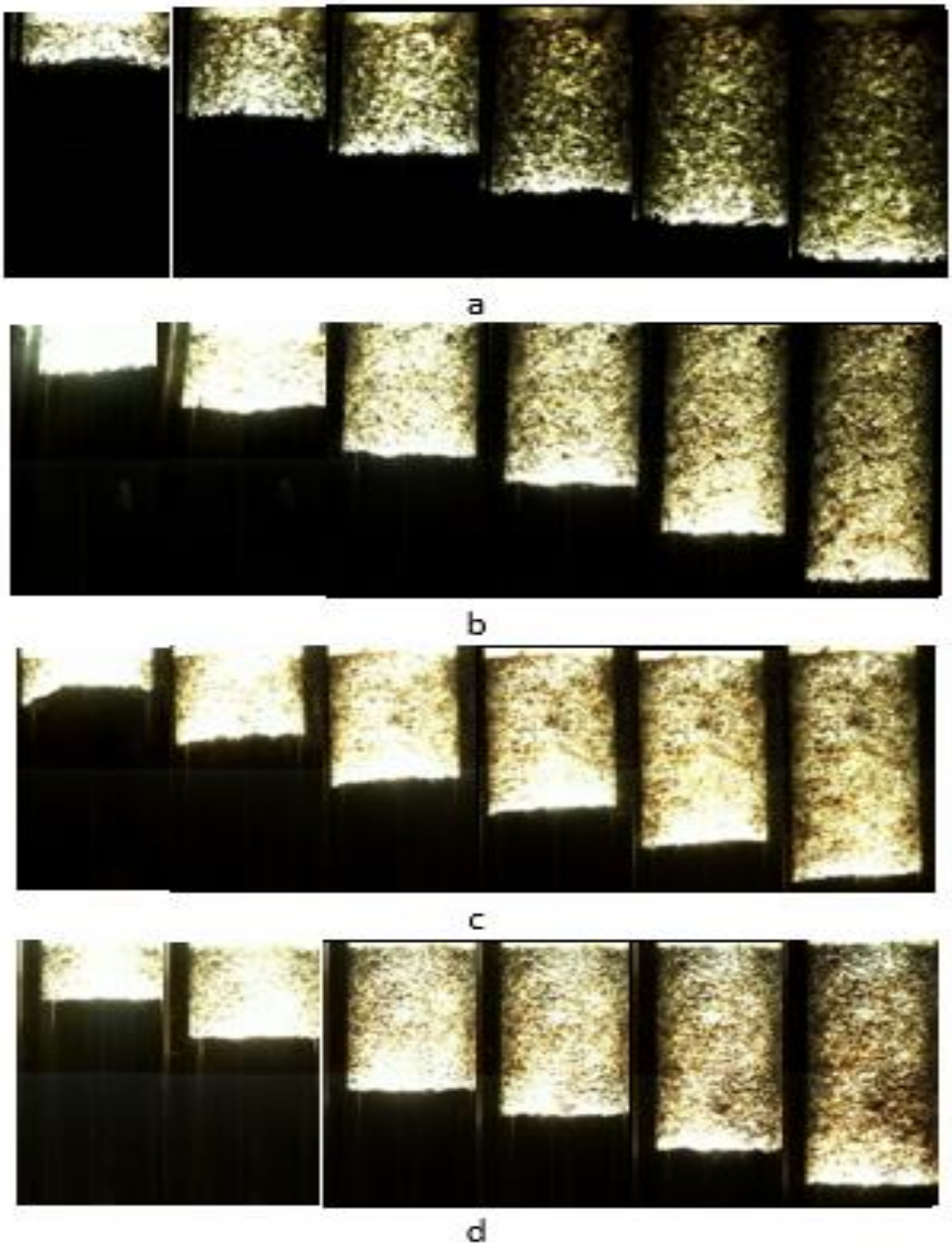

Figure 61 - Burning images of AN/Mg/CRH/NiO composites at pressures (a) - 1 MPa, (b) - 2 MPa, (c) - 3 MPa and (d) - 3.5 MPa

By adding activated CRH and NiO, the burning rate of the propellant composites increased by 3-4 $mm \cdot s^{-1}$ in average at each pressure.

Characteristics of the burning rates of composite propellants AN/Mg/NC, AN/Mg/NC/CRH and AN/Mg/CRH-NiO at different pressures are shown in Fig. 62.

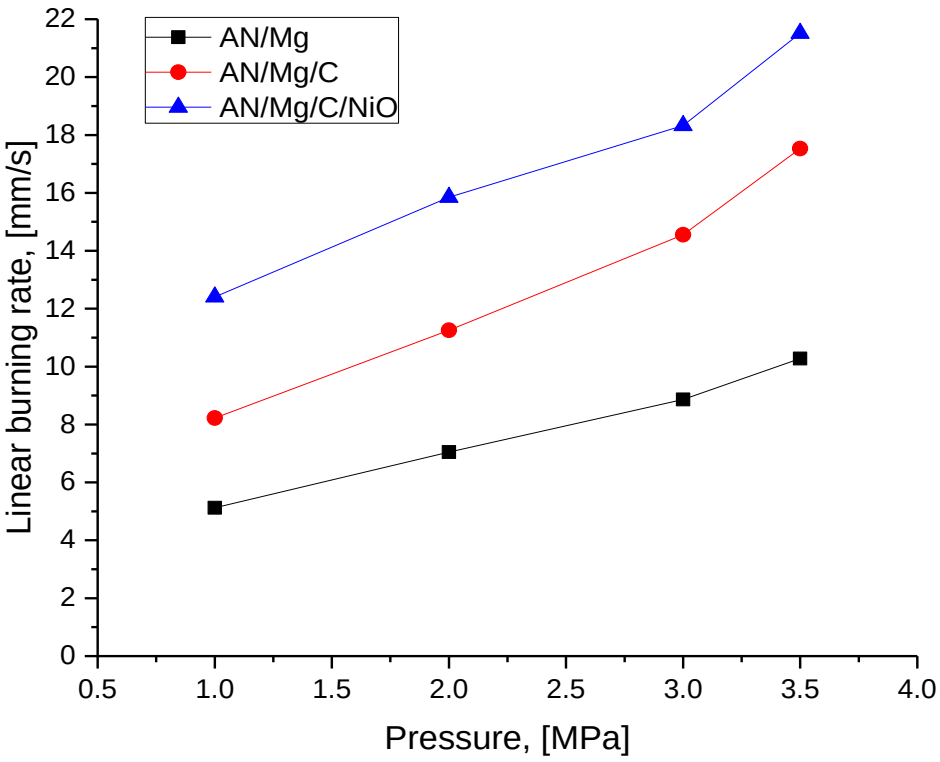

Figure 62 - Dependencies of the burning rates of AN/Mg, AN/Mg/CRH and AN/Mg/CRH-NiO composites on the pressure

Table 15 - The burning rates (mm/s) of composites the dependencies on the pressure

Pressure, MPa	AN/Mg/NC/CRH	**AN/Mg/NC/CRH**	AN/Mg/NC/CRH-TiO	AN/Mg/NC/CRH-Zr_2O	AN/Mg/NC/CRH-NiO	**AN/Mg/NC/CRH-CuO**
1	5.126	8.225	9.073	9.157	10.422	11.658
2	7.046	11.254	10.175	10.875	13.615	14.968
3	8.862	14.557	14.881	15.463	16.298	17.668
3,5	10.067	17.531	17.706	17.990	19.176	20.468

Table 15 demonstrates the dependencies of burning rates of studied composites with various metal oxides in relation to various pressures. Among these composites, AN/Mg/NC/CRH-CuO composite showed the highest burning rate (addition of nanosized CuO low the thermal decomposition temperature of ammonium nitrate from 276 to 209°C almost lower for 60°C) for that reason reaction was provided faster.

3.11.3 Combustion of AN/Mg/NC/AC-FeO MOFs compositions

Fig. 63 shows the phenomena of combustion of AN/Mg/CRH-based activated carbon compositions in the atmospheric air. Activated carbon has been considered as a technological additive capable of working as a promotion agent which has a high activity, high specific surface area and good recovery ability.

It should be noted, that the combustion system is stable and has a laminar flame, accompanied by the release of a large amount of heat with a combustion temperature of approximately 1100°C, and has no solid combustion products.

Table 16 shows the results of the combustion temperature and combustion rate of composites based on activated CRH.

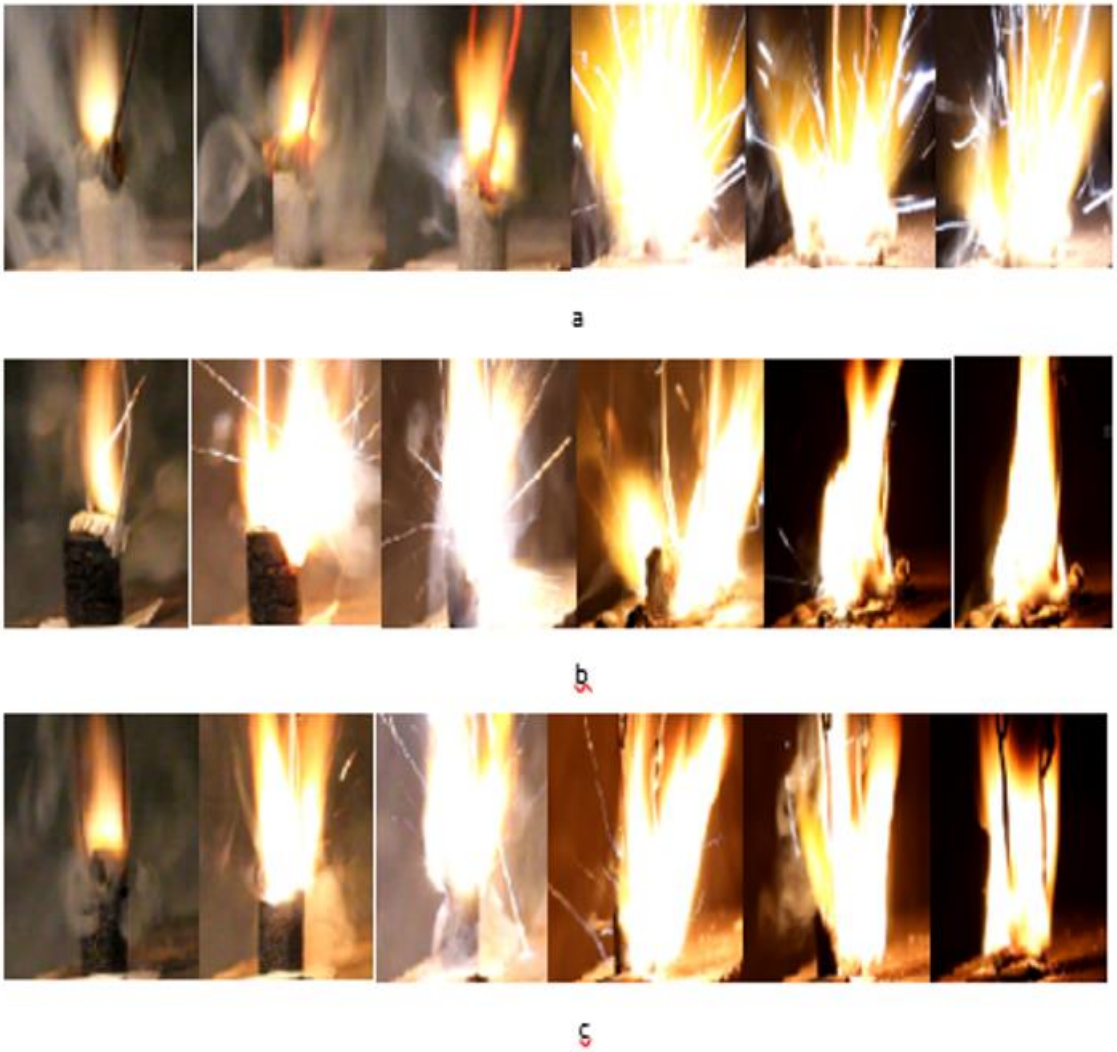

Figure 63 - Burning of pyrotechnic compositions: a) AN/Mg/NC, b) AN/Mg/NC/CRH, c) AN/Mg/NC/CRH-FeO

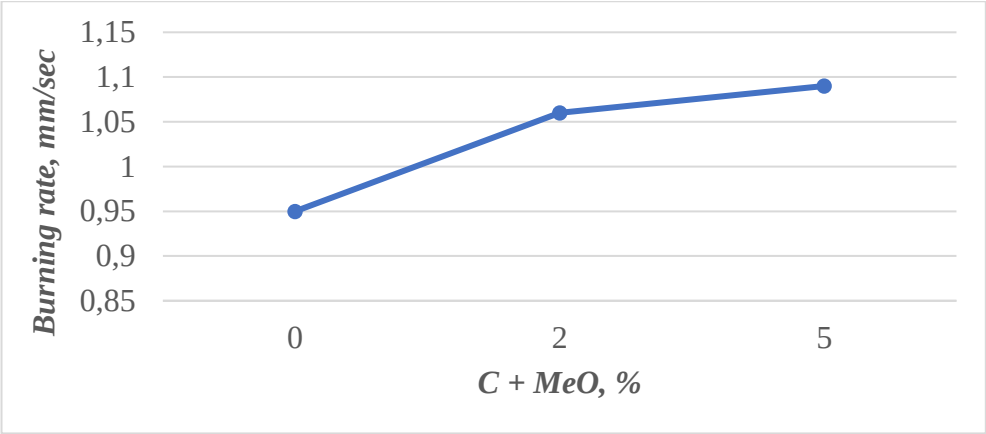

Figure 64 - Dependencies of the burning rates of AN/Mg/NC/FeO on the concentration CRH+MeO, %

Analysis of the results showed an increase in the burning rate composite compositions by adding different concentrations of activated carbons with metal oxides (Fig. 64). Analysis of the linear combustion rate of this sample showed the highest result.

Table 16 - The combustion temperature and the burning rate of activated CRH compositions

№	Samples	Ratio, %	T, ^{0}C (combustion temperature)	U [mm/s] Burning rate
1	AN/Mg/NC	75/24.7/0.3	906	0,950
2	AN/Mg/NC/CRH	75/21.8/0.3/2.9	944	1,062
3	AN/Mg/NC/CRH-FeO	75/21.7/0.3/2.9/0.1	1070	1,097

Application of the activated CRH as a fuel for the pyrotechnic compositions increases the burning rate and condensed system reduces the phase exchange, melting and decomposition temperatures of ammonium nitrate. Addition of metal oxides (FeO) stabilizes the composition of the system and increases the burning rate significantly.

It can be concluded that, activated CRH and multilayer graphenes (according to the results of SEM, Raman, BET) have many reactive centers on the surface in the form of pores and defects, free atoms at corners and faces, and are also characterized by a large specific surface. It is believed that on the structural inhomogeneities, defects and pores of carbon, active centers are formed that promote chemical processes. It can be assumed that during the decomposition of ammonium nitrate in the presence of activated carbons, heat accumulation occurs precisely in these centers, which, in turn, raises the temperature of the entire system. The above factors undoubtedly play a role in increasing the rate of oxidation and the burning rate of fuel.

CONCLUSION

The main results of this study:

1. Activated carbon-based MOF (CRH/Me_xO_y) metal-organic frameworks have been created based on carbonized rice husk and transition metal oxide nanoparticles, which were first used as a combustion catalyst in pyrotechnic compositions.

2. The effect of CRH doped with CuO on the combustion AN/Mg/NC based energetic mixture was investigated. The decomposition kinetics and combustion characteristics of the mixture with additives have been investigated using a DSC technique and a high-pressure combustion chamber. Under the effect of CRH-CuO the behavior of AN/Mg/NC mixture decomposition changed from the three–stage character into two–stages. After adding of CRH–CuO, the heat release is increased from 1.2 to 7.2 mW. The addition of AC in energetic mixture shift exothermic peaks to low temperatures side and decrease the onset decomposition temperature in range from 276 to 209°C.

3. It was found that the additives MOF (CRH-CuO) provide the pyrotechnic composition AN/Mg/NC with a high burning rate of 11.6 to 20.5 mm/s at an initial pressure in the system of 1 to 3.5 MPa, while the calculated value of the indicator pressure n is in the range of 0.53-0.42. From the results obtained, an important conclusion follows that the addition of MOF provides the opportunity to significantly increase the burning rate of the pyrotechnic composition without the transition of the combustion process to explosive mode.

4. It was established that the developed pyrotechnic compositions AN/Mg/NC/CRH/Me_xO_y are highly energy-efficient materials suitable for direct ignition by laser radiation. The developed combustible composition does not require the addition of optical sensitizers to ensure stable ignition by laser radiation, which means the preservation of its chemical properties. The pyrotechnic composition AN/Mg/NC/CRH/CuO stably ignites at a laser energy of ≥4.35 J (without MOF, the laser energy was 25.97 J), the ignition delay time is 506 ms (without MOF, the ignition delay time was 902 ms).

5. It was revealed that the additives MOF (CRH/Me_xO_y) have a direct effect on the decomposition mechanism of the pyrotechnic composition AN/Mg/NC and reduce its activation energy to 8 kJ/mol.

REFERENCES

1. Murray J.S. Energetic Materials: Part 1. Decomposition, Crystal and Molecular Properties (University of New Orleans). From the series: Theoretical and Computational Chemistry, Volume 12. Elsevier: Amsterdam. 2003. – P.466.
2. Bakulin V.N., Dubovkin N.F., Sorokin V.A. and other. Powerful fuel for aviation and rocket engines. M.: Physmathlit, 2009. – P.400.
3. Sheremetev A. B. Energy materials on the base of heterocycles. Chemistry of heterocyclic compounds 2017, 53 (6/7), 629.
4. J. J. Perry Iv, J. A. Perman and M. J. Zaworotko, Chem Soc Rev., 2009, 38, 1400-1417.
5. S. Zhang, X.-Y. Liu, Q. Yang, Z.-Y. Su, W.-J. Gao, Q. Wei, G. Xie, S.-P. Chen and S.-L. Gao, Chem.-Eur. J., 2014, 20, 7906-7910.
6. O. S. Bushuyev, G. R. Peterson, P. Brown, A. Maiti, R. H. Gee, B. L. Weeks and L. J. Hope-Weeks, Chem. Eur. J., 2013, 19, 1706-1711.
7. X. Liu, Q. Yang, Z. Su, S. Chen, G. Xie, Q. Wei and S. Gao, RSC Adv., 2014, 4, 16087-16093.
8. Chandan Dey, Tanay Kundu, Bishnu P. Biswal, Arijit Mallick and Rahul Banerjee. Crystalline metal-organic frameworks (MOFs): synthesis, structure and functionActa Crystallographica Section B. Structural Science, Crystal Engineering and Materials. -2014. V.70. P.3–10.
9. Shenghua Li, Yuan Wang, Cai Qi, Xiuxiu Zhao, Jichuan Zhang, Shaowen Zhang and Siping Pang*. 3D Energetic Metal–Organic Frameworks: Synthesis and Properties of High Energy Materials // Angew. Chem. Int. Ed. –2013. P.1 – 6. Vol. 52.
10. Shibashis Halder, Pritam Ghosh, Corrado Rizzoli, Priyabrata Banerjee, Partha Roy. Nitroaromatic explosives detection by a luminescent Cd(II) based metal organic framework. Journal Polyhedron 123. -2017. P. 217–225.
11. R. A. Yetter, G. A. Risha and S. F. Son, Proc. Combust. Inst., 2009, 32, 1819–1838.
12. C. Wu, K. Sullivan, S. Chowdhury, G. Jian, L. Zhou and M. R. Zachariah, Adv. Funct. Mater., 2012, 22, 78–85.
13. G. Jian, J. Feng, R. J. Jacob, G. C. Egan and M. R. Zachariah, Angew. Chem., 2013, 125, 9925–9928.
14. E. Vega, H. Ruiz, S. Escalona, A. Cervantes, D. LopezVeneroni, E. Gonzalez-Avalos and G. Sanchez-Reyna, Atmos. Pollut. Res., 2011, 2, 477–483.
15. S. B. Kim, K. J. Kim, M. H. Cho, J. H. Kim, K. T. Kim and S. H. Kim, ACS Appl. Mater. Interfaces, 2016, 8, 9405–9412.
16. M.C. Adams, Recent advances in ablation, ARS J. 29 (1959) 625e652.
17. M. Atamanov., Zh.K. Yelemessova., A. Imangazy., K. Kamunur., B. Lesbayev., Z. Mansurov., T. Yue., R. Shen., Q.L. Yan. The Journal of Physical Chemistry C, 2019, 123, 22941−22948. DOI: 10.1021/acs.jpcc.9b05094.

18. Jauhari Ashish, Gharde Swaroop, Kandasubramanian Balasubramanian. "Effect of Ammonium Perchlorate Particle Size on Flow, Ballistic, and Mechanical Properties of Composite Propellant", Elsevier BV, 2019
19. Glossary for the Worldwide Transportation of Dangerous Goods and Hazardous Materials, 1999.
20. Weigand, Jan Josef (2005): High energy density materials based on tetrazole and nitramine compounds: Synthesis, scale-up and testing. Dissertation, LMU München: Faculty of Chemistry and Pharmacy
21. C. Oommen. "Ammonium nitrate: a promising rocket propellant oxidizer", Journal of Hazardous Materials, 1999
22. Hui Su, Jichuan Zhang, Yao Du, Pengcheng Zhang, Shenghua Li, Tao Fang, Siping Pang. "New roles for metal–organic frameworks: fuels for environmentally friendly composites", RSC Advances, 2017
23. Li, Shenghua, Yuan Wang, Cai Qi, Xiuxiu Zhao, Jichuan Zhang, Shaowen Zhang, and Siping Pang. "3D Energetic Metal-Organic Frameworks: Synthesis and Properties of High Energy Materials", Angewandte Chemie International Edition, 2013.
24. Dey, C., Kundu, T., Biswal, B. P., Mallick, A., & Banerjee, R. (2013). Crystalline metal-organic frameworks (MOFs): synthesis, structure and function. Acta Crystallographica Section B Structural Science, Crystal Engineering and Materials, 70(1), 3–10. doi:10.1107/s2052520613029557
25. Yan, Q.-L., Gozin, M., Liu, P.-J., & He, G.-Q. (2019). Insensitive Energetic Materials Containing Two-Dimensional Nanostructures as Building Blocks. Nanomaterials in Rocket Propulsion Systems, 81–111. doi:10.1016/b978-0-12-813908-0.00003-4
26. Herreros, D. N., & Fang, X. (2017). Laser ignition of elastomer-modified cast double-base (EMCDB) propellant using a diode laser. Optics & Laser Technology, 89, 21–26. doi: 10.1016/j.optlastec.2016.09.033
27. C.T. Morrow, L.D. Ely, M.R. Smith (Eds.), Proceedings of the 6th Symposium on Ballistic Missile and Aerospace Technology, vol. IV, Academic Press Inc., New York, 1961, pp. 189e204.
28. P. Sutton, O. Biblarz, Rocket Propulsion Elements, Wiley-IEEE, 2000, pp. 268e340. ISBN 0471326429, 9780471326427.
29. Adam, D.; Karaghiosoff, K.; Klapötke, T. M.; Holl, G.; Kaiser, M. *Propellants, Expl. Pyrotech.* 2002, *27*, 7.
30. Köhler, J.; Meyer, R., 'Explosivstoffe', Wiley-VCH, D-Weinheim, D, 9. Auflage, 1998.
31. Deal, W. E. *J. Chem. Phys.* 1957, *27(1)*, 796.
32. Mader, C. L. Report LA-2900, *Los Alomos Scientific Laboratory, Fortran BKW Code for computing the detonation properties of explosives*, Los Alamos, NM, July 1963.
33. Pagoria, P. F.; Lee, G. S.; Michell, A. R.; Schmidt, R. D. *Thermochim. Acta* 2002, *384*, 187.

34. Shimizu, T. *Fireworks − Art, Science and Technique*, Maruzen Co Ltd., Tokyo, J, 1981.
35. Lancaster, R.; Shimizu, T.; Butler, R. E. A.; Hall, R. G. *Fireworks − Principle and Practise*, Chemical Publishing Company Inc., New York, USA, 1974.
36. Ineichen, H.; Berger, B. *Chimia*, 2004, *58*, 369.
37. Cord, P. P.; Labourdique, A.; Fauconnier, A.; Rouby, T. 16th Int. Annual Conf. of ICT, Karlsruhe, Germany,1985, 44/1.
38. Reed, R.; Brady, V. L.; Hirtner, J. M. 20th International Pyrotechnics Seminar, Colorado Springs, Colorado, USA, IPSUSA, Inc. 1994, 815; b) Galbraith, L. D. Unites States Patent 5,449,041, 1995;
39. Lane, G. A.; Torkleson, T. R.; Dergarzarian, T. E.; Staudacher, G. R. 3rd International Pyrotechnics Seminar, Colorado Springs, Colorado, USA, IPSUSA, Inc. 1972, 25;
40. Engelen, K.; Lefebvre, M. H. Propellants, Expl. Pyrotech. 2003, 28(4), 201.
41. Kirk-Othmer Encyclopedia of Chemical Technology, Vol. 2, 4th edn., Wiley, New York, 1992, pp. 698–705.
42. Ullmann's Encyclopedia of Industrial Chemistry, Vol. A2, 5th edn., VCH, Germany, 1989, pp. 243–252.
43. G.P. Sutton, Rocket Propulsion Elements, 5th edn., Wiley, New York, 1986, p. 296.
44. J.R. Glauber, De Natura Salium, Amsterdam, 1659, Pharmacopoeia Spagyrica, Amsterdam, 1667.
45. J.W. Mellor, A Comprehensive Treatise on Inorganic and Theoretical Chemistry, Vol. 2, Longmans Green, London, 1922, pp. 829–846.
46. B.T. Fedroff, Encyclopedia of Explosives and Related Items, Vol. 1, Picatinny Arsenal, NJ, 1960, pp. A311–A379.
47. H. Ellern, Military and Civilian Pyrotechnics, Chemical Publishing, New York, 1968, pp. 176–177.
48. S. Fordham, High Explosives and Propellants, Pergamon, London, 1966, p. 40
49. M.K. Atamanov, K.Hori., M.A. Yeleuov., Zh.K. Yelemesova. New energetic graphene oxide frameworks (GOFs) for combustion on han based monopropellant. The First International Conference on Defense Technology (Beijing, China, Oct.21-25, 2018).
50. Q. L. Zhu, J. Li and Q. Xu, J. Am. Chem. Soc., 2013, 135, 10210–10213.
51. N. L. Rosi, J. Eckert, M. Eddaoudi, D. T. Vodak, J. Kim, M. O. Keeffe and O. M. Yaghi, Science, 2003, 300, 1127–1129.
52. M. P. Suh, H. J. Park, T. K. Prasad and D. W. Lim, Chem. Rev., 2012, 112, 782–835.
53. Y. He, R. Krishna and B. Chen, Energy Environ. Sci., 2012, 5, 9107–9120.
54. Q. Zhai, Q. Lin, T. Wu, L. Wang, S. Zheng, X. Bu and P. Feng, Chem. Mater., 2012, 24, 2624–2626.
55. H. B. Zhang, M. J. Zhang, P. Lin, V. Malgras, J. Tang, S. M. Alshehri, Y. Yamauchi, S. W. Du and J. Zhang, Chem.–Eur. J., 2016, 22, 1141–1145.
56. J. Zhang and J. M. Shreeve, Dalton Trans., 2016, 45, 2363–2368.

57. S. Zhang, Q. Yang, X. Liu, X. Qu, Q. Wei, G. Xie, S. Chen and S. Gao, Coord. Chem. Rev., 2016, 307, 292–312.
58. Hui Su, Jichuan Zhang, Yao Du, Pengcheng Zhang, Shenghua Li, Tao Fangb and Siping Pang. New roles for metal–organic frameworks: fuels for environmentally friendly composites. Journal RSC Advances. 2017, 7, 11142.
59. Chandan Dey, Tanay Kundu, Bishnu P. Biswal, Arijit Mallick and Rahul Banerjee. Crystalline metal-organic frameworks (MOFs): synthesis, structure and functionActa Crystallographica Section B. Structural Science, Crystal Engineering and Materials. -2014. V.70, P.3–10.
60. Shenghua Li, Yuan Wang, Cai Qi, Xiuxiu Zhao, Jichuan Zhang, Shaowen Zhang and Siping Pang*. 3D Energetic Metal–Organic Frameworks: Synthesis and Properties of High Energy Materials//Angew. Chem. Int. Ed. –2013. P.1 –6. Vol. 52.
61. Shibashis Halder, Pritam Ghosh, Corrado Rizzoli, Priyabrata Banerjee, Partha Roy. Nitroaromatic explosives detection by a luminescent Cd(II) based metal organic framework. Journal Polyhedron 123. -2017. P. 217–225.
62. Hui Su, Jichuan Zhang, Yao Du, Pengcheng Zhang, Shenghua Li, Tao Fangb and Siping Pang. New roles for metal–organic frameworks: fuels for environmentally friendly composites. RSC Adv., 2017, 7, 11142.
63. Dr. S. Li, Y. Wang, C. Qi, X. Zhao, J. Zhang, Prof. S. Pang. 3D Energetic Metal–Organic Frameworks: Synthesis and Properties of High Energy Materials. Angew. Chem. Int. Ed. 2013, 52, 1 – 6.
64. Jacobs, P.W.M., Russel-Jones, A., The thermal decomposition and ignition of mixtures of ammonium perchlorate copper chromite. In: Eleventh Symposium (International) on Combustion, V. 11, P. 457-462 (1967).
65. Hussain, G., Rees, G.J.: Combustion of NH_4NO_3 and carbon based mixtures. Fuel 72(11), - P. 1475–1479 (1993).
66. Hussain, G., Rees, G.J.: Combustion of ammonium perchlorate based mixture with and without black powder, studied by d.s.c and TG/DTG. Fuel 71, - P. 471-473 (1992).
67. Geim, A.K. and Novoselov, K.S. (2007) The Rise of Graphene. Nature Materials, 6, 183-191. https://doi.org/10.1038/nmat1849.
68. Saxena, S. and Tyson, A. (2010) Interacting Quasi-Two-Dimensional Sheets of Interlinked Carbon Nanotubes: A High-Pressure Phase of Carbon. ACS Nano, 4, 3515-3521. https://doi.org/10.1021/nn100626z.
69. Brodie, B.C. (1859) On the Atomic Weight of Graphite. Philosophical Transactions of the Royal Society of London, 149, 249-259. https://doi.org/10.1098/rstl.1859.0013.
70. Staudenmaier, L. (1898) Verfahren zur Darstellung der Graphitsaure. Berichte der Deutschen Chemischen Gesellschaft, 31, 1481-1487. https://doi.org/10.1002/cber.18980310237.
71. Hummers, W.S. and Offeman, R.E. (1958) Preparation of Graphitic Oxide. Journal of The American Chemical Society, 80, 1339. https://doi.org/10.1021/ja01539a017

72. D.V. Rosato, Other properties and characteristics, in: D.V. Rosato, R.T. Schwartz (Eds.), Environmental Effects on Polymeric Materials, Environments, Interscience Publishers, 1968, pp. 807-808.
73. G. Epstein, H.A. King, Plastic for rocket motor nozzles, Ind. Eng. Chem. 52 (1960) 764e767.
74. M. Favaloro, Ablative materials, in: Kirk-Othmer Encyclopedia of Chemical Technology, 2001, https://doi.org/10.1002/0471238961.0102120106012201.a01.
75. Cory S. American Fuel & Petrochemical Manufacturers. American Fuel & Petrochemical Manufacturers. Retrieved 18 December 2016.
76. Khezami L., Chetouan, A., Taou, B., Capar, R. Production and characterisation of activated carbon from wood components in powder: cellulose, lignin, xylan // Powder Technol. - 2005. - № 157. - P.48–56.
77. Alekhina M.B. Intended business: educational aid - M.: PXTY after D.I. Mendelev, 2007.- 116 p.
78. Romanos J.; et al. (2012). "Nanospace engineering of KOH activated carbon". Nanotechnology. 23 (1): 015401. doi:10.1088/0957-4484/23/1/015401.
79. Komarov V.C., Besarab C.V. Accessories and catalysts Day-to-day adjustments to a good structure. - M.: INFPA-M, 2014.- 203 p.80.
80. Ishitha K. and Ramakrishna P. A. Activated charcoal: as burn rate modifier and its mechanism of action in non-metalized composite solid propellants Int J Adv Eng Sci Appl Math, 2014. 6(1–2):76–96.
81. Kubota, N.: Propellants and Explosives. Wiley, Germany (2002).
82. Verma, S., Ramakrishna, P.A.: Investigations on activated charcoal, a burn rate enhancer in composite solid propellant. J. Propuls. Power 29(5), 1214–1219 (2013).
83. Verma, S., Ramakrishna, P.A.: Activated charcoal: a novel burn rate enhancer of aluminized composite propellants. Combust. Flame 157, 1202–1210 (2010).
84. Verma, S., and Ramkrishana, P. A., “Development of Low Burn Rate Pressure Index Composite Solid Propellant,” 8th Asia Pacific Conference on Combustion, The Combustion Institute – Indian Section (CIIS), Hyderabad, India, 2010, pp. 619–626.
85. Kumar P, Joshi CP, Kumar R, Biswas S. Catalytic effects of Cu-Co* on the thermal decomposition of AN and AN/KDN based green oxidizer and propellant samples. Defence Technology 2018;14(3):250-60.
https://doi:10.1016/j.dt.2018.03.002.
86. Rao DCK, Yadav N, Joshi PC. Cu–Co–O nano-catalysts as a burn rate modifier for composite solid propellants. Defence Technology 2016;12(4):297– 304. https://doi:10.1016/j.dt.2016.01.001.
87. GOST 4453-74. An active, illuminated wooden illuminated apron [Electronic pecypc]. - URL: http: // http: //docs.cntd.ru/document/gost-4453-74.
88. Babuk V.A., Dolotkazin I.N., Glebov A.A., Burning Mechanisms of Aluminized Solid Rocket Propellants Based on Energetic Binders // Propellants Explosives, Pyrotechnics. – 2005. – Vol. 30, № 4. – P. 281-290.
89. Risha G, Ulas A, Kuo K, Koch D, Ludwig C, Glick R. Combustion behavior of TAL-1308 composite solid propellant for airbag applications. 35th Joint Propulsion

Conference and Exhibit. 20-24 June 1999 Los Angeles, California. https://doi:10.2514/6.1999-2632.
90. Hoeflich, T.C.; LaBarge, M. S. Journal of Loss Prevention in the Process Industries 2002, 15, 163.
91. Standard Test Method for Arrhenius Kinetic Constants for Thermally Unstable Materials, ASTM Designation E698-99, 1999.
92. Ozawa, T. Bull. Chem. Chem. Soc. Jpn. 1965, 38, 1881.
93. Kissinger, H. E. Anal. Chem. 1957, 29, 1702.
94. Tomoki Naya and Makoto Kohga. "Burning characteristics of ammonium nitrate-based composite propellants supplemented with MnO2" Propellants explosive, pyrothec. V.38. P. 87–94. (2013).
95. Tomoki Naya and Makoto Kohga, "Burning characteristics of ammonium nitrate-based composite propellants supplemented with Fe2O3". Propellants explosive, pyrothec. Issue 4, August. V. 38. P.547–554. (2013).
96. McIntyre D. A Laser Spark Plug Ignition System fora Stationary Lean-Burn Natural Gas Reciprocating Engine. Ph.D. thesis. West Virginia University, 2007.
97. Gordon, S., and McBride, B.J. 1994. Computer program for calculation of complex chemical equilibrium composition and applications. NASA RP-1311-P2.
98. R. Saito, M. Hofmann, G. Dresselhaus et. al., Raman Spectroscopy of Graphene and Carbon nanotubes. Adv. Phys. 66 (3), 413-550, 2011. https://doi.org/10.1080/00018732.2011.582251.
99. J. M. Jandosov, N. V. Shikina, M. A. Biisenbayev, et al., "Evaluation of Synthetic Conditions for H3PO4 Chemically Activated Rice Husk and Preparation of Honeycomb Monoliths," Eurasian Chem. Technol. J. 11 (30, 245–252 (2009); https://doi.org/10.18321/ectj287.
100. M. K. Atamanov, I. Noboru, T. Shotaro, et al., "Investigation of Combustion and Thermal Analysis of Ammonium Nitrate with Carbonaceous Materials," Combust. Sci. Technol. 118 (11-12), 2003–2011 (2016); https://doi.org/ 10.1080/00102202.2016.1220143.
101. Yelemessova Zh.K., Mansurov Z.A., Lesbayev B.T., Ruiqi Shen. Laser ignition of energetic materials based on carbon containing metal oxide propellant. Chemical Journal of Kazakhstan (2019), 2 (66):163-168.
102. Izato Y, Miyake A, Date S. Combustion characteristics of ammonium nitrate and carbon mixtures based on a thermal decomposition mechanism. Propellants, Explosives, Pyrotechnics 2013;38(1):129–35. https://doi:10.1002/prep.201100106.
103. Yelemessova Zh.K., Atamanov M.K., Kamunur K., Lesbayev B.T., Ruiqi Shen. Investigation of the transitional metal oxides effects on combustion and thermal characteristics of AN/Mg/C-activated carbon composites. Chemical Journal of Kazakhstan (2019), 1 (65):273-279.
104. Sudhakar AOR, Mathew S. Thermal behaviour of CuO doped phase-stabilised ammonium nitrate. Thermochim Acta. 2006:451(1-2):5–9. https://doi:10.1016/ j.tca.2006.08.013.

105. Klimova I, Kaljuvee T, Türn L, Bender V, Trikkel A, Kuusik R. Interactions of ammonium nitrate with different additives. Journal of Thermal Analysis and Calorimetry 2011;105(1), 13–26. https://doi:10.1007/s10973-011-1514-9.
106. Yelemessova Zh.K., Kamunur K., Pustovalov I.A., Imangazy A.M., Lesbayev B.T., Ruiqi Shen. Burning of pyrotechnic compositions with metal salt supplements. Combustion and Plasmachemistry (2017), 4 (15): 338-344.
107. Yelemessova Zh.K., Pustovalov I.A., Kamunur K., Shen R. Research of the colorful pyrotechnic compositions based on binders with various color scale. XV All-Russian with an international school-seminar accessory for young males and girls named after Academician A.G. Merzhanova. (Chernogolovka, November 22-24, 2017).
108. Kamunur K., Jandosov J.M., Abdulkarimova R.G., Hori K., Yelemessova Z.K. «Combustion study of different transitional metal oxide based on AN/MgAl composites gas generators»// Eurasian Chemico-Technological Journal, 2017, 19, 341-346, DOI: https://doi.org/10.18321/ectj682.
109.Yelemessova Zh.K., Ruiqi Shen. Metal-organic frameworks-based energy propellant: effect on combustion of ammonium nitrate and magnesium composition. Chemical Journal of Kazakhstan (2019), 4 (68):99-111.
110. K. Kamunur, J.M. Jandosov, R.G. Abdulkarimova, K.Hori, Zh. Yelemessova, Z.A. Mansurov. Effect of Cr2O3 on burning characteristics of gas generators based on AN/MgAl. IX International Symposium «Combustion and Plasmochemistry» (Almaty, Kazakhstan, 13-15 September, 2017).
111. Yelemessova Zh.K., Lesbayev B.T., Ruiqi Shen. Investigation of the effect of activated carbon (from plant raw material) based on metal oxides for pyrotechnical purposes. X International Symposium «The physics and chemistry of carbon and nanoenergetic materials» (Almaty, Kazakhstan, 12-14 September, 2018);
112.Yan QL, Gozin M, Zhao FQ, Cohen A, Pang SP. Highly energetic compositions based on functionalized carbon nanomaterials. Nanoscale 2016;8(9):4799-851. DOI: 10.1039/c5nr07855e.
113. Singh H, Shekhar H. Problems associated with the combustion modelling of solid rocket propellants, 5th International Seminar On Flame Structure And Combustion, Novosibirsk (Russia), 11–14 July 2005.
114. Liau YC, Yang V. Analysis of RDX monopropellant combustion with two-phase subsurface reactions. Journal of Propulsion and Power 1995;11(4):729– 39. https://doi:10.2514/3.23898.
115. Hosseini SG, Eslami A. Thermoanalytical investigation of relative reactivity of some nitrate oxidants in tin-fueled pyrotechnic systems. Journal of Thermal Analysis and Calorimetry 2010;101(3):1111–9. https://doi:10.1007/s10973-01.0-0813-x.
116. Nanoshel LLC web site: www.nanoshel.com/metal-organic-frameworks